PICOF'06

Laboratoire J.-A. Dieudonné
Université de Nice Sophia-Antipolis
Parc Valrose

Nice, France
5-7 avril 2006

Résumés

3ème Colloque sur les Problèmes Inverses, le Contrôle et l'Optimisation de Formes

Abstracts

3rd Conference on Inverse Problems Control and Shape Optimization

ENIT LAMSIN
INRIA SOPHIA ANTIPOLIS
Université Nice SOPHIA ANTIPOLIS

Third Conference on Inverse Problems, Control and Shape Optimization

Troisième Colloque sur les Problèmes Inverses, le Contrôle et l'optimisation de Formes

Book of abstracts

April 5-7, 2006
Nice (France)

Introduction

Bien que leurs outils d'analyse et de calcul soient en grande partie communs, les scientifiques travaillant dans les trois axes que regroupe le colloque (Problèmes Inverses, Contrôle, Optimisation de Formes) n'ont que peu d'opportunités de réunion, d'échange et de confrontation de points de vue. C'était le constat fondateur de PICOF, qui veut d'abord être un lien régulier, susceptible de favoriser les synthèses ainsi que de susciter et d'approfondir les collaborations. Il a l'ambition de conforter ainsi son statut de manifestation d'envergure internationale sur ce sujet dans l'espace francophone, en particulier méditerranéen.

Cette troisième édition du Colloque, faisant suite à celles tenues à Carthage (Tunisie) en 1998 et en 2002, s'inscrit dans la fidélité aux objectifs et à l'esprit initiaux, en même temps qu'elle marque une nouvelle étape dans la poursuite de ces objectifs.

Fidélité aux origines, puisque le colloque reste un événement à dimension humaine, sans sessions parallèles pour que tous les participants puissent s'écouter et échanger, largement ouvert aux jeunes aussi bien par le biais des conférences invitées que par celui de la « session posters » nouvellement introduite, ainsi qu'à la coopération scientifique sur le pourtour méditerranéen enfin. Mais il s'agit aussi d'une nouvelle étape, puisque le colloque adopte une fréquence biennale, et qu'il se tiendra désormais à tour de rôle sur chacune des deux rives du bassin méditerranéen, afin de mieux tenir son rôle d'aiguillon d'une coopération Nord-Sud au meilleur niveau. La manifestation se veut de la sorte pleinement engagée dans le développement conjoint des mathématiques appliquées sur le pourtour de la Méditerranée. A cet égard, le colloque ne constitue que la figure de proue d'un dispositif permanent d'échanges, mis en place depuis plusieurs années déjà, dispositif qui concerne autant les scientifiques confirmés que les plus jeunes et dont le potentiel de progression demeure très important.

Le cru 2006 de PICOF, matérialisé par l'ouvrage que vous tenez entre les mains, s'annonce à cet égard d'une qualité rare. Les quelques 34 conférences et posters couvriront largement le spectre des problèmes inverses, du contrôle et de l'optimisation de formes. Ils en balayeront les aspects théoriques d'existence, d'unicité, de stabilité, de contrôlabilité, aussi bien que les aspects de la modélisation dans de multiples domaines applicatifs, sans oublier les aspects algorithmiques et les méthodes numériques qui deviennent, le travail des chercheurs et le développement des moyens de calcul aidant, de plus en plus effectives.

Les organisateurs de la conférence sont ravis de la transformation des deux essais de 1998 et de 2002 que la présente session constitue. Nous la devons en premier lieu aux conférenciers qui ont accepté notre invitation, au travail rigoureux des membres du Comité Scientifique, et en particulier à celui de son président Jacques Blum, ainsi qu'aux efforts et au dévouement des membres du Comité d'Organisation. Nous la devons également à l'appui apporté par les trois institutions organisatrices : ENIT (École Nationale d'Ingénieurs de Tunis), INRIA (Institut National de Recherche en Informatique et Automatique) et UNSA (Université de Nice-Sophia Antipolis), ainsi que par le Conseil Régional PACA (Provence-Alpes-Côte d'Azur), l'AUF (Agence universitaire de la francophonie), le CIMPA (Centre International de Mathématiques Pures et Appliquées), le MAE (Ministère Français des Affaires Étrangères) et le Conseil Général des Alpes Maritimes. Que toutes et tous trouvent ici l'expression de notre profonde gratitude.

Les Présidents de PICOF'06

Henda El Fekih Mohamed Jaoua Juliette Leblond

Introduction

Although sharing numerous analytical and computational tools, the researchers involved in the three topics of the conference seldom meet and exchange ideas in conferences. This established fact was the reason for founding PICOF, which aims to constitute a steady link, capable of fostering syntheses and partnerships, and to consolidate its position as the main conference on these topics in the French-speaking area.

Following the two first meetings, which were held in Carthage, Tunisia, in 1998 and 2002, the present one, though characterized by its faithfulness to the initial spirit and goals of the Conference, shows a new step in pursuing these objectives.

Loyal to its original spirit, the Conference remains at a personal level, with no parallel sessions, in order to allow all those attending to listen to each other and to exchange ideas. It also remains open to younger researchers, through the invited conferences as well as the newly created poster session. Finally, it is still widely open to cooperative action between scientists from all around the Mediterranean sea.

On the other hand, the present meeting also represents a new move towards effectiveness, by adopting a 2-year periodicity, and by crossing for the first time the Mediterranean sea, to be held in turn on its Northern and Southern shores, in order to better fulfill its role as a spearhead of a North/South partnership at the highest possible level. Besides conforming to the highest scientific standards, the conference is fully concerned with the joint development of Applied Mathematics all around the Mediterranean sea. It is actually the figurehead of a full arrangement, that has been set up for a few years, including a collection of tools intended to promote scientific exchanges, with a special focus on young researchers.

As evidenced by the booklet you have in your hands, the 2006 PICOF crop seems to be exceptional. The 34 conferences and posters will cover the whole range of inverse problems, control and shape optimization. They will deal with theoretical aspects related to existence, uniqueness, stability, and controllability. They will also take care of the modeling aspects in several areas of applications, as well as the algorithmic aspects and those related to numerical methods, which are becoming more effective every day, thanks to the work of researchers and the development of computing power.

The organizers are clearly delighted that this meeting continues in this way from the first two experiments of Carthage 1998 and 2002. We owe this in the first instance to the guest speakers who accepted the invitation, to the Scientific Commitee's rigorous work, and especially that of its President, Jacques Blum, as well as to the efforts and devotion of the Organization Committee members. We also owe it to the support of three organizing institutions: ENIT (École Nationale d'Ingénieurs de Tunis), INRIA (Institut National de Recherche en Informatique et Automatique) and UNSA (Université de Nice-Sophia Antipolis), as well as the support of the Conseil Régional PACA (Provence-Alpes-Côte d'Azur), AUF (Agence universitaire de la francophonie), CIMPA (International Centre for Pure and Applied mathematics), the MAE (Foreign Affairs French Ministry) and the Conseil Général des Alpes Maritimes To all of them, we here express our deep gratitude.

The Chairs of the Conference

Henda El Fekih Mohamed Jaoua Juliette Leblond

Scientific Comittee

Chair: Jacques Blum (UNSA, JAD)

Members: Amina Amassad (Nice), Laurent Baratchart (Sophia Antipolis), Amel Ben Abda (Tunis), Rajae Aboulaïch (Rabat), Jean-Antoine Désidéri (Sophia Antipolis), Henda El Fekih (Tunis), Caroline Fabre (Nice), Abderrahmane Habbal (Nice), Mohamed Jaoua (Nice), Rainer Kress (Göttingen), Karl Kunisch (Graz), Juliette Leblond (Sophia Antipolis), Mohamed Masmoudi (Toulouse), Jean-Pierre Raymond (Toulouse), Gunther Uhlmann (Washington), Michael Vogelius (New Brunswick), Enrique Zuazua (Madrid).

Organisation Team

Co-Chairs:

Henda El Fekih (ENIT-LAMSIN)
Mohamed Jaoua (UNSA, JAD)
Juliette Leblond (INRIA, Apics)

Members:

Amina Amassad (UNSA, JAD)
Amel Ben Abda (ENIT-LAMSIN)
José Grimm (INRIA, Apics)
Abderrahmane Habbal (UNSA, JAD)
Dany Sergeant (INRIA, Relext)

Contents

Stability and Reconstruction for the determination of nonlinear corrosion

Giovanni Alessandrini [1] *Eva Sincich*[2]

We shall discuss an inverse boundary value problem arising in *corrosion* detection. The aim of such a problem is to determine a *nonlinear* term in a boundary condition, which models the possible presence of corrosion damage, by performing a finite number of current and voltage measurements on the boundary. The physical problem is modeled as follows. A bounded Lipschitz domain Ω in $\mathbb{R}^n$ represents the region occupied by the electrostatic conductor which contains no sources and no sinks and this is modeled by the Laplace operator, so that the voltage potential u satisfies

$$\Delta u = 0 \text{ in } \Omega. \tag{1.1}$$

The simplified model of corrosion appearance reduces to the problem of recovering a coefficient $\varphi = \varphi(x)$ in a *linear* boundary condition of the type

$$\frac{\partial u}{\partial \nu} = -\varphi u, \tag{1.2}$$

where ν is the outward unit normal at the boundary and $\varphi \geq 0$ is the so-called *Robin coefficient*. The study of such a problem has been developed by many authors, among them we mention Alessandrini, Del Piero, Rondi [1], Chaabane, Fellah, Jaoua, Leblond [6, 7, 8] and Fasino and Inglese [11, 12, 13].

A more accurate model of corrosion requires a nonlinear relationship between voltage and current density on the corroded surface. A model of this kind, known as the Butler and Volmer model, postulates the boundary condition

$$\frac{\partial u}{\partial \nu} = \lambda(\exp(\alpha u) - \exp(-(1-\alpha)u)). \tag{1.3}$$

Such a *nonlinear* boundary value problem, has been recently discussed by Bryan, Kavian, Vogelius and Xu in [5, 16, 24]. The authors have examined the questions of the existence and the uniqueness of the solution of the problem with a given nonlinearity of the type (1.3).

In the following we shall consider a more general choice of the nonlinear profile, namely of the form

$$\frac{\partial u}{\partial \nu} = f(u) \ , \tag{1.4}$$

[1] alessang@univ.trieste.it
[2] esincich@sophia.inria.fr

and we shall deal with the inverse problem of determining the nonlinear term f in the boundary value problem

$$\begin{cases} \Delta u = 0 & \text{in } \Omega, \\ \dfrac{\partial u}{\partial \nu} = g & \text{on } \Gamma_2, \\ \dfrac{\partial u}{\partial \nu} = f(u) & \text{on } \Gamma_1, \\ u = 0 & \text{on } \Gamma_D. \end{cases} \tag{1.5}$$

Let us now give the formulation of our problem. We assume that the boundary of the conductor, which is modeled by the domain Ω, is decomposed in three open, nonempty and disjoint portions $\Gamma_1, \Gamma_2, \Gamma_D$, one of which, say Γ_2, is accessible to the electrostatic measurements, whereas the portion Γ_1, where the corrosion takes place, is out of reach. The remaining portion Γ_D, which separates Γ_1 from Γ_2, is assumed to be grounded. The inverse corrosion problem thus consists in the determination of f when one pair of Cauchy data $\{u|_{\Gamma_2}, \frac{\partial u}{\partial \nu}|_{\Gamma_2}\}$ is available on the accessible portion Γ_2 of the conductor.

Since the direct problem (1.5) might not be well-posed, it seems natural to require an a priori energy bound on the electrostatic potential u within the conductor,

$$\int_\Omega |\nabla u(x)|^2 \leq E^2 \ . \tag{1.6}$$

Next, we require an a priori bound of the Lipschitz continuity of f, namely

$$|f(u) - f(v)| \leq L|u - v| \ , \ \text{for every } u, v \ \in \mathbb{R} \ . \tag{1.7}$$

Moreover, we shall assume the knowledge of some additional information on the measured current density g on the accessible part of the boundary Γ_2. More precisely, we assume a bound on the Hölder continuity of g

$$\|g\|_{C^{0,\alpha}(\Gamma_2)} \leq G \ . \tag{1.8}$$

Also, we shall require a lower bound on the same current density g. Namely, we shall prescribe that, for a given inner portion $\Gamma_2^{2r_0}$ of Γ_2, and a given number $m > 0$, we have

$$\|g\|_{L^\infty(\Gamma_2^{2r_0})} \geq m > 0 \ . \tag{1.9}$$

It has to be noticed that, since one can expect to identify the corrosion profile f only on the range of values taken by the voltage potential u on the corroded part of the boundary and since it is not a priori given, it follows that the unknown of the problem are indeed the domain upon which f may be determined, beyond the profile f on such a domain. Thus in [2], as preliminary step of the treatment of this inverse problem, we proved a lower bound on the oscillation of u on Γ_1, namely

$$\operatorname*{osc}_{\Gamma_1} u \geq \textit{const.} \exp\Big(-\big(\textit{const.}\ m\big)^{-\gamma}\Big) , \tag{1.10}$$

where γ is a positive exponent such that $\gamma > 1$.

Next, as the main result achieved in [2], we showed that if u_1 and u_2 are two potentials corresponding to nonlinearities f_1 and f_2 whose Cauchy data are close

$$\begin{aligned} &\|u_1 - u_2\|_{L^2(\Gamma_2)} \leq \varepsilon \ , \\ &\left\| \frac{\partial u_1}{\partial \nu} - \frac{\partial u_1}{\partial \nu} \right\|_{L^2(\Gamma_2)} \leq \varepsilon \ , \end{aligned}$$

then the ranges of u_1 and u_2 on Γ_1 agree on an interval V, such that

$$\text{length of } V \ \sim \ \exp\left[-\left(\frac{m}{c}\right)^{-\gamma}\right]. \tag{1.11}$$

On such an interval the nonlinearities f_1 and f_2 agree up to an error of the type

$$\left|\log\left(\frac{1}{\varepsilon}\right)\right|^{-\theta}, \tag{1.12}$$

where $0 < \theta < 1$.

For what concerns the reconstruction issue, let us recall that we shall term reconstruction the inverse problem of the approximate identification of the nonlinear term f by the approximate electrostatic measurements $\{u|_{\Gamma_2}, \frac{\partial u}{\partial \nu}|_{\Gamma_2}\}$, u being the solution to (1.5). Indeed the Cauchy data will be affected by errors since they are given by finitely many samples. Thus, as a consequence, we can expect to recover the nonlinearity f only in an approximate manner.

In this setting the stability analysis just discussed, can be understood as a preliminary result for the reliability of the reconstruction procedure.

Since the main cause of the ill-posedness of such an inverse problem relies on the solution of a the severely ill-posed Cauchy problem with Cauchy data $\{u|_{\Gamma`_2}, \frac{\partial u}{\partial \nu}|_{\Gamma_2}\}$, in [3] we have proposed a method for the approximate resolution of the Cauchy problem. Such a method is based on the reformulation of the Cauchy problem to a regularized inversion of a suitable compact operator, fitting our problem in the widely developed theory of regularization for equations of the first kind. Indeed, with appropriate reductions of the problem, we proved that the operator that maps the unknown Cauchy data on Γ_1 into the Cauchy data on Γ_2, is compact. Such a compactness result is strongly based on well-known regularity property for solution of elliptic equations. This reformulation allows the method of singular value decomposition and the approximate inversion by the technique of Tikhonov regularization.

Let us mention the most recent contributions to the approximate solution of the Cauchy problem due to Berntsson, Cheng, Eldén, Elliott, Engl, Fomin, Hào, Heggs, Hon, Ingham, Kabanikhin, Karchevskiĭ, Kozlov, Marin, Maz'ya, Leit˜ao, Lesnic, Maz'ya, Wei, [4], [9], [10], [14], [15], [18], [19], [20], [21], [22].

Finally we suggested an approximate expression of the nonlinearity f. Indeed by a formal computation we selected a candidate minimizer of the so-called best-fit functional and we proved, under further a priori assumptions, the pointwise convergence of such candidate minimizers to the exact nonlinearity f (see [23]).

Bibliography

[1] G. Alessandrini, L. Del Piero, L. Rondi. *Stable determination of corrosion by a single electrostatic boundary measurement*, Inverse Problems, 19 (2003), no.4, 973-984.

[2] G. Alessandrini, E. Sincich. *Detecting nonlinear corrosion by electrostatic measurements*, Applicable Anal. 85, 1-3, January-March 2006, 107-128.

[3] G. Alessandrini, E. Sincich. *Solving elliptic Cauchy problems and the identification of nonlinear corrosion*, to appear on J. Computational Appl. Math.

[4] F. Berntsson, L. Eldén. Numerical solution of a Cauchy problem for the Laplace equation, Inverse Problems, Vol.17, no.4, 839-853, (2001).

[5] K. Bryan, M. Vogelius. *Singular solutions to a nonlinear elliptic boundary value problem originating from corrosion modeling*, Quart. Appl. Math., 60 (2002), 675-694.

[6] S. Chaabane, I. Fellah, M. Jaoua, J. Leblond. *Logarithmic stability estimates for a Robin coefficient in two-dimensional Laplace inverse problems*, Inverse Problems, 20 (2004), no.1, 47-59.

[7] S. Chaabane, M. Jaoua, J. Leblond. *Parameter identification for Laplace equation and approximation in Hardy classes*, J. Inverse Ill-Posed Probl. 11 (2003), no. 1, 33–57.

[8] S. Chaabane, M. Jaoua. *Identification of Robin coefficients by the means of boundary measurements*, Inverse Problems 15 (1999), no. 6, 1425–1438.

[9] J. Cheng, Y.C. Hon, T. Wei. Computation for multidimensional Cauchy problem, SIAM J. Control Optim., Vol.42, no.2, 381-396, (2003).

[10] H.W. Engl, A. Leitão. A Mann iterative regularization method for elliptic Cauchy problems, Numer. Funct. Anal. Optim., Vol.22, no.7-8, 861-884, (2001).

[11] D. Fasino, G. Inglese. *An inverse Robin problem for Laplace equation: theoretical results and numerical methods*, Inverse Problems, 15 (1999), 41-48.

[12] D. Fasino, G. Inglese. *Discrete methods in the study of an inverse problem for Laplace's equation*, IMA J. Numer. Anal. 19 (1999), no. 1, 105–118.

[13] D. Fasino, G. Inglese. *Stability of the solutions of an inverse problem for Laplace's equation in a thin strip*, Numer. Funct. Anal. Optim. 22 (2001), no. 5-6, 549–560.

[14] D.N. Hào, D. Lesnic. The Cauchy problem for Laplace's equation via the conjugate gradient method, IMA J. Appl. Math. Vol.65, no.2, 199-217, (2000).

[15] S.I. Kabanikhin, A.L. Karchevskiĭ. An optimization algorithm for solving the Cauchy problem for an elliptic equation, Dokl. Akad. Nauk., Vol.359, no.4, 445-447, (1998).

[16] O. Kavian, M. Vogelius. *On the existence and "blow-up" of solutions of a two dimensional nonlinear boundary value problem arising in corrosion modeling*, Proc. Roy. Soc. Edinburgh, 133A, (2003), 119-149.

[17] R. Kohn, M. Vogelius. *Determining conductivity by boundary measurements*, Comm. Pure Appl. Math. 37 (1984), no.3, 289-298.

[18] V.A. Kozlov, V.G. Maz'ya. On iterative procedure for solving ill-posed boundary value problems that preserve differential equations, Leningrad Math. J., Vol.1, no.5, 1207-1228, (1990).

[19] V.A. Kozlov, V.G. Maz'ya, A.V. Fomin. An iterative method for solving the Cauchy problem for elliptic equations, U.S.S.R. Comput. Math. and Math. Phys. Vol.31, no.1, 45-52, (1992).

[20] A. Leitão. An iterative method for solving elliptic Cauchy problem, Numer. Funct. Anal. Optim., Vol.21, no.5-6, 715-742, (2000).

[21] L. Marin, D. Lesnic. Boundary element solution of the Cauchy problem in linear elasticity using singular value decomposition, Comput. Methods Appl. Mech. Engrg. Vol.191, no. 29-30, 3257-3270, (2002).

[22] L. Marin, L. Elliott, P.J. Heggs, D.B. Ingham, D. Lesnic, X. Wen. Comparison of regularization methods for solving the Cauchy problem associated with the Helmholtz equation, Internat. J. Numer. Methods Engrg. Vol.60, no.11, 1933-1947, (2004).

[23] E. Sincich. Stability and Reconstruction for the Determination of Boundary Terms by a Single Measurement, PhD.Thesis, S.I.S.S.A.-I.S.A.S. Trieste, 2005 (down-loadable at http://www.sissa.it/library/).

[24] M. Vogelius, J.-M. Xu. *A nonlinear elliptic boundary value problem related to corrosion modeling*, Quart. Appl. Math., 56, (1998), 479-505.

Shape and Topology Optimization by the Level Set Method

Grégoire Allaire[1] *François Jouve*[2]

2.1 Introduction

Numerical methods of shape and topology optimization based on the level set representation and on shape differentiation make possible topology changes during the optimization process. But they do not solve the inherent problem of ill-posedness of shape optimization which manifests itself in the existence of many local minima, usually having different topologies. The reason is that the level set method can easily remove holes but can not create new holes in the middle of a shape. In practice, this effect can be checked by varying the initialization which yields different optimal shapes with different topologies. This absence of a nucleation mechanism is an inconvenient mostly in 2-d: in 3-d, it is less important since holes can appear by pinching two boundaries.

In [1] we have proposed, as a remedy, to couple our previous method with the topological gradient method (cf. [5][6][7][13]). Roughly speaking it amounts to decide whether or not it is favorable to nucleate a small hole in a given shape. Creating a hole changes the topology and is thus one way of escaping local minima. Our coupled method of topological and shape gradients in the level set framework is therefore much less prone to finding local, non global, optimal shapes. For most of our 2-d numerical examples of compliance minimization, the expected global minimum is attained from the trivial full domain initialization.

2.2 Setting of the problem

We restrict ourselves to linear elasticity. A shape is a bounded open set $\Omega \subset \mathbb{R}^d$ ($d = 2$ or 3) with a boundary made of two disjoint parts Γ_N and Γ_D, submitted to respectively Neumann and Dirichlet boundary conditions. All admissible shapes Ω are required to be a subset of a working domain $D \subset \mathbb{R}^d$. The shape Ω is occupied by a linear isotropic elastic material with Hooke's law A defined, for any symmetric matrix ξ, by $A\xi = 2\mu\xi + \lambda\big(\operatorname{Tr}\xi\big)\mathrm{Id}$, where μ and λ are the Lamé moduli. The displacement field u is the solution of the linearized elasticity system

$$\left\{\begin{array}{rcll} -\operatorname{div}\left(A\,e(u)\right) & = & f & \text{in } \Omega \\ u & = & 0 & \text{on } \Gamma_D \\ \big(A\,e(u)\big)n & = & g & \text{on } \Gamma_N, \end{array}\right. \tag{2.1}$$

[1] gregoire.allaire@polytechnique.fr
[2] francois.jouve@polytechnique.fr

where $f \in L^2(D)^d$ and $g \in H^1(D)^d$ are the volume forces and the surface loads. If $\Gamma_D \neq \emptyset$, (2.1) admits a unique solution in $u \in H^1(\Omega)^d$. The objective function is denoted by $J(\Omega)$. In this paper, only the compliance will be considered:

$$J(\Omega) = \int_\Omega f \cdot u \, dx + \int_{\Gamma_N} g \cdot u \, ds = \int_\Omega A\, e(u) \cdot e(u) \, dx. \tag{2.2}$$

To avoid working on a problem with a volume constraint, we introduce a Lagrange multiplier ℓ and consider the minimization

$$\inf_{\Omega \subset D} \mathcal{L}(\Omega) = J(\Omega) + \ell |\Omega|. \tag{2.3}$$

2.3 Shape derivative

To apply a gradient method to the minimization of (2.3) we recall the classical notion of shape derivative (see e.g. [9][12]). Starting from a smooth open set Ω, we consider domains of the type $\Omega_\theta = (\mathrm{Id} + \theta)(\Omega)$, with Id the identity mapping of $\mathbb{R}^d$ and θ a vector field in $W^{1,\infty}(\mathbb{R}^d, \mathbb{R}^d)$.

Definition 2.1 *The shape derivative of J at Ω is defined as the Fréchet derivative at 0 of the application $\theta \to J\big((Id+\theta)(\Omega)\big)$, i.e.*

$$J\big((Id+\theta)(\Omega)\big) = J(\Omega) + J'(\Omega)(\theta) + o(\theta) \quad \textit{with} \quad \lim_{\theta \to 0} \frac{|o(\theta)|}{\|\theta\|} = 0 \,,$$

where $J'(\Omega)$ is a continuous linear form on $W^{1,\infty}(\mathbb{R}^d, \mathbb{R}^d)$.

We recall the following classical result (see [3] and references therein).

Theorem 2.1 (shape derivative for the compliance) *Let Ω be a smooth bounded open set and $\theta \in W^{1,\infty}(\mathbb{R}^d; \mathbb{R}^d)$. If $f \in H^1(\Omega)^d$, $g \in H^2(\Omega)^d$, $u \in H^2(\Omega)^d$, then the shape derivative of (2.2) is*

$$\begin{aligned} J'(\Omega)(\theta) = &\int_{\Gamma_N} \left(2 \left[\frac{\partial (g \cdot u)}{\partial n} + Hg \cdot u + f \cdot u \right] - Ae(u) \cdot e(u) \right) \theta \cdot n \, ds \\ &+ \int_{\Gamma_D} Ae(u) \cdot e(u) \, \theta \cdot n \, ds, \end{aligned} \tag{2.4}$$

where H is the mean curvature defined by $H = \operatorname{div} n$.

2.4 Topological derivative

One drawback of the method of shape derivative is that no nucleation of holes inside the domain are allowed. Numerical methods based on the shape derivative may therefore fall into a local minimum. A remedy to this inconvenience has been proposed as the bubble method, or topological asymptotic method, [6], [7], [13]. The main idea is to test the optimality of a domain to topology variations by removing a small hole with appropriate boundary conditions.

Consider an open set $\Omega \subset \mathbb{R}^d$ and a point $x_0 \in \Omega$. Introduce a fixed model hole $\omega \subset \mathbb{R}^d$, a smooth open bounded subset containing the origin. For $\rho > 0$ we define the translated and rescaled hole $\omega_\rho = x_0 + \rho\omega$ and the perforated domain $\Omega_\rho = \Omega \setminus \bar{\omega}_\rho$. The goal is to study the variations of the objective function $J(\Omega_\rho)$ as $\rho \to 0$.

Definition 2.2 *If the objective function admits the following so-called topological asymptotic expansion for small $\rho > 0$*

$$J(\Omega_\rho) = J(\Omega) + \rho^d D_T J(x_0) + o(\rho^d),$$

then $D_T J(x_0)$ is called the topological derivative at point x_0.

If the model hole ω is the unit ball, the following result gives the expression of the topological derivative for the compliance $J(\Omega)$ with Neumann boundary conditions on the hole in 2d (see [7], [13]).

Theorem 2.2 *Let ω be the unit ball of $\mathbb{R}^2$. If $f = 0$, $g \in H^2(\Omega)^2$ and $u \in H^2(\Omega)^2$, then $\forall x \in \Omega \subset \mathbb{R}^2$, if $C_2 = \pi(\lambda + 2\mu)/(2\mu(\lambda + \mu))$,*

$$D_T J(x) = C_2\big\{4\mu Ae(u) \cdot e(u) + (\lambda - \mu)\,\mathrm{Tr}(Ae(u))\,\mathrm{Tr}(e(u))\big\}(x).$$

The above expression is nonnegative. This means that, for compliance minimization, there is no interest in nucleating holes if there is no volume constraint. However, if a volume constraint is imposed, the topological derivative may have negative values due to the addition of the term $-\ell|\omega|$. For the minimization problem (2.3), the corresponding topological gradient is $D_T\mathcal{L}(x) = D_T J(x) - \ell|\omega|$. At the points where $D_T\mathcal{L}(x) < 0$, holes are introduced into the current domain.

2.5 Level set method for shape optimization

Consider $D \subset \mathbb{R}^d$ a bounded domain in which all admissible shapes Ω are included, i.e. $\Omega \subset D$. Following the idea of Osher and Sethian [10], the boundary of Ω is represented by means of a level set function ψ such that $\psi(x) < 0 \Leftrightarrow x \in \Omega$. The normal n to the shape Ω is recovered as $\nabla\psi/|\nabla\psi|$ and the mean curvature H is given by $\mathrm{div}\,(\nabla\psi/|\nabla\psi|)$.

During the optimization process, the shape $\Omega(t)$ is going to evolve according to a fictitious time parameter $t > 0$ which corresponds to descent stepping. The evolution of the level set function is governed by the following Hamilton-Jacobi transport equation [10]

$$\frac{\partial\psi}{\partial t} + V|\nabla\psi| = 0 \quad \text{in} \quad D, \tag{2.5}$$

where $V(t, x)$ is the normal velocity of the shape's boundary. The choice V is based on the shape derivative computed in Theorem 2.1

$$\mathcal{L}'(\Omega)(\theta) = \int_{\partial\Omega} v\,\theta \cdot n\,ds, \tag{2.6}$$

where the integrand $v(u, n, H)$ depends on the state u, the normal n and the mean curvature H. The simplest choice is to take the steepest descent $\theta = -vn$. This yields a normal velocity for the shape's boundary $V = -v$. Another choice consists in smoothing the velocity field vn by applying the Neumann-to-Dirichlet map to $-vn$. The method described in details in [8] is used in the numerical computations.

The main point is that the Lagrangian evolution of the boundary $\partial\Omega$ is replaced by the Eulerian solution of a transport equation in the whole fixed domain D. Likewise the elasticity equations for the state u are extended to the whole domain D by using the so-called "ersatz material" approach. The Hamilton-Jacobi equation (2.5) is solved by an explicit upwind scheme

(see e.g. [11]) on a Cartesian grid with a time stepping satisfying a CFL condition. To regularize the level set function (which may become too flat or too steep), it is periodically reinitialized by solving another Hamilton-Jacobi equation which admits, as a stationary solution, the signed distance to the initial interface [11].

2.6 Optimization algorithm

For the minimization problem (2.3) we propose an iterative coupling of the level set method and of the topological gradient method. Both methods are gradient-type algorithms, so our coupled method can be thought of as an alternate directions descent algorithm.

The level set method relies on the shape derivative $\mathcal{L}'(\Omega)(\theta)$ of Section 2.3, while the topological gradient method is based on the topological derivative $D_T\mathcal{L}(x)$ of Section 2.4. These two types of derivative define independent descent directions that we simply alternate as follows.

In a first step, the level set function ψ is advected according to the velocity $-v$. Then, holes are introduced into the current domain Ω where the topological derivative $D_T\mathcal{L}(x)$ is minimum and negative.

Our proposed algorithm is structured as follows:

1. Initialization of the level set function ψ_0 corresponding to an initial guess Ω_0 (usually the full working domain D).

2. Iteration until convergence, for $k \geq 0$:

   (a) **Elasticity analysis.** Computation of the state u_k solving a problem of linear elasticity on Ω_k. This yields the shape derivative, the velocity v_k and the topological gradient.

   (b) **Shape gradient.** If $\mod(k, n_{top}) < n_{top}$, the current shape Ω_k, characterized by the level set function ψ_k, is deformed into a new shape Ω_{k+1}, characterized by ψ_{k+1} which is the solution of the Hamilton-Jacobi equation (2.5) after a time interval Δt_k with the initial condition ψ_k and a velocity $-v_k$. Δt_k is chosen such that $\mathcal{L}(\Omega_{k+1}) \leq \mathcal{L}(\Omega_k)$.

   (c) **Topological gradient.** If $\mod(k, n_{top}) = 0$, nucleation step: Ω_{k+1} is obtained by inserting new holes into Ω_k according to the topological gradient.

For details about the shape gradient step and the topological gradient step, we refer to our previous works [1][2][3].

2.7 A numerical example in 2-d

It is a variation of the classical cantilever, but its optimal solution have a more complex topology. It consists in a rectangular domain of dimensions 10×8 with a square hole whose boundaries are submitted to an homogeneous Dirichlet boundary condition. The domain is meshed with a regular 150×120 grid. Figure 2.1 shows the solution obtained by the algorithm coupling shape and topological sensitivity, starting from the full domain, with 1 step of topological gradient every 10 iterations.

The convergence history of Figure 2.2, for different numbers of initial holes, ranging from 0 to 160, gives some hints on the efficiency of the level set method without topological gradient: first, it confirms that a "topologically poor" initialization cannot convergence to a good solution;

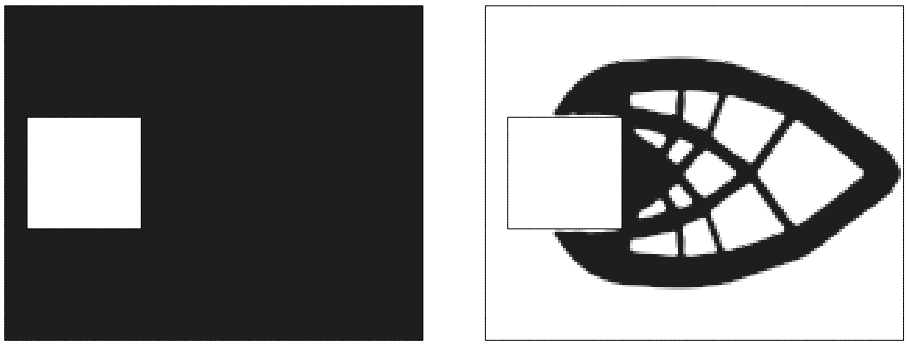

Figure 2.1: *The initial configuration (full domain) and the solution obtained by the level set method with topological gradient.*

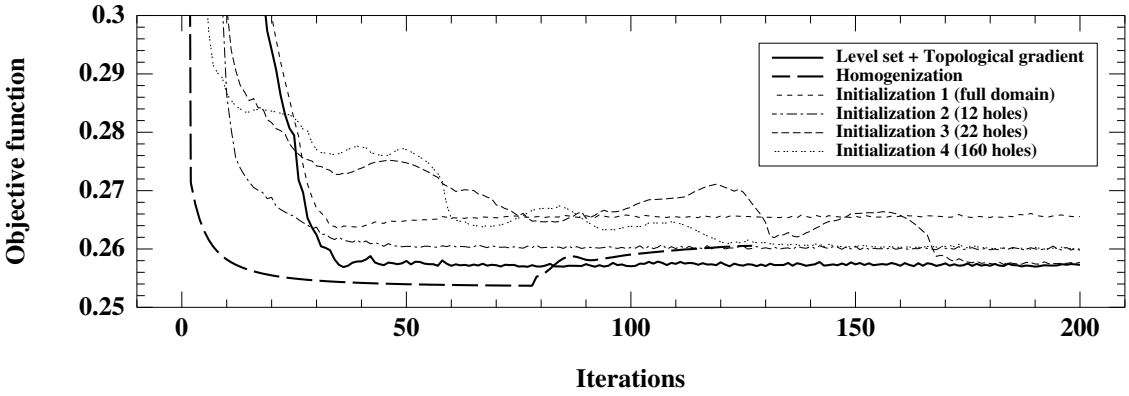

Figure 2.2: *Convergence history of the homogenization method, the level set method with topological gradient (full domain initialization), and the plain level set method with 4 different initial states.*

second, it shows that initializing with "many holes" is not a good idea too. The good strategy lies in between, but it is generally not easy to find. The topological gradient allows the convergence to a good solution, starting from the full domain, without the need of adjusting any tricky numerical parameters. Remark that the solution computed from initialization 3 (22 holes) is also good, but it has been reached after an history where it had to escape from many local minima, using the tolerance of the algorithm to small increases of the objective function.

Bibliography

[1] G. Allaire, F. De Gournay, F. Jouve, A.-M. Toader. Structural optimization using topological and shape sensitivity via a level set method, *Control and Cybernetics*, **34**, 59-80 (2005).

[2] G. Allaire, F. Jouve, A.-M. Toader. A level set method for shape optimization, *C. R. Acad. Sci. Paris, Série I*, **334**, 1125-1130 (2002).

[3] G. Allaire, F. Jouve, A.-M. Toader. Structural optimization using sensitivity analysis and a level set method, *J. Comp. Phys.*, **194**/1, 363-393 (2004).

[4] M. Burger, B. Hackl, W. Ring. Incorporating topological derivatives into level set methods, *J. Comp. Phys.*, **194**/1, 344-362 (2004).

[5] J. Céa, S. Garreau, P. Guillaume, M. Masmoudi. The shape and topological optimizations connection, IV WCCM, Part II (Buenos Aires, 1998), *Comput. Methods Appl. Mech. Engrg.*, 188, 713-726 (2000).

[6] H. Eschenauer, A. Schumacher. Bubble method for topology and shape optimization of structures, *Structural Optimization*, **8**, 42-51 (1994).

[7] S. Garreau, P. Guillaume, M. Masmoudi. The topological asymptotic for PDE systems: the elasticity case, *SIAM J. Control Optim.*, **39**(6), 1756-1778 (2001).

[8] F. de Gournay. Velocity extension for the level-set method and multiple eigenvalues in shape optimization. SIAM J. on Control and Optim. to appear.

[9] F. Murat, S. Simon. Etudes de problèmes d'optimal design. *Lecture Notes in Computer Science 41*, 54-62, Springer Verlag, Berlin (1976).

[10] S. Osher, J.A. Sethian. Front propagating with curvature dependent speed: algorithms based on Hamilton-Jacobi formulations, *J. Comp. Phys.*, **78**, 12-49 (1988).

[11] J.A. Sethian. *Level set Methods and fast marching methods: evolving interfaces in computational geometry, fluid mechanics, computer vision and materials science*, Cambridge University Press (1999).

[12] J. Simon. Differentiation with respect to the domain in boundary value problems, *Num. Funct. Anal. Optimz.*, **2**, 649-687 (1980).

[13] J. Sokołowski, A. Żochowski. Topological derivatives of shape functionals for elasticity systems. *Mech. Structures Mach.*, **29**, no. 3, 331-349 (2001).

3-D electromagnetics, asymptotic models and MUSIC-type imaging of a collection of small scatterers

Habib Ammari[1] *Ekaterina Iakovleva*[2] *Dominique Lesselier*[3]
Gaële Perrusson[4]

3.1 Introduction

We consider a collection of small ellipsoidal electromagnetic inclusions buried within a homogeneous medium, with arbitrary contrasts of permittivity, conductivity and permeability vis-à-vis this embedding medium. We assume that there exists a finite number m of electromagnetic inclusions, each of the form $z_j + \alpha B_j$, where the domains B_j are ellipsoids containing the origin. The points $z_j \in \mathbb{R}^3$, $j = 1, \ldots, m$, which determine the location of the inclusions, are assumed to satisfy the following: $|z_j - z_l| \geq d_0 > 0$ for all $j \neq l$. The value of α, the common order of magnitude of the diameters of the inclusions, is taken as a small fraction of the wavelength of the wavefield at the operation frequency (time-harmonic regime), which enables us to speak of small inclusions.

The collection is illuminated by an planar array (parallel to the xOy plane) of N vertical electric and/or magnetic dipoles (parallel to the z axis), located at some, not necessary large distance from it, see Fig. 3.1. (A general configuration is considered in [3].) The resulting electric and/or magnetic field is collected by the same array as the transmitter one. This procedure yields the multistatic data response (MSR) matrix that is characteristic of the collection of inclusions for given sets (*e.g.*, arrays) of transmitters and receivers at the (single) frequency of operation.

Extending our previous works in two-dimensional scalar scattering situations [1, 2] to full three-dimensional vector electromagnetics, we show how the eigenvalue structure of the multistatic data response matrix can be employed within the framework of the MUSIC method in order to retrieve either dielectric inclusions, or magnetic inclusions, or combinations thereof, with the limiting perfectly electric conductor (PEC) or perfectly magnetic conductor (PMC) encompassed as well.

In practice one is carrying out two steps: first, the calculation of singular values (and the corresponding eigenvectors), the number of nonzero ones depending upon the number and the electromagnetic nature of the inclusions and upon the transmitters and/or receivers' geometrical arrangement and polarization; second, the orthogonal projection of a properly built vector

[1] ammari@cmap.polytechnique.fr
[2] iakov@cmap.polytechnique.fr
[3] lesselier@lss.supelec.fr
[4] perrusson@lss.supelec.fr

propagator onto the null space of the MSR matrix, coincidence with an inclusion being then associated to a peak of the inverse norm of the projection, the makeup of the indicator being itself function of the nature of the inclusions.

In the case of a single triaxial ellipsoidal inclusion with arbitrary semi-axes and location with respect to the transmitter and receiver arrays, the single vectors and values are exhibited in closed form. Notice that this also enables us to retrieve as a particular case the results described earlier by Chambers and Berryman [9] for a lossless dielectric or PEC sphere with symmetric position with respect to a common transmitter/receiver array.

Let us emphasize here that our MUSIC-type method makes use of asymptotic expansions of the scattered electric and/or magnetic fields. Starting from application of Green's theorems to Maxwell's equations satisfied by the electromagnetic fields, we formally derive asymptotic formulations of the scattered electric and/or magnetic fields as series expansions in terms of the average diameter of the inclusions, here limiting ourselves for simplicity to the leading-order terms. Such formulations involve the polarization tensors associated to the inclusions. We refer to the closely related works [4, 6, 7, 8]. As for the use of duality it easily yields the magnetic counterpart of an electric case and vice-versa.

3.2 The MultiStatic data Response (MSR) matrix

Let μ_0 and ε_0 denote the magnetic permeability and the electric permittivity of the free space; we shall assume that μ_0, $\mathrm{Im}\, m(\varepsilon_0)$, and $\mathrm{Re}\, e(\varepsilon_0)$ are positive constants. Let $k = \omega\sqrt{\varepsilon_0\mu_0} > 0$ be the wavenumber, where $\omega > 0$ is a given frequency. Positive real and imaginary parts are chosen for the square root.

The incident electric field $E_0^{(n)}$ in a homogeneous medium due to a point-like current density at the position r_n and directed in the $\hat{e}_z$ direction, $J_0^{(n)}(r) = \delta(r - r_n)\hat{e}_z Il_n$, is given by

$$E_0^{(n)}(r) = i\omega\mu_0\, G(r, r_n) \cdot \hat{e}_z\, Il_n, \tag{3.1}$$

where the constant Il_n is the current moment and

$$G(r, r_n) = \left[I + \frac{\nabla\,\nabla}{k^2} \right] \frac{e^{ik|r-r_n|}}{4\pi|r - r_n|}$$

is the dyadic Green's function of the background medium. The magnetic field is given by

$$H_0^{(n)}(r) = \nabla\times G(r, r_n) \cdot \hat{e}_z\, Il_n. \tag{3.2}$$

The incident field $E_0^{(n)}$ interacts with the inclusions and generates a total electric field $E_\alpha^{(n)}$ which satisfies the Lippman-Schwinger equation

$$E_\alpha^{(n)}(r_p) - E_0^{(n)}(r_p) = \sum_{j=1}^{m} \int\limits_{z_j+\alpha B_j} dr' \Big[- i\omega\, (\mu_j - \mu_0)\, \nabla'\times G(r_p, r') \cdot H_\alpha^{(n)}(r') \\ + \omega^2\mu_0\, (\varepsilon_j - \varepsilon_0)\, G(r_p, r') \cdot E_\alpha^{(n)}(r') \Big], \tag{3.3}$$

where the constants μ_j and ε_j denote the permeability and the complex permittivity of the jth inclusion, $z_j + \alpha B_j$, and r_p is the location of the pth receiver.

For ellipsoids much smaller than a wavelength ($\alpha k \ll 1$) we can show that

$$E_\alpha^{(n)}(r_p) - E_0^{(n)}(r_p) = \alpha^3 \sum_{j=1}^{m} \Big[-i\omega\mu_0 \, \nabla' \times G(r_p, z_j) \cdot M_j^\mu \, H_0^{(n)}(z_j) + k^2 G(r_p, z_j) \cdot M_j^\varepsilon \, E_0^{(n)}(z_j) \Big] + O(\alpha^4), \tag{3.4}$$

where $M_j^q = M^q(B_j)$ is a polarization tensor which, for inclusion B_j, reads in the ellipsoidal co-ordinate system attached to it as

$$M_j^q = \left(\frac{q_j}{q_0} - 1 \right) \begin{bmatrix} m_{j1} & 0 & 0 \\ 0 & m_{j2} & 0 \\ 0 & 0 & m_{j3} \end{bmatrix} |B_j|,$$

where the coefficients $m_{jl}, l = 1, 2, 3$, are equal to $q_0/(q_0 + L_l(q_j - q_0))$, the L_l being the well-known depolarization factors of the ellipsoid proportional to harmonic elliptic integrals of degree 1. See [5, 10, 13]. Here $\{q\}$ denote either the set $\{\mu\}$ or $\{\varepsilon\}$.

The voltages induced on the pth receiving element can be expressed as

$$V_p = \hat{e}_z \cdot \left(E_\alpha^{(n)}(r_p) - E_0^{(n)}(r_p) \right),$$

where the perturbation $E_\alpha^{(n)}(r_p) - E_0^{(n)}(r_p)$ is given by (3.4), in which we have neglected the asymptotic term of order α^4.

In the general case, if all transmitters are simultaneously activated, the raw data measured at the receivers at the fixed frequency ω are given by

$$V = A\, J,$$

where $V = [V_1 \dots V_N]^T$ is a N dimensional linear array of voltages; $J = [Il_1 \dots Il_N]^T$ is the N dimensional column vector of applied source excitations and A is the $N \times N$ data matrix called the multistatic data response (MSR) matrix.

For any point $z \in \mathbb{R}^3 \setminus \{r_1, \dots, r_N\}$, introduce the matrices $g_z^\varepsilon, g_z^\mu \in \mathbb{C}^{N\times 3}$

$$\begin{aligned} g_z^\varepsilon &= \left(G(z, r_1) \cdot \hat{e}_z \dots G(z, r_N) \cdot \hat{e}_z \right)^T, \\ g_z^\mu &= \left(\nabla \times G(z, r_1) \cdot \hat{e}_z \dots \nabla \times G(z, r_N) \cdot \hat{e}_z \right)^T. \end{aligned}$$

We consider separately the following three cases:

case 1: $\mu_j = \mu_0$ for all $j = 1, \dots, m$; $g_{z_j} = g_{z_j}^\varepsilon$ and $M_j = i\omega\mu_0 \, k^2 \, M_j^\varepsilon$.

case 2: $\varepsilon_j = \varepsilon_0$ for all $j = 1, \dots, m$; $g_{z_j} = g_{z_j}^\mu$ and $M_j = i\omega\mu_0 \, M_j^\mu$.

case 3: $\mu_j \neq \mu_0$ and $\varepsilon_j \neq \varepsilon_0$ at least for one $j \in \{1, \dots, m\}$; $g_{z_j} = [g_{z_j}^\mu \;\; g_{z_j}^\varepsilon]$ and $M_j = i\omega\mu_0 \, \mathrm{diag}(M_j^\mu, k^2 M_j^\varepsilon)$.

Then the MSR matrix A decomposes as

$$A = \sum_{j=1}^{m} g_{z_j} \, M_j \, g_{z_j}^T.$$

Now our goal is to estimate the location z_j of each inclusion.

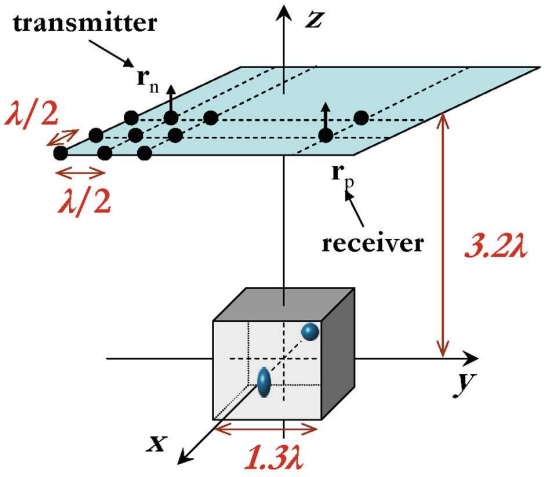

Figure 3.1: *Sketch of the configuration under numerical study.*

3.3 The MUSIC-type algorithm

Next is a MUSIC characterization of the locations of the electromagnetic inclusions [12, 3].

Proposition 3.1 *Let $a \in \mathbb{R}^d \setminus \{0\}$ be such that $g_z \cdot a \neq 0$, for any point $z \in \mathbb{R}^3 \setminus \{r_1, \ldots, r_N\}$. Then*

$$g_z \cdot a \in \mathcal{R}(AA^*) \quad \textit{iff} \quad z \in \{z_1, \ldots, z_m\}.$$

The dimension of the vector a is equal to 3 (cases 1 and 2) and 6 (case 3).

Moreover, it can be shown, that $r = \text{rank}(g_z) = 3$ in case 1; $r = 2$ in case 2 and $r = 5$ in case 3.

Let the SVD of the matrix A be defined by $A = U\Sigma W^*$. From Proposition 3.1, A has rank mr. Then the first mr columns of U provide an orthonormal left basis for the image space of A, denoted by U_S, and the rest of the matrix U provides the basis for the left null space of A, denoted by U_N. Then the orthogonal projection onto the left null space of A are given by $P = U_N U_N^*$. A test point z coincides with one of the positions z_j if and only if $P(g_z \cdot a) = 0$. Thus we can form an image of $z_j, j = 1, \ldots, m$, by plotting, at each point z, the quantity

$$F(z) = \frac{1}{||P(g_z \cdot a)||}. \tag{3.5}$$

The resulting image does not depend on the shape of the inclusions.

3.4 Numerical example of MUSIC reconstructions

The configuration of interest is schematized in Fig. 3.1. One is considering two coincident transmitter and receiver arrays centered within the plane $z = z_a = 5$ and covering a square area of side 10, both consisting of $N = 13^2$ vertical electric dipoles radiating or receiving with unit amplitudes Il and operated at circular frequency $\omega = 4$ —the corresponding wavelength in the embedding free space, with as usual unit permittivity and permeability value ($\varepsilon_0 = \mu_0 = 1$), is $\lambda = \pi/2$. Two identical dielectric prolate spheroidal inclusions $z_1 + \alpha B_1$ and $z_2 + \alpha B_2$ with size parameter $\alpha = 0.1$ and orthogonal orientations (the longest semi-axis of B_1 is orientated along

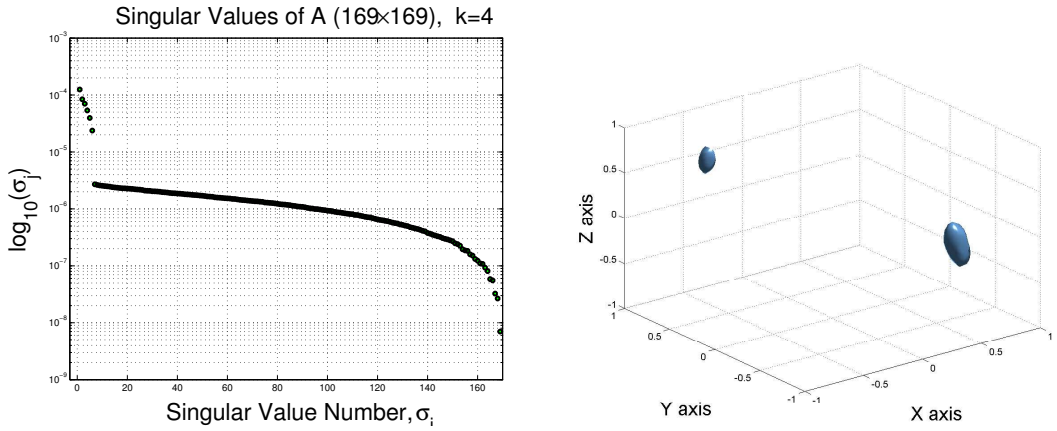

Figure 3.2: *(Dielectric contrasts only): distribution of the singular values of A for 13^2 singly-polarized dipolar transmitters and receivers in the case of noisy data with 20dB signal-to-noise ratio (left); corresponding 3D plots of $F(z)$ (right).*

z, the longest one of B_2 along x) are to be retrieved within a cubical box $\Omega = [-1, 1]^3 \subset \mathbb{R}^2$ assumed situated below the arrays. The points z_1 and z_2 have the coordinates $(.6, -.6, -.1)$ and $(-.6, .6, .7)$ respectively. The domains B_1 and B_2 are characterized by shape equations $x^2 + y^2 + (z/3)^2 = 1$ and $(x/3)^2 + y^2 + z^2 = 1$. Their dielectric permittivities are set to $\varepsilon_1 = 5$, $\varepsilon_2 = 2$. (In this purely dielectric cases, the permeabilities are set to 1.)

In terms of the probing wavelength the array step size is about $\lambda/2$, *i.e.*, the traditional half-a-wave-length sampling step. So the sought inclusions lie in the near field of the array, strongly aspect-limited data (with view angles of 45 degrees or less) being available, whilst one is facing the severe hypothesis of single polarization electric field data, good amount of noise being added to them also.

Within the above setting, the retrieval involves the calculation of the SVD of the MSR matrix $A \in \mathbb{C}^{169\times 169}$. Then, for each discrete location $z \in \Omega$ (the sampling step is henceforth chosen as $h = 0.06$), the identifier of interest is given by (3.5) with $a = (1, 1, 1) \in \mathbb{R}^3$, which is calculated within Ω. The plot of $z \to F(z)$ illustrates the result achieved. Other accompanying results displayed consist of the singular values of the MSR matrix A, shown using a standard log scale.

Bibliography

[1] H. Ammari, E. Iakovleva, and D. Lesselier. *A MUSIC algorithm for locating small inclusions buried in a half-space from the scattering amplitude at a fixed frequency.* Multiscale Modeling Simulation, 3 (2005), pp. 597–628.

[2] H. Ammari, E. Iakovleva, and D. Lesselier. *Two numerical methods for recovering small inclusions from the scattering amplitude at a fixed frequency.* SIAM J. Sci. Comput., 27 (2005), pp. 130–158.

[3] H. Ammari, E. Iakovleva, D. Lesselier and G Perrusson. *MUSIC-type electromagnetic imaging of a collection of small three-dimensional bounded inclusions.* submitted to SIAM J. Sci. Comput., Sept. 2005.

[4] H. Ammari and H. Kang. *Reconstruction of Small Inhomogeneities from Boundary Measurements*. Lecture Notes in Mathematics, Volume 1846, Springer-Verlag, Berlin, 2004.

[5] H. Ammari and H. Kang. *Polarization and Moment Tensors with Applications to Inverse Problems and Effective Medium Theory*. book, to appear.

[6] H. Ammari and H. Kang. *Boundary layer techniques for solving the Helmholtz equation in the presence of small inhomogeneities.* J. Math. Anal. Appl., 296 (2004), pp. 190–208.

[7] H. Ammari and A. Khelifi. *Electromagnetic scattering by small dielectric inhomogeneities*. J. Math. Pures Appl., 82 (2003), pp. 749–842.

[8] H. Ammari, M. Vogelius, and D. Volkov. *Asymptotic formulas for perturbations in the electromagnetic fields due to the presence of imperfections of small diameter* II. *The full Maxwell equations*. J. Math. Pures Appl. (9), 80 (2001), pp. 769–814.

[9] D.H. Chambers and J.G. Berryman. *Analysis of the time-reversal operator for a small spherical scatterer in an electromagnetic field*. IEEE Trans. Antennas Propagat., 52 (2004), pp. 1729–1738.

[10] G. Dassios and R.E. Kleinman. *Low Frequency Scattering*. Oxford Science Publications, The Clarendon Press, Oxford University Press, New York, 2000.

[11] A.J. Devaney. *Time reversal imaging of obscured targets from multistatic data*. IEEE Trans. Antennas Propagat., 523 (2005), pp. 1600–1610.

[12] A. Kirsch. *The MUSIC algorithm and the factorisation method in inverse scattering theory for inhomogeneous media*. Inverse Problems, 18 (2002), pp. 1025–1040.

[13] R.E. Kleinman and T.B.A. Senior. *Rayleigh scattering in Low and High Frequency Asymptotics*. pp. 1–70, edited by V.K. Varadan and V.V. Varadan, North-Holland, 1986.

[14] G. Pólya and G. Szegö. *Isoperimetric Inequalities in Mathematical Physics*. Annals of Mathematical Studies Number 27, Princeton University Press, Princeton, NJ, 1951.

Sensitivity analysis of spectral properties of high contrast band-gap materials

Habib Ammari[1] *Hyeonbae Kang*[2] *Sofiane Soussi* *Habib Zribi*

4.1 Problem statement

We investigate the band-gap structure of the frequency spectrum for waves in a high-contrast, two-component periodic medium. We consider two-dimensional photonic crystals consisting of a background medium which is perforated by an array of holes periodic along each of the two orthogonal coordinate axes. We perform a high-order sensitivity analysis with respect to the index ratio. Our method, which is based on a boundary integral perturbation theory, gives a new tool for the optimal design problem in photonic crystals.

The photonic crystal we consider consists of a homogeneous background medium of constant index k which is perforated by an array of arbitrary-shaped holes periodic along each of the two orthogonal coordinate axes in $\mathbb{R}^2$. These holes are assumed to be of index 1, see Figure 4.1. We assume that the structure has unit periodicity and define the periodic domain $Y = \mathbb{R}^2/\mathbb{Z}^2$, which can be identified with the unit square $[0,1]^2$.

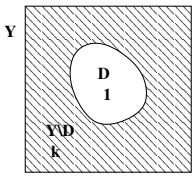

Figure 4.1: *Unit cell of the photonic crystal*

Suppose $\alpha \neq 0$. We seek for eigenfunctions u of

$$\begin{cases} \nabla \cdot (1 + (k-1)\chi_{Y\setminus\overline{D}})\nabla u + \omega^2 u = 0 & \text{in } Y, \\ e^{-i\alpha\cdot x} u \quad \text{is periodic,} \end{cases} \tag{4.1}$$

[1]Centre de Mathématiques Appliquées, CNRS UMR 7641 and Ecole Polytechnique, 91128 Palaiseau Cedex, France (ammari@cmapx.polytechnique.fr, soussi@cmapx.polytechnique.fr, zribi@cmapx.polytechnique.fr).

[2]School of Mathematical Sciences, Seoul National University and RIM, Seoul 151-747, Korea (hkang@math.snu.ac.kr)

where $\chi_{Y\setminus\overline{D}}$ is the indicator function of $Y \setminus \overline{D}$. The problem (4.1) can be rewritten as

$$\begin{cases} k\Delta u + \omega^2 u = 0 & \text{in } Y \setminus \overline{D}, \\ \Delta u + \omega^2 u = 0 & \text{in } D, \\ u|_+ = u|_- & \text{on } \partial D, \\ k\dfrac{\partial u}{\partial \nu}\Big|_+ = \dfrac{\partial u}{\partial \nu}\Big|_- & \text{on } \partial D, \\ e^{-i\alpha\cdot x}u \text{ is periodic.} \end{cases} \tag{4.2}$$

For each quasi-momentum variable α and k, let $\sigma_\alpha(D,k)$ be the (discrete) spectrum of (4.1). Then the spectral band of the photonic crystal is given by

$$\bigcup_{\alpha\in[0,2\pi]^2} \sigma_\alpha(D,k).$$

We shall investigate the behavior of $\sigma_\alpha(D,k)$ when $k \to \infty$.

4.2 Sensitivity analysis with respect to the index ratio

In this section we give the main result concerning the asymptotic expansion of the eigenvalues ω^2 with respect to the index ratio k.

Using an integral representation formula for the solutions to problem 4.1, we obtain a new way of looking at the spectrum of 4.1 by examining the characteristic values of a certain operator-valued function $\mathcal{A}_k^\alpha$. Expanding this operator-valued function in terms of k:

$$\mathcal{A}_k^\alpha(\omega) = \begin{cases} \mathcal{A}_0^\alpha(\omega) + \displaystyle\sum_{l=1}^{+\infty} \frac{1}{k^l}\mathcal{A}_l^\alpha(\omega) & \text{if } \alpha \neq 0, \\ \dfrac{k}{\omega^2}\begin{pmatrix} 0 & -\int_{\partial D}\cdot \\ 0 & 0 \end{pmatrix} + \mathcal{A}_0^0(\omega) + \displaystyle\sum_{l=1}^{+\infty} \frac{1}{k^l}\mathcal{A}_l^0(\omega) & \text{if } \alpha = 0, \end{cases}$$

we calculate asymptotic expressions of its characteristic values with the help of the generalized Rouché's theorem [1].

The following theorem holds.

Theorem 4.1 *Suppose $\alpha \neq 0$. Let ω_0^2 be a simple eigenvalue of the Dirichlet-Laplacian in D. Then, there exists a unique eigenvalue $(\omega_k^\alpha)^2$ of problem (4.1), such that (ω_k^α) converges to ω_0 as $k \to +\infty$. Moreover, we have the following complete asymptotic expansion for the eigenvalue perturbations:*

$$\omega_k^\alpha - \omega_0 = \frac{1}{2i\pi}\sum_{p=1}^{+\infty}\frac{1}{p}\sum_{n=p}^{+\infty}\frac{1}{k^n}\operatorname{tr}\int_{\partial V}(\mathcal{A}_0^\alpha)^{-p}(\omega)B_{n,p}^\alpha(\omega)d\omega, \tag{4.3}$$

where V is a small complex neighborhood of ω_0 and

$$B_{n,p}^\alpha(\omega) = (-1)^p \sum_{\substack{n_1+\ldots+n_p=n \\ n_i\geq 1}} \mathcal{A}_{n_1}^\alpha(\omega)\ldots\mathcal{A}_{n_p}^\alpha(\omega). \tag{4.4}$$

For the case $\alpha = 0$, we have the following theorem.

Theorem 4.2 *Suppose $\alpha = 0$. Let ω_0^2 be a simple eigenvalue of the Dirichlet-Laplacian in D. Then, there exists a unique eigenvalue $(\omega_k^0)^2$ of (4.1), such that ω_k^0 converges to $\widetilde{\omega}_0$ (defined from ω_0) as $k \to +\infty$. Moreover, the following complete asymptotic expansion holds:*

$$\omega_k^0 - \widetilde{\omega}_0 = \frac{1}{2i\pi} \sum_{p=1}^{+\infty} \frac{1}{p} \sum_{n=p}^{+\infty} \frac{1}{k^n} \operatorname{tr} \int_{\partial V} (\mathcal{A}_0^0)^{-p}(\omega) B_{n,p}^0(\omega) d\omega, \tag{4.5}$$

where V is a small complex neighborhood of $\widetilde{\omega}_0$ and $B_{n,p}^0(\omega)$ is given by (4.4) with $\alpha = 0$.

Here, $\widetilde{\omega}_0$ is given in terms of the eigenvalue ω_0 and of its associated eigenvector u_0 through the relation:

$$\widetilde{\omega}_0 - \omega_0 = -\frac{\left(\int_{\partial D} \frac{\partial u_0}{\partial \nu} d\sigma_x \right)^2}{2\omega_0^3 |Y \setminus \overline{D}| \int_D |u_0^2| dx}. \tag{4.6}$$

Note that the zero-order term $\tilde{\omega}_0$ has already been given by a completely different argument by R. Hempel and K. Lienau [3].

The following corollary which gives us explicitly the first-order term of the expansion.

Corollary 4.1 *Let ω_0^2 be a simple eigenvalue of the Dirichlet-Laplacian in D and let u_0 be its associated eigenvector. Let v_0 be the unique α-quasi-periodic solution to the problem:*

$$\begin{cases} \Delta v_0 = 0 & \text{in } Y \setminus \overline{D}, \\ \dfrac{\partial v_0}{\partial \nu}\Big|_+ = \dfrac{\partial u_0}{\partial \nu}\Big|_- & \text{on } \partial D, \end{cases}$$

Then, we have:

$$\omega_k^\alpha - \omega_0 = -\frac{1}{k} \frac{\int_{Y \setminus D} |\nabla v_0|^2 dx}{2\omega_0 \int_D |u_0|^2 dx} + O(k^{-2}) \quad \text{as } k \to +\infty.$$

A similar result holds for the periodic case ($\alpha = 0$).

Bibliography

[1] I.T.S. Gohberg and E.I. Sigal. *Operator extension of the logarithmic residue theorem and Rouché's theorem.* Mat. Sb. (N.S.) 84 (1971), 607–642.

[2] H. Ammari, H. Kang, S. Soussi, and H. Zribi. *Layer Potential Techniques in Spectral Analysis. Part II: Sensitivity Analysis of Spectral Properties of High Contrast Band-Gap Materials* Preprint 2005.

[3] R. Hempel and K. Lienau. *Spectral properties of periodic media in the large coupling limit.* Commun. Part. Diff. Equat., 25 (2000), 1445–1470.

Image restoration and classification by topological asymptotic expansion

Didier Auroux[1] *Lamia Jaafar Belaïd*[2] *Mohamed Masmoudi*[3]

Introduction

The aim of this paper is to propose a new method for both the grey-level image restoration and classification problems. For each of these two problems, we first present the classical variational approach and then we introduce an application of the topological asymptotic analysis.

5.1 Image restoration using the topological gradient theory

Nonlinear variational approach

Let Ω be an open bounded domain of $\mathbb{R}^2$ and $v \in L^2(\Omega)$ the noised image. The idea of the nonlinear variational approach is to minimize the following cost function

$$J(u) = \frac{1}{2}\int_\Omega |v-u|^2 \, dx + \int_\Omega c \, \psi(|\nabla u|) \, dx. \tag{5.1}$$

To find a minimum of J is equivalent to solve the associated Euler-Lagrange equation:

$$\left\{ \begin{array}{rl} -\operatorname{div}\left(c \, \psi'(|\nabla u|)\frac{\nabla u}{|\nabla u|}\right) + u = v & \text{in } \Omega, \\ \partial_n u = 0 & \text{in } \Gamma = \partial\Omega. \end{array} \right. \tag{5.2}$$

Let us remark that if $\psi(|\nabla u|) = \frac{1}{2}|\nabla u|^2$, we obtain the linear variational approach:

$$\left\{ \begin{array}{rl} -\operatorname{div}(c\nabla u) + u = v & \text{in } \Omega, \\ \partial_n u = 0 & \text{in } \Gamma = \partial\Omega. \end{array} \right. \tag{5.3}$$

One simply has to solve equation (5.2) and its solution u is the restored image.

Topological gradient approach

For a small $\rho \geq 0$, let $\Omega_\rho = \Omega \backslash \sigma_\rho$ the perturbed domain by the insertion of a crack $\sigma_\rho = x_0 + \rho\sigma(n)$, where $x_0 \in \Omega$, $\sigma(n)$ is a straight crack, and n a unit vector normal to the crack.

[1] auroux@mip.ups-tlse.fr
[2] lamia.belaid@esstt.rnu.tn
[3] masmoudi@mip.ups-tlse.fr

Consider the following partial differential equation

$$\begin{cases} -\operatorname{div}(c\nabla u) + u = u_0 & \text{in } \Omega, \\ \partial_n u = 0 & \text{on } \Gamma = \partial\Omega, \end{cases} \tag{5.4}$$

where we have the following partition $\Omega = \Omega_\rho \cup \sigma_\rho$ and $c = c_0$ in Ω_ρ and $c = \varepsilon$ in σ_ρ. Theoretically, c should be equal to 0 in the crack, but numerically, c will then be set to a small value ε.

We consider the following cost function

$$j(\rho) = J(u_\rho) = \int_{\Omega_\rho} \|\nabla u_\rho\|^2 \; dx, \tag{5.5}$$

where u_ρ is the solution of the latest equation.

The cost function J, and the bilinear and linear forms associated to equation (5.4) satisfy the hypothesis of the topological asymptotic theory (see [4, 1] for more details).

In the present case, we denote by v the adjoint state, solution of the adjoint problem

$$\begin{cases} -\operatorname{div}(c\nabla v) + v = -\partial_u J(u) & \text{in} \quad \Omega, \\ \partial_n v = 0 & \text{on} \quad \partial\Omega, \end{cases} \tag{5.6}$$

and we obtain the following topological asymptotic expansion [3, 1]

$$j(\rho) - j(0) = \rho^2 G(x_0, n) + \circ(\rho^2), \tag{5.7}$$

with

$$G(x_0, n) = -\pi(\nabla u(x_0).n)(\nabla v(x_0).n) - \pi|\nabla u(x_0).n|^2. \tag{5.8}$$

Then the topological gradient could be written as

$$G(x, n) = \langle M(x)n, n\rangle, \tag{5.9}$$

where $M(x)$ is the symmetric matrix defined by

$$M(x) = -\pi \frac{\nabla u(x)\nabla v(x)^T + \nabla v(x)\nabla u(x)^T}{2} - \pi \nabla u(x)\nabla u(x)^T. \tag{5.10}$$

For a given x, $G(x, n)$ takes its minimal value when n is the eigenvector associated to the lowest eigenvalue $\lambda_{\min}$ of M. This value will be considered as the topological gradient associated to the optimal orientation of the crack $\sigma_\rho(n)$.

The resolution algorithm is the following

- Initialization : $c = c_0$.
- Calculation of u_0 and v_0 : solutions of the direct (5.2) and adjoint (5.6) problems.
- Computation of the 2×2 matrix M and its lowest eigenvalue $\lambda_{\min}$ at each point of the domain.
- Set

$$c_1 = \begin{cases} \varepsilon \text{ if } x \in \Omega \text{ such that } \lambda_{\min} < \alpha < 0, \quad \varepsilon > 0 \\ c_0 \text{ elsewhere.} \end{cases} \tag{5.11}$$

- Calculation of u_1 solution to problem (5.2) with $c = c_1$.

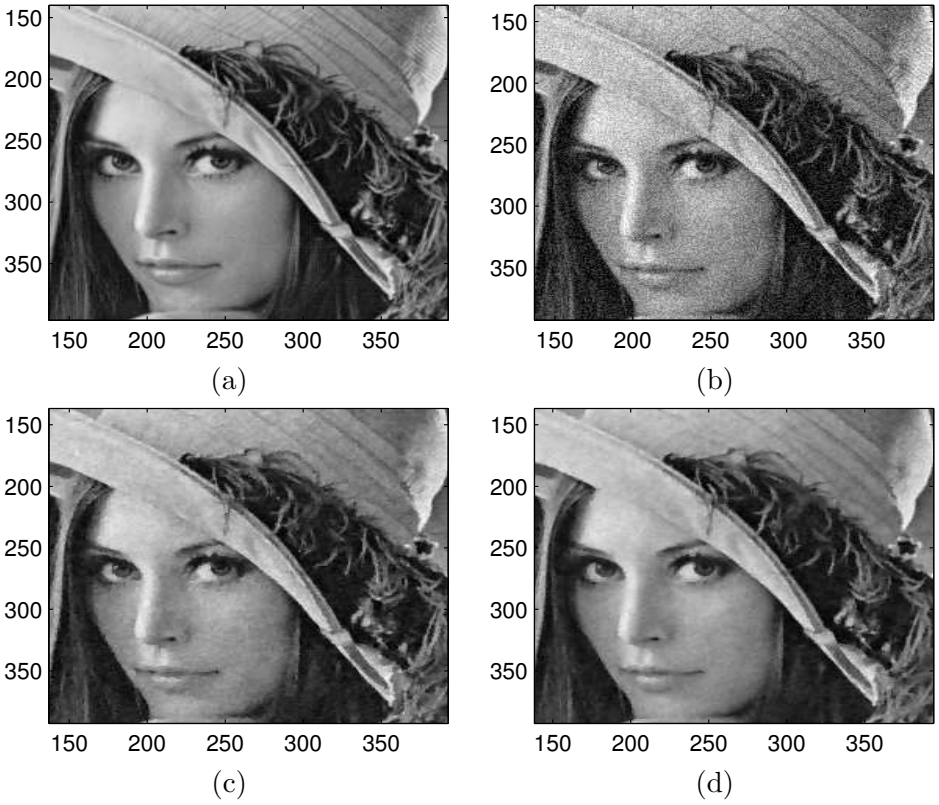

Figure 5.1: *Original image (a), noised image (b), restored image by nonlinear diffusion (c) and restored image by topological gradient (d).*

One can see [3] for more details. This algorithm finds the contours of the image, and smooths the image everywhere else. The idea is then to simply apply the closest class algorithm to the smothered image.

As the first resolution of the direct problem is performed with a constant value of c, it is possible to greatly speed up the computation by using the DCT (Discrete Cosine Transform) method. Then, for the second resolution of the direct problem with a non constant c, we use as preconditioner the DCT in the preconditioned conjugate gradient algorithm. See [3] for more details.

Figure 5.1 shows the original and noised images, and the restored images by nonlinear diffusion and by topological gradient. The edges reconstruction is very good. Figure 5.2 shows the computational cost versus the image size, and the DCT method allows a nearly linear complexity.

5.2 Regularized Image classification

Topological gradient applied to the classical approach

Let u_0 be the original image defined on an open set Ω of $\mathbb{R}^2$. We want to classify the image u_0 using n predefined classes $C_i, 1 \leq i \leq n$, and we choose the grey level intensity as a classifier. The goal of image classification is then to find a partition of Ω in subsets $\{\Omega_i\}_{i=1,..,n}$, such that u_0 is close to C_i in Ω_i. The classified image u will then be defined by

$$u(x) = C_i \quad \forall x \in \Omega_i, \tag{5.12}$$

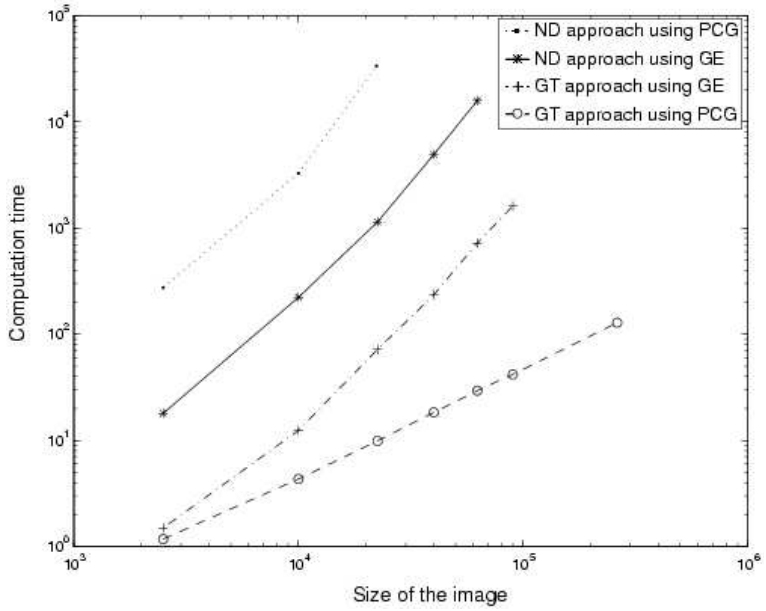

Figure 5.2: *Computational cost versus the image size for nonlinear diffusion (ND) and topological gradient (GT), using a Gauss elimination method (GE) or a preconditioned (by a discrete cosine transform) conjugate gradient method (PCG).*

where $\{\Omega_i\}_{i=1,..,n}$ are defined by

$$\Omega_i = \left\{ x \in \Omega; x \text{ belongs to the } i^{th} \text{ class} \right\}. \tag{5.13}$$

In order to obtain a classified image with smoother contours, we consider the following cost function

$$J\left((\Omega_i)_{i=1,..,n}\right) = \sum_{i=1}^{n} \int_{\Omega_i} (u_0(x) - C_i)^2 \, dx + \sum_{i \neq j} |\Gamma_{ij}|, \tag{5.14}$$

measuring the root mean square difference between the original image and the classified image. The second part of J is a regularization term. $|\Gamma_{ij}|, i \neq j$ represents the one-dimensional Hausdorff measure of Γ_{ij} [2].

We have to solve the equation

$$u(x) = C_i \quad \text{in } \omega_{\rho_i}, \tag{5.15}$$

where ω_{ρ_i} $(1 \leq i \leq n-1)$ is the subset of pixels that should be reassigned to the class C_i and $\omega_{\rho_n} = \Omega \backslash (\bigcup_{i=1}^{n-1} \overline{\omega_{\rho_i}})$.

The variation of the cost function upon reassigning the pixel x to the class C_i is

$$\begin{array}{rcl} \delta \tilde{J}_i(x) = & \int_{\omega_{\rho_i}} & (C_n - C_i)(2u_0(x) - C_i - C_n) \, dx \\ & + & \alpha(|\partial(\Omega_i \cup \omega_{\rho_i})| - |\partial \Omega_i|), \end{array} \tag{5.16}$$

and the pixel x is still reassigned to the class which minimizes mostly the cost function.

The algorithm is then the following

- for each $1 \leq i \leq n-1$, compute $g_i(x)$ for each pixel x,

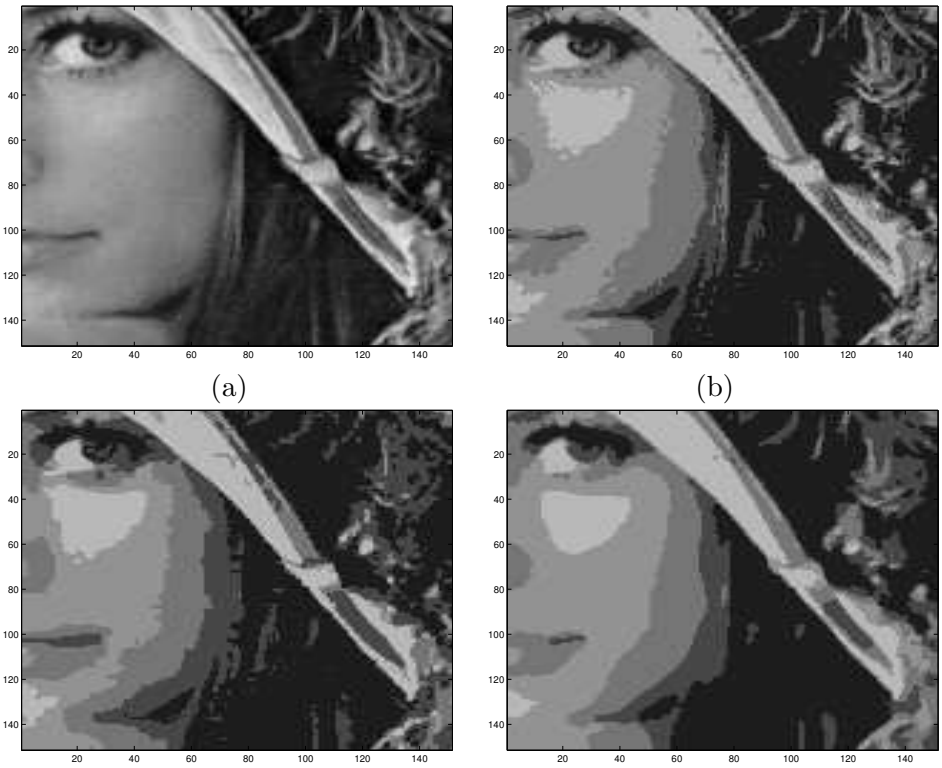

Figure 5.3: *Original image (a) and 5-classes classified images: without regularization (b), with regularization (c), smoothed by topological gradient and then classified (d).*

- for each pixel x, find i_0 so that $g_{i_0}(x) \leq g_i(x)\ \forall i$,
- if $g_{i_0}(x) < 0$ (or $< -\varepsilon$), reassign x to the class C_{i_0}.

Let us remark that (5.16) is not an asymptotic expansion, because the first part of (5.16) is proportional to ρ^2 whereas the second one is proportional to ρ. Hence, if $\rho \to 0$, only the second term subsists. In our problem, ρ will be set so that the crack σ_ρ is one pixel, and then (5.16) is valid for this given value of ρ.

Because of the regularization term, it is important to run again the algorithm with the classified image as initial guess, because some pixels which had positive topological gradients may have negative ones at next iteration. If for example all neighbors of x have been reassigned to class i but not x, which is still assigned to the class C_n, at the next iteration, the regularization term in $\delta\tilde{J}_i(x)$ may be strongly negative, and then x may be reassigned to the class C_i. So, we have to iterate the algorithm until all functional variations $\delta\tilde{J}_i$ are everywhere non negative.

A restoration-based preprocessing method using the topological gradient

We still consider the following equation

$$\left\{\begin{array}{rl} -\operatorname{div}(c\nabla u) + u = u_0 & \text{in } \Omega, \\ \partial_n u = 0 & \text{on } \Gamma = \partial\Omega, \end{array}\right. \tag{5.17}$$

with $c = \dfrac{1}{\varepsilon}$ in Ω_ρ and $c = \varepsilon$ in σ_ρ. σ_ρ still represents the contours of the image. As ε is supposed to be small, if we are on a contour, $c = \varepsilon$ and then u and u_0 are almost the same. But otherwise,

$c = \frac{1}{\varepsilon}$ and then the P.D.E. is nearly equivalent to $\Delta u = 0$, which will provide a really smooth image.

In comparison with the previous section, the topological gradient $g(x)$ and the general algorithm remains unchanged. After smoothing, the image is then classified in the same way as in the previous section.

Figure 5.3 shows the original image and three 5-classes classified images. The first one corresponds to a classification without regularization, and has then unsmooth contours. The second one corresponds to a regularized classification and has smoother contours. The last one has been smoothed by the topological gradient preprocessing method, and then classified. It has clearly much smoother contours.

Conclusion

The topological asymptotic expansion (with a DCT preconditioned conjugate gradient method) gives promising results for both the restoration and classification problems.

Bibliography

[1] Samuel Amstutz, Imen Horchani, and Mohamed Masmoudi. Crack detection by the topological gradient method. *Contr. Cybernetics*, 34(1): 81–101, 2005.

[2] Gilles Aubert and Pierre Kornprobst. *Mathematical problems in image processing.* Appl. Math. Sci., Vol. 147, Springer-Verlag, New York, 2002.

[3] Lamia Jaafar Belaid, Mohamed Jaoua, Mohamed Masmoudi, and Lassaad Siala. Image restoration and edge detection by topological asymptotic expansion. *C. R. Acad. Sci. Ser. I*, 342(5): 313–318, 2006.

[4] Bessem Samet, Samuel Amstutz, and Mohamed Masmoudi. The topological asymptotic for the helmholtz equation. *SIAM J. Control Optim.*, 42(5): 1523–1544, 2003.

An energy approach to solve Cauchy problems

Thouraya Baranger[1] *Stéphane Andrieux*[2] *Amel Ben Abda*[3]

Abstract

An energy approach is introduced in the context of the ill-posed problem of boundary data recovering, which is well known as a Cauchy problem. The problem is converted into an optimization one. Numerical experiments highlight the efficiency of the proposed method as well as its robustness in the model context of Laplace equation, but also for elasticity problems.

6.1 Introduction

We are interested in the problem of data completion, which consists in recovering the data on an inaccessible part of the boundary of a solid using overspecified data on the other part of it. This is an old problem mathematically known as the Cauchy one. This situation may arises in many industrial, engineering or biomedical applications under various forms: identification of boundary conditions on unreachable part of the boundary, expansion of measured surface fields inside a body from partial boundary measurements. But also it can be the first step in general parameters identification problems and damage detection where only partial boundary data are under control. Hence, robust and efficient data completion method is an essential and basic tool in structural identification. In this paper we present a method for data completion based on the minimization of an energy-like error functional depending on the lacking data.

6.2 Data Completion

Let us consider the above Cauchy problem (6.1). Assuming the data (Φ, T) are compatible, i.e. that this pair is indeed the trace and normal trace of a unique harmonic function u, extending the data means finding (φ, t) such that:

$$\begin{cases} \nabla \cdot k(x)\nabla u = 0 & \text{in } \Omega \\ u = T,\ k(x)\nabla u.n = \Phi & \text{on } \Gamma_c \\ u = t,\ k(x)\nabla u.n = \varphi & \text{on } \Gamma_i \end{cases} \tag{6.1}$$

The question is to recover numerically the pair (φ, t). However, in practical problems data are not expected to be compatible, since data errors may occur from measurement discretization

[1]Thouraya.Baranger@insa-lyon.fr.fr, LDMS UMR CNRS 5006, ISTIL-UCBL, France.
[2]LaMSID, UMR CNRS-EDF 2832, Clamart, France.
[3]LAMSIN-ENIT, Tunisie.

and modelling errors. The ill-posedness in Hadamard's sense arises –dramatically– when one tries to approximate a given data (Φ, T): it is possible to approach it as closely as desired on Γ_c by traces of a single harmonic function, the "surprise" being a hectic behavior of this function on the remaining part of the boundary, see for instance [5]. The approach in the error functional method developed here follows two steps. First, we consider, for a given pair (η, τ), the two following mixed well-posed problems:

$$\begin{cases} \nabla \cdot k(x)\nabla u_1 = 0 & \text{in } \Omega \\ u_1 = T & \text{on } \Gamma_c \\ k(x)\nabla u_1.n = \eta & \text{on } \Gamma_i \end{cases} \tag{6.2}$$

$$\begin{cases} \nabla \cdot k(x)\nabla u_2 = 0 & \text{in } \Omega \\ u_2 = \tau & \text{on } \Gamma_i \\ k(x)\nabla u_2.n = \Phi & \text{on } \Gamma_c \end{cases} \tag{6.3}$$

The next step is to build an error functional on the pair (η, τ) using a seminorm E. Indeed, u_1 and u_2 are obviously equal only when the pair (η, τ) meets the real data (φ, t) on the boundary Γ_i. We propose then to solve the data completion problem via the following minimization:

$$(\varphi, t) = arg \min_{\eta,\tau} E(\eta, \tau) \tag{6.4}$$

$$E(\eta, \tau) = \int_\Omega (k(x)\nabla u_1 - k(x)\nabla u_2).(\nabla u_1 - \nabla u_2) \tag{6.5}$$

where $\eta \in H^{-1/2}(\Gamma_i)$, $\tau \in H^{1/2}(\Gamma_i)$, u_1 and u_2 being the solution of (6.2) and (6.3). Using the properties of the fields u_1 and u_2, it is straightforward to derive an alternative expression of the E functional:

$$E(\eta, \tau) = \int_{\Gamma_i} (\eta - k(x)\nabla u_2.n)(u_1 - \tau) + \int_{\Gamma_c} (k(x)\nabla u_1.n - \Phi)(T - u_2). \tag{6.6}$$

This expression shows that the error between the two fields u_1 and u_2 can be expressed equivalently by an integral involving only the boundary of the domain Ω. E is convex, quadratic and positive with a minimum equal to zero. It reaches this minimum for $u_1 = u_2 + Cte = u$, where u is the unique solution to our data recovering problem. The last expression of E shows that the energy error can be expressed only with a boundary error term, which can be used for the computation of it. Unlike in least squares methods, the error on the flux is weighted by the error on the temperature. This feature illustrates the more symmetric formulation that can be obtained by error functional based on the energy of the problem: no choice of an adimensionalizing parameter is needed, in opposition to mixed least-square objective functionals where it is essential.

The implementation of this method was carried out using finite element method (FEM). Hence, the derivative of E was carried out by the adjoint state and is preferably established on the basis of the FEM-discretized problem. The advantage of this fully-discrete approach is that the exact gradient of the discrete objective function is obtained; moreover it is easily implementable see [1]. The computations are run under *Matlab Software* environment [12] and also by using *Code-Aster* [10] for the three dimensional elasticity problems.

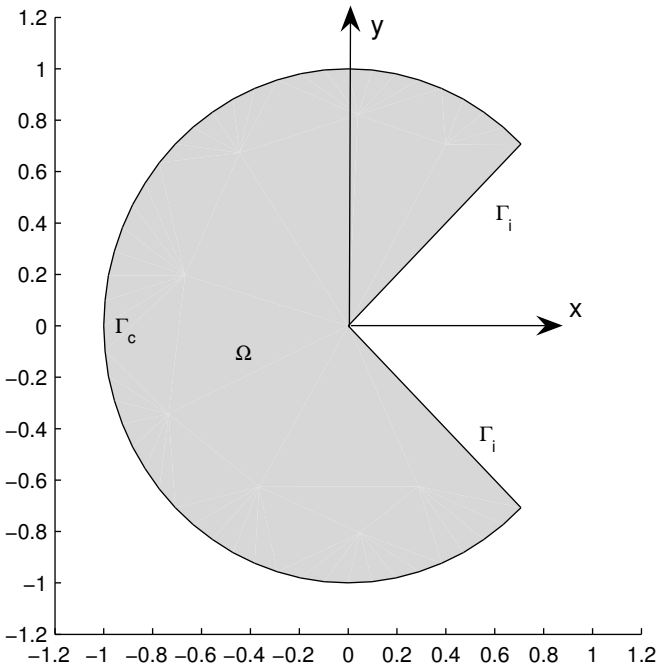

Figure 6.1: *Geometric data*

6.3 Results

The following example has been treated by Cimetière et al. in [8] using a first order inverse method. It is a thermostatics problem defined on the domain shown on the figure 6.1. The overspecied data are available on the circular boundary. These data are obtained from the exact field $u = \frac{y}{(x-0.5)^2+y^2}$. The figure 6.2 and 6.3 show the reconstructed temperature and heat flux as well as the exact ones. The results obtained in this example (13 iterations of the optimization algorithm) illustrate the robustness of the proposed method in so far as the data is singular.

6.4 Conclusion

We proposed in this work a method for data matching based on the minimization of an energy error functional. Our data recovering process has two main features that make it an efficient method. The first feature is undoubtedly the versatility of the present method: even though the results are performed in the 2D-Cauchy-Poisson setting, it can be developed for other operators as well as in 3D-situations. This method is quite general and has wide applications ranging from bioelectrical field (EEG, ECG) to mechanical engineering (cracks, corrosion). The second feature we would like to point out concerns the accuracy of the present method. The peculiar character of the method lies on the treatment of the reconstructed trace and normal trace simultaneously: both of them are well recovered. We tested successfully the matching method in the case of temperature and heat flux recovering, and also elasticity problem. This procedure compares then very favorably with iterative data matching existing method.

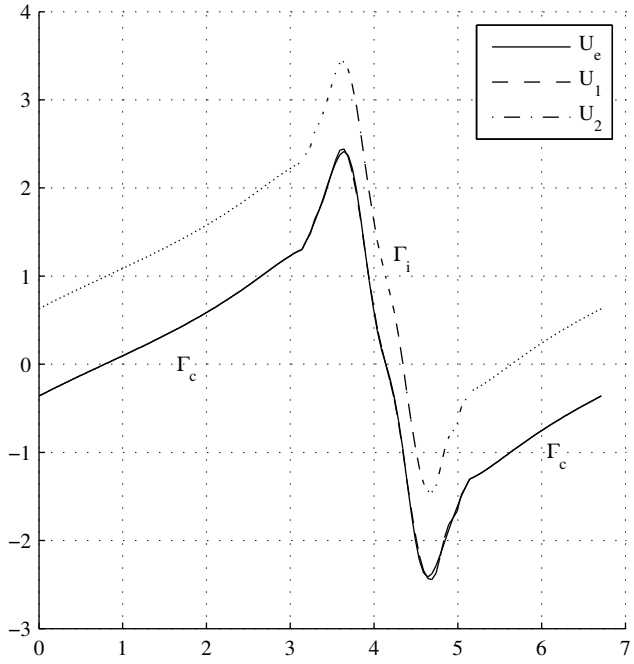

Figure 6.2: *Reconstructed temperature on* Γ_i *from overspecified data generated by* $u = \dfrac{y}{(x-0.5)^2+y^2}$. *This results are performed with finite elements of class* C^o. *The mesh of* Ω *is regular and consists of triangular elements with linear interpolation.*

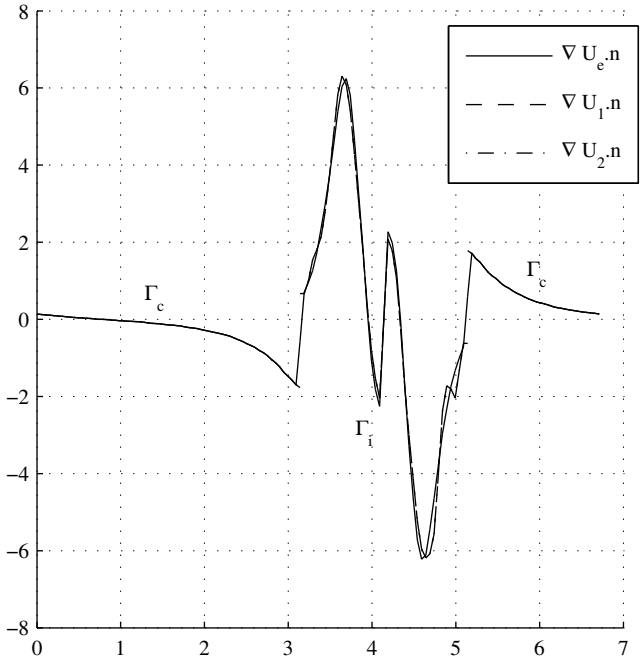

Figure 6.3: *Reconstructed flux on* Γ_i *from overspecified data generated by* $u = \dfrac{y}{(x-0.5)^2+y^2}$. *This results are performed with finite elements of class* C^o. *The mesh of* Ω *is regular and consists of triangular elements with linear interpolation.*

Bibliography

[1] S. Andrieux, T.N. Baranger and A. Ben Abda. 2006, Solving Cauchy problems by minimizing an energy-like functional, *Inverse Problems*, **22**, 115-133 1177-1191.

[2] S. Andrieux, A. Ben Abda and T.N. Baranger. 2005, Data completion via an energy error functional, *C.R. Mecanique* **333**, 171-177.

[3] S. Andrieux, A. Ben Abda. 1992, Fonctionnelles de Kohn-Vogelius et identification de domaines, *Collection de notes internes de la direction des etudes et de recherche*, EDF 92 NI J 0006.

[4] S. Andrieux, A. Ben Abda. 1994, Determination of planar cracks by external measurements via reciprocity gap functionals: Identifiability results and direct location methods, *Inverse Problems in Engineering and Mechanics* Edited by H. D. Bui, M. Tanaka

[5] L. Baratchart and J. Leblond. 1998, Hardy approximation to L^p functions subsets of the circle with $1 \leq p \leq \infty$, *Constructive Approximation*, **40**, 41-56.

[6] A. Ben Abda. 1993, *Sur quelques problèmes inverses géométriques via des équations de conduction elliptiques: Etude théorique et numérique* Ph.D Ecole Nationale d'Inénieurs de Tunis, Tunisia.

[7] M. Bonnet and A. Constaninescu. 2005, Inverse problems in elasticity, *Inverse Problems*, **21**, 1-50.

[8] A. Cimetière, F. Delvare, M. Jaoua and F. Pons. 2001, Solution of the Cauchy problem using iterated Tikhonov regularization, *Inverse Problems*, **17**, 553-570.

[9] A. Cimetière, F. Delvare and F. Pons. 2004, A first order inverse method for the data completion problem, *C.R. Mecanique*, **333**, 123-126.

[10] Code-Aster. EDF-R&D, www.Code-Aster.org

[11] J. Hadamard. 1953, *Lectures on Cauchy's Problem in Linear Partial Differential Equation* Dover New York USA.

[12] Matlab Software. Copyright 1984-2000 The MathWorks, Inc.

[13] L. Rota. 1994, An inverse approach for identification of dynamic constitutive equations, *Inverse Problems in Engineering and Mechanics* Edited by H. D. Bui, M. Tanaka

Controllability of Schrödinger equations

Karine Beauchard[1]

7.1 Introduction

A quantum particle, in a 1D space, is represented by its wave function

$$\begin{array}{rccccc} \psi: & \mathbb{R} & \times & \mathbb{R} & \to & \mathbb{C} \\ & (t & , & q) & \mapsto & \psi(t,q). \end{array}$$

The physical meaning of $|\psi(t,q)|^2 dq$ is the probability of the particle to be in the volume dq surrounding the point q at time t. Thus, at any time t, we have

$$\int_{\mathbb{R}} |\psi(t,q)|^2 dq = 1.$$

When the particle is in a potential $V(q)$, its wave function solves the Schrödinger equation

$$i\hbar \frac{\partial \psi}{\partial t}(t,q) = -\frac{\hbar^2}{2m}\frac{\partial^2 \psi}{\partial q^2}\psi(t,q) + V(q)\psi(t,q).$$

Let us consider a particle in an infinite square potential well

$$V(q) = 0 \text{ when } q \in I := (-1/2, 1/2), V(q) = +\infty \text{ when } q \notin I$$

which moves in $\mathbb{R}$ along time. Up to renormalisation, the dynamic of the wave function in the moving system of reference is given by

$$(\Sigma) \begin{cases} i\dfrac{\partial \psi}{\partial t}(t,q) = -\dfrac{1}{2}\dfrac{\partial^2 \psi}{\partial q^2}(t,q) - \langle u(t), q\rangle \psi(t,q), & q \in (-1/2,1/2), t \in \mathbb{R}_+, \\ \psi(t, \pm 1/2) = 0, \end{cases}$$

where $u := -\ddot{D}$ is the acceleration of the well. The system (Σ) is a control system in which

- the state is the wave function ψ of the particle, which, for every $t \in \mathbb{R}_+$, belongs to the $L^2(I,\mathbb{C})$-unitary sphere $\mathcal{S}$,
- the control is the acceleration $t \mapsto u(t) \in \mathbb{R}$ of the well.

[1]Karine.Beauchard@cmla.ens-cachan.fr

This control system is nonlinear: it is bilinear with respect to the couple (ψ, u).

Section 7.2 presents a local controllability result, around the ground state, for the system (Σ), and a sketch of its proof. The main tools are Coron's return method, moment theory and a Nash-Moser implicit function theorem. Section 7.3 presents a steady-state controllability result for (Σ), got thanks to local controllability results. Finally, section 7.4 proposes controllability results on other PDEs proved with the technique introduced for the study of (Σ).

7.2 Local controllability of (Σ)

7.2.1 Main result of [2]

In [2] one proves the local controllability of the system (Σ) around the ground state for $u \equiv 0$, which is the function

$$\psi_1(t,q) := \varphi_1(q) e^{-i\lambda_1 t}.$$

Here, $\lambda_1 := \pi^2/2$ is the smallest eigenvalue of the operator A defined on

$$D(A) := (H^2 \cap H_0^1)(I, \mathbb{C}), \text{ by } A\varphi := -\frac{1}{2}\frac{d^2\varphi}{dq^2}$$

and $\varphi_1(q) := \sqrt{2}\cos(\pi q)$ is the associated eigenvector. This behaviour was conjectured by Rouchon in [9].

Theorem 7.1 *Let $\phi_0, \phi_1 \in \mathbb{R}$. There exist $T > 0$ and $\eta > 0$ such that, for every ψ_0, ψ_f in $\mathcal{S} \cap D(A^{7/2})$ satisfying*

$$\|\psi_0 - \varphi_1 e^{i\phi_0}\|_{H^7(I,\mathbb{C})} < \eta, \quad \|\psi_f - \varphi_1 e^{i\phi_1}\|_{H^7(I,\mathbb{C})} < \eta,$$

there exists a trajectory (ψ, u) of the control system (Σ) on $[0,T]$ such that $\psi(0) = \psi_0$, $\psi(T) = \psi_f$ and $u \in H_0^1((0,T), \mathbb{R})$.

Let us state few remarks about the regularity assumption H^7.

Following arguments from Ball, Marsden and Slemrod in [1], Turinici proved in [7, chap.4] that the control system (Σ) is not controllable in $H^2 \cap H_0^1(I, \mathbb{C})$ with control functions $u \in L^r_{\text{loc}}(\mathbb{R}_+, \mathbb{R})$, $r > 1$.

Theorem 7.1 emphasises that his negative result is due to a choice of functional spaces which does not allow controllability. More precisely, the system (Σ) can be controlled

- in $H^2(I, \mathbb{C})$, but with a control functions set larger than $L^r_{\text{loc}}(\mathbb{R}_+, \mathbb{R})$, $r > 1$, for instance $H^{-1}_{\text{loc}}(\mathbb{R}_+, \mathbb{R})$,
- with control functions $u \in L^2_{\text{loc}}(\mathbb{R}_+, \mathbb{R})$, but in a smaller space than $H^2(I, \mathbb{C})$, for instance $H^3(I, \mathbb{C})$.

The proof given in [2] gives the controllability of (Σ) in H^7 with control functions in H_0^1. The exponent 7 is only technical and related to the application of the Nash-Moser theorem. With the same strategy and strengthened estimates, it is now possible to prove the same theorem with every where $H^7(I, \mathbb{C})$ replaced by $H^{5+\epsilon}$, $\epsilon > 0$. One conjectures that the optimal result is the local controllability in H^5 with control functions $u \in H_0^1$.

7.2.2 Sketch of the proof of Theorem 7.1

A classical approach to get local controllability around a trajectory consists in proving the controllability of the linearised system around this trajectory and concluding thanks to an inverse mapping theorem. This method does not work here: Rouchon proved in [9] that, around any state of definite energy, the linear tangent approximate system is not controllable.

The proof of Theorem 7.1 relies on Coron's return method and quasi-static deformations. The return method was introduced by Coron, in 1992, and has already been used to prove many controllability results for PDEs.

This method is in two steps. First, one finds a trajectory $(\widetilde{\psi}, \widetilde{u})$ of the control system (Σ) such that the linearised control system around $(\widetilde{\psi}, \widetilde{u})$ is controllable in time T. Then, using an implicit function theorem, one gets the local controllability in time T of the nonlinear system (Σ) around $(\widetilde{\psi}(0), \widetilde{\psi}(T))$: there exist a neighbourhoods V_0 of $\widetilde{\psi}(0)$ and V_T of $\widetilde{\psi}(T)$ such that the system (Σ) can be moved in time T from any point $\xi \in V_0$ to any point $\zeta \in V_T$.

In a second step, given two points ψ_0, ψ_f closed enough to $\varphi_1 e^{i\phi_0}$, $\varphi_1 e^{i\phi_1}$, one proves that the system (Σ) can be moved

- from ψ_0 to a point $\xi \in V_0$, using quasi-static transformations,
- from one point $\zeta \in V_T$ to ψ_f, using again quasi-static transformations,
- from ξ to ζ using the local controllability around $(\widetilde{\psi}(0), \widetilde{\psi}(T))$.

The trajectory $(\widetilde{\psi}, \widetilde{u})$ used in [2] is the ground state for a constant acceleration $u \equiv \gamma$, $\gamma \in \mathbb{R}^*$,

$$\psi_{1,\gamma}(t,q) := \varphi_{1,\gamma} e^{-i\lambda_{1,\gamma} t}.$$

Here, $\lambda_{1,\gamma}$ is the first eigenvalue of the operator A_γ defined on

$$D(A_\gamma) := (H^2 \cap H_0^1)(I, \mathbb{C}), \text{ by } A_\gamma \varphi := -\frac{1}{2}\frac{d^2\varphi}{dq^2} - \gamma q \varphi.$$

and $\varphi_{1,\gamma}$ is an associated eigenvector. More precisely, thanks to **moment theory**, one proves that the linearised system around $(\psi_{1,\gamma}, u \equiv \gamma)$ is controllable in $D(A_\gamma^{3/2})$, with control functions in $L^2((0,T),\mathbb{R})$, for every $T > 0$, when $\gamma \in \mathbb{R}^*$ is small enough.

Unfortunately, this controllability result for the linearised system around $(\psi_{1,\gamma}, u \equiv \gamma)$ is not sufficient to get the local controllability of the nonlinear system (Σ) around $\psi_{1,\gamma}$ by applying the classical implicit function theorem. Indeed, the map Φ which associates to any couple of initial condition and control (ψ_0, v) the couple of initial and final conditions (ψ_0, ψ_T) for the system (Σ) with $u = \gamma + v$, is well defined and of class C^1 between the following spaces,

$$\begin{array}{rccccccc} \Phi: & [S \cap D(A_\gamma^{3/2})] & \times & H^1((0,T),\mathbb{R}) & \to & [S \cap D(A_\gamma^{3/2})] & \times & [S \cap D(A_\gamma^{3/2})] \\ & (\psi_0 & , & v) & \mapsto & (\psi_0 & , & \psi_T). \end{array}$$

Its differential map $d\Phi(\varphi_{1,\gamma}, 0)$ at the point $(\varphi_{1,\gamma}, 0)$ maps the space

$$E := [T_S(\varphi_{1,\gamma}) \cap D(A_\gamma^{3/2})] \times H^1((0,T),\mathbb{R})$$

into the space

$$F := [T_S(\psi_{1,\gamma}(0)) \cap D(A_\gamma^{3/2})] \times [T_S(\psi_{1,\gamma}(T)) \cap D(A_\gamma^{3/2})],$$

where $T_S(\xi)$ is the tangent space to the L^2-sphere $\mathcal{S}$ at the point ξ. It admits a right inverse, $d\Phi(\varphi_{1,\gamma},0)^{-1}$, but it does not map F into E : it only maps F into

$$[T_S(\psi_{1,\gamma}(0)) \cap D(A_\gamma^{3/2})] \times L^2((0,T),\mathbb{R}).$$

One deals with this loss of regularity using a **Nash-Moser implicit function theorem** adapted from [8] and one gets the following theorem.

Theorem 7.2 *Let $T := 4/\pi$. There exists $\gamma^* > 0$ such that, for every $\gamma \in (0,\gamma^*)$, there exists $\eta > 0$ such that, for every $(\psi_0,\psi_T) \in \mathcal{S} \cap D(A_\gamma^{7/2})$ satisfying*

$$\|\psi_0 - \psi_{1,\gamma}(0)\|_{H^7(I,\mathbb{C})} \leqslant \eta, \quad \|\psi_T - \psi_{1,\gamma}(T)\|_{H^7(I,\mathbb{C})} \leqslant \eta,$$

there exists a trajectory (ψ,u) of the control system (Σ) such that $\psi(0) = \psi_0$, $\psi(T) = \psi_T$ and $(u-\gamma) \in H_0^1((0,T),\mathbb{R})$.

It is at this step of the proof that the regularity assumption H^7 appears : in order to prove the convergence of the Nash iterations, one needs regularity on the initial and final conditions.

In the second step of the return method, one constructs explicitly, for $\gamma > 0$ small enough, trajectories

$$(\psi,u) : [0,T^1] \to H^7(I,\mathbb{C}) \times \mathbb{R}$$

such that

$$u(0) = 0, \quad u(T^1) = \gamma, \quad \psi(0) = \varphi_1 e^{i\phi_0}, \quad \psi(T^1) \in D(A_\gamma^{7/2}),$$
$$\|\psi(T^1) - \varphi_{1,\gamma}\|_{H^7} < \eta/2.$$

Then, for $\psi_0 \in D(A^{7/2})$ closed enough to $\varphi_1 e^{i\phi_0}$, the same control moves the system from ψ_0 to ξ which satisfies

$$\xi \in D(A_\gamma^{7/2}) \text{ and } \|\xi - \varphi_{1,\gamma}\|_{H^7} < \eta,$$

thanks to the continuity with respect to initial conditions. The control used in this step moves slowly from 0 to γ : one makes **quasi-static transformations**.

7.3 Steady-state controllability of (Σ)

In [3], we study the same physical system, but we want to control not only the wave function ψ of the particle but also the position D and the speed S of the potential well. Thus, we consider the control system

$$(\widetilde{\Sigma}) \begin{cases} i\dfrac{\partial\psi}{\partial t}(t,q) = -\dfrac{1}{2}\dfrac{\partial^2\psi}{\partial q^2}(t,q) - \langle u(t),q\rangle\psi(t,q), & q \in (-1/2,1/2), t \in \mathbb{R}_+, \\ \psi(t,\pm 1/2) = 0, \\ \dot{S} = u, \\ \dot{D} = S, \end{cases}$$

in which the state is (ψ,S,D) and the control is the function u. Let us introduce orthonormal eigenvectors $(\varphi_n)_{n\in\mathbb{N}^*}$ of the operator A,

$$\varphi_n(q) := \sqrt{2}\cos(n\pi q) \text{ when } n \text{ is odd}, \qquad \varphi_n(q) := \sqrt{2}\sin(n\pi q) \text{ when } n \text{ is even},$$

and the eigenstates $\psi_n(t,q) := \varphi_n(q)e^{-i\lambda_n t}$ where $\lambda_n := -(n\pi)^2/2$. The main result of [3] is the following one.

Theorem 7.3 *For every $n_0, n_f \in \mathbb{N}^*$, there exists a time $\mathcal{T} > 0$ and a trajectory (ψ, S, D, u) of $(\widetilde{\Sigma})$ on $[0, \mathcal{T}]$ such that $(\psi(0), S(0), D(0)) = (\varphi_{n_0}, 0, 0)$, $(\psi(\mathcal{T}), S(\mathcal{T}), D(\mathcal{T})) = (\varphi_{n_f}, 0, 0)$, and $u \in H_0^1((0, \mathcal{T}), \mathbb{R})$.*

Let us explain how we prove this theorem with $n_0 = 1$, $n_f = 2$.

First, we prove the local controllability of $(\widetilde{\Sigma})$ around all the trajectories

$$(Y_\theta := (\xi_\theta := \sqrt{1-\theta}\psi_1 + \sqrt{\theta}\psi_2, S \equiv 0, D \equiv 0), u \equiv 0), \text{ for } \theta \in [0, 1].$$

Then, we conclude thanks to the compactness of the segment $[Y_0, Y_1]$.

The local controllability results are proved in a similar way as in section 7.2. However the introduction of S and D makes the proof more difficult. For instance, the linearised system around

$$(Z_\gamma := (\psi_{1,\gamma}, S \equiv \gamma t, D \equiv \frac{1}{2}\gamma t), u \equiv \gamma)$$

is not controllable anymore because the variables ψ and S are not independent. We get the local controllability of (ψ, D) for $(\widetilde{\Sigma})$ around $Z_\gamma(0)$, thanks to the **Nash-Moser theorem**, as in section 7.2. Then, we use the **second order term** of Φ to control S: we find a control which fixes the first order term $d\Phi(Z_\gamma(0), 0)$, and a control which moves the second order term $d^2\Phi(Z_\gamma(0), 0)$ only in the direction S. We conclude the local controllability of (ψ, S, D) for $(\widetilde{\Sigma})$ around $Z_\gamma(0)$, thanks to the intermediate values theorem.

7.4 The same technique on other PDEs

The technique introduced for the study of (Σ) gave positive controllability results for others PDEs. Note that these PDEs were known to be not controllable in particular functional spaces, thanks to the argument of [1]. One proves their controllability in other spaces.

The first PDE is the following 1D beam equation

$$(\mathcal{P}) \begin{cases} u_{tt} + u_{xxxx} + p(t)u_{xx} = 0, & x \in (0,1), t \in \mathbb{R}_+ \\ u(t,.) = u_x(t,.) = 0 & \text{at } x = 0, 1, \end{cases}$$

in which the state variable is $u(t, x)$ and the control is the function $p(t)$. Thanks to the Nash-Moser theorem, one proves, in [4], the local controllability of $(\mathcal{P})$ in $H^{5+\epsilon} \times H^{3+\epsilon}((0,1), \mathbb{R})$, $\epsilon > 0$ around reference trajectories of the form

$$(u_{\text{ref}}(t, x) := v_k(x)\sin(\sqrt{\lambda_k}t) + v_{k+1}(x)\sin(\sqrt{\lambda_{k+1}}t), u \equiv 0),$$

where, for every $n \in \mathbb{N}^*$,

$$\frac{d^4}{dx^4}v_n = \lambda_n v_n, \quad v_n(0) = v_n(1) = v_n'(0) = v_n'(1) = 0.$$

The second PDE represents a quantum particle in a 1D infinite square potential well with variable length. The state variable is the wave function ψ of the particle and the control is the length $l(t)$ of the potential. After changes of variable and wave functions, one works on the equivalent control system

$$(\mathcal{V}) \begin{cases} i\dot{\psi} = -\psi'' + (\dot{u} - u^2)x^2\psi, & x \in (0,1), t \in \mathbb{R}_+, \\ \psi(t,0) = \psi(t,1) = 0, \end{cases}$$

in which the state is ψ and the control u is subjected to $u(0) = u(T) = \int_0^T u(t)dt = 0$. Thanks to the Nash-Moser theorem and expansion to the second order, one proves, in [5], local controllability results in $H^{5+\epsilon}((0,1),\mathbb{C})$ for $(\mathcal{V})$. Then, a compactness argument provides global controllability between eigen states.

Conclusion

The technique introduced for the study of (Σ) are general enough to be applied on other equations. They probably also give a positive controllability theorem for the general bilinear control systems which are proved to be not controllable (in particular spaces) in [1]. This constitutes an open problem.

Another interesting question about (Σ) is the existence of a minimal time for the controllability. An affirmative answer is given in [6], the value of this minimal time is still open.

Bibliography

[1] J.M. Ball, J.E. Marsden and M. Slemrod. *Controllability for distributed bilinear systems,* SIAM J. Control and Optim., 20, July 1982.

[2] K. Beauchard. *Local Controllability of a 1-D Schrödinger equation,* J. Math. Pures et Appl., 84, July 2005, p. 851-956.

[3] K. Beauchard and J.-M. Coron. *Controllability of a quantum particle in a 1D moving potential well,*. J. Funct. Analysis, 232, March 2006, p. 328-389.

[4] K. Beauchard. *Local controllability of a 1D beam equation,* prépublication du CMLA N.2005-24 (soumis).

[5] K. Beauchard. *Controllability of a quantum particle in a 1D infinite square potential well with variable length,* prepublication du CMLA N. 2005-25 (soumis).

[6] J.-M. Coron. *On the small-time local controllability of a quantum particule in a moving one-dimensional infinite square potential well,* C.R.A.S. (to appear).

[7] M. Defranceschi and C. Le Bris. *Mathematical Models and Methods for Ab Initio Quantum Chemistry,* Springer-Verlag Berlin Heidelberg New York, 2000.

[8] L. Hörmander. *On the Nash-Moser Implicit Function Theorem,* Annales Academiae Scientiarum Fennicae, 1985, p. 255-259.

[9] P. Rouchon. *Control of a quantum particule in a moving potential well,* 2nd IFAC Workshop on Lagrangian and Hamiltonian Methods for Nonlinear Control, Seville, 2003.

Reconstruction methods for the three-dimensional inverse acoustic obstacle scattering problems

Fahmi Ben Hassen[1] *Klaus Erhard*[2] *Roland Potthast*[3]

8.1 Introduction

Inverse scattering problems are concerned with the reconstruction of objects and parameter functions from the knowledge of scattered waves. Today, basically three different categories of methods for the treatment of the full nonlinear scattering problem are known: iterative methods, decomposition methods and sampling/probe methods.

The point source method (PSM) is a scheme for the reconstruction of a scattered field from its far field pattern which was introduced by Potthast in [2]. It belongs to the class of decomposition methods since it solves the inverse shape reconstruction problem by a decomposition of the nonlinear ill-posed problem into the linear ill-posed problem to reconstruct the scattered field from the far field pattern and the nonlinear but well-posed problem to find the zeros of the total field (for a sound-soft obstacle). The PSM can also be regarded as an analytic continuation method extending the far field of a scattered wave to its near field. This feature is used as an ingredient for the singular sources method. The reconstructions of fields are also of general interest for several applications, as for identifying sources of acoustic or electromagnetic waves[4].

The singular sources method (SSM), first proposed in [3], is another technique for the reconstruction of the shape of an obstacle, from the knowledge of the far field pattern of scattered plane waves. It belongs to the class of *sampling and probe methods*. The basic idea behind these methods is to sample the unknown area by constructing an indicator function. The unknown shapes can be found from the behaviour of this indicator function. Its main advantage compared to the PSM is that the boundary condition on the scatterer does not need to be known. This independence of the method on the physical properties of obstacles is of great practical importance, since in many cases knowledge about these properties of the objects to be reconstructed is not available. However, this scheme needs the knowledge of the far field patterns of many incident waves.

In this work, we study numerical applicability of the PSM and the SSM for three-dimensional reconstructions. Moreover, we give new proofs of convergence, by which our methods can be

[1]LAMSIN-ENIT, BP 37, 1002 Tunis, Tunisia. fahmi.benhassen@enit.rnu.tn
[2]NAM, University of Göttingen, Germany. kerhard@math.uni-goettingen.de
[3]NAM, University of Göttingen, Germany. potthast@math.uni-goettingen.de
[4]The design of an acoustical camera generating 3d reconstructions of acoustic sources within cars has been nominated for the German future price "Deutscher Zukunfspreis" 2005.

shown to work for arbitrary incident fields, limited aperture and arbitrary boundary conditions.

8.2 Acoustic scattering problems

We consider acoustic scattering from a bounded impenetrable scatterer $\mathcal{D}$. The scatterer $\mathcal{D}$ consists of a domain $D \subset \mathbb{R}^3$ and a boundary condition for the total field on ∂D. We assume that ∂D is of class C^2 and that $\mathbb{R}^3 \setminus \overline{D}$ is connected.

Given an incident field u^i and a scatterer $\mathcal{D}$, the direct acoustic obstacle scattering problem is to find a scattered field $u^s \in C^2(\mathbb{R}^3 \setminus \overline{D}) \cap C(\mathbb{R}^3 \setminus D)$, which solves the Helmholtz equation

$$\triangle u^s + \kappa^2 u^s = 0 \tag{8.1}$$

in $\mathbb{R}^3 \setminus \overline{D}$ and satisfies the Sommerfeld radiation condition

$$r\Big(\frac{\partial u^s}{\partial r} - i\kappa u^s\Big) \to 0, \quad r = |x| \to \infty, \tag{8.2}$$

uniformly in all directions $\hat{x} = x/|x|$, such that the total field $u = u^i + u^s$ satisfies Dirichlet, Neumann or impedance boundary conditions given, respectively, as

$$u|_{\partial D} = 0, \qquad \frac{\partial u}{\partial \nu}|_{\partial D} = 0 \qquad \frac{\partial u}{\partial \nu}|_{\partial D} + \lambda u|_{\partial D} = 0, \tag{8.3}$$

with the impedance function $\lambda \in C(\partial D)$. Here, the letter ν denotes the outward unit normal vector to ∂D.

The solution of each of this problems exists and is unique (see [1]). In addition, a solution of the Helmholtz equation (8.1) in the exterior of some ball B satisfying (8.2) is called radiating. A radiating solution u^s has the asymptotic behaviour of an outgoing spherical wave (see Theorem 2.5 in [1]) :

$$u^s(x,d) = \frac{e^{i\kappa|x|}}{|x|}\left\{u^\infty(\hat{x},d) + O\left(\frac{1}{|x|}\right)\right\}, \tag{8.4}$$

as $|x| \to \infty$ uniformly in all directions $\hat{x} := x/|x|$. The function u^∞ is known as the *far field pattern* of u^s and it is defined on the unit sphere $\mathbb{S}^2 := \big\{x \in \mathbb{R}^3 : |x| = 1\big\}$.
It is a basic result known as Rellich Lemma that a scattered field u^s is determined by the knowledge of the far field pattern u^∞ on an open subset of $\mathbb{S}^2$.

8.3 The point source method

Here we show how the PSM reconstructs the scattered field u^s from its limited aperture far field pattern $u^\infty|_\Lambda$ given on an open nonempty subset Λ of $\mathbb{S}^2$. Then, we might search for the boundary ∂D of a sound-soft scatterer D by searching for the zeros of the total field $u = u^i + u^s$.

8.3.1 The main result

Given $x \in \mathbb{R}^3 \setminus \overline{D}$, the idea of the point-source method is to choose an *approximation domain* $G(x)$, with $x \notin \overline{G(x)}$ and such that $G(x)$ is large enough to contain the unknown domain D, and approximate the point source $\Phi(x,y)$ for $y \in \overline{G(x)}$ by a *superposition of plane waves*, also called a Herglotz wave function,

$$v[g_x](y) := \int_\Lambda e^{i\kappa y\cdot d} g_x(d)\, ds(d), \tag{8.5}$$

with a density g_x obtained from an approximate solution of the integral equation

$$\int_\Lambda e^{i\kappa y\cdot d} g_x(d)\, ds(d) = \Phi(x,y),\ \ y \in \partial G(x). \tag{8.6}$$

Under appropriate conditions on $G(x)$, the approximations are always possible up to any approximation error ε with a Herglotz wave function with density $g_{x,\varepsilon} \in L^2(\Lambda)$ (see Lemma 3.1.2. in [4]).

Definition 8.1 *Consider a set of sampling domains $G(x)$ parameterized by $x \in \mathbb{R}^3$, such that $x \notin \overline{G(x)}$. Let D be a bounded domain in $\mathbb{R}^3$. We define the* illuminated area

$$\mathcal{E} := \{x \in \mathbb{R}^3 :\ \overline{D} \subset G(x)\}. \tag{8.7}$$

The main result of the point source method can be stated as follows :

Theorem 8.1 *Consider the scattering of an acoustic wave by an impenetrable obstacle D, with ∂D of class C^2. Assume that the incident wave u^i satisfies (8.1) in D. Then, the back-projection operator*

$$(A_\varepsilon u^\infty)(x) := 4\pi \int_\Lambda u^\infty(-d) g_{x,\varepsilon}(d)\, ds(d),\ \ x \in \mathbb{R}^3 \setminus \overline{D}, \tag{8.8}$$

with a density $g_{x,\varepsilon}$, converges uniformly to the scattered field on any compact subset M of the illuminated area $\mathcal{E}$, i.e.

$$\lim_{\varepsilon\to 0} \max_{x\in M} |u^s(x) \ - \ A_\varepsilon u^\infty(x)| = 0. \tag{8.9}$$

8.3.2 Realization of the point source method

A basic numerical step of the point source method is the approximation of a point source $\Phi(x,\cdot)$ on some domain of approximation $G(x)$ by a Herglotz wave function (8.5). In general, $\Phi(x,\cdot)$ is not in the range of the compact operator $H : L^2(\Lambda) \to L^2(\partial G(x))$ defined by

$$(Hg)(y) := \int_\Lambda e^{i\kappa y\cdot d} g(d)\, ds(d)\ , \quad y \in \partial G(x), \tag{8.10}$$

and we need some regularization scheme for the calculation of an approximate solution to the ill–posed integral equation (8.6). Here, we stabilize the calculation of g_x by applying a Tikhonov regularization scheme, i.e. by solving the regularized equation

$$(\alpha I + H^*H)g = H^*\Phi(x,\cdot) \tag{8.11}$$

for $g = g_{x,\alpha} \in L^2(\Lambda)$, with a small regularization parameter $\alpha = \alpha(\varepsilon) > 0$, such that $\|\Phi(x,\cdot) - Hg_{x,\alpha}\|_{L^2(\partial G)} < \varepsilon$.

From a computational point of view, we have to solve the regularized integral equation (8.11) for every $x \in \Omega$, when using arbitrary approximation domains $G(x)$. This computational cost can be reduced by the following strategy:
We solve the regularized integral equation (8.11) only once for $x = 0$ and a chosen $G(0)$ to obtain $g_{0,\alpha}$. Then, we define a family of approximation domains

$$\mathcal{G} := \{G(x) = G(0) + x : x \in \Omega\}. \tag{8.12}$$

This set consists of translations of the original geometric configuration $(0, G(0))$ to the configuration $(x, G(x))$. In this case, we can calculate the density $g_{x,\alpha}$ of the approximation of

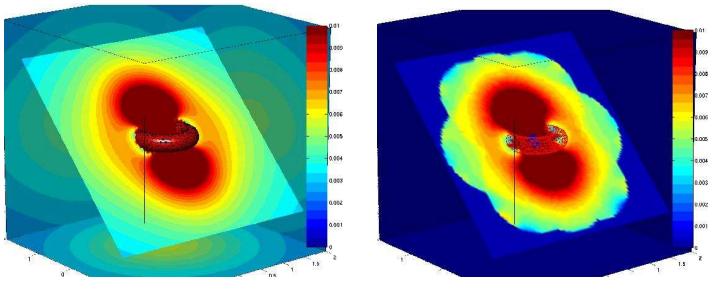

Figure 8.1: *The modulus of the calculated and the reconstructed total fields for the sound soft ring with an incident point source in the origin and* $\kappa = 2$.

$\Phi(x,\cdot)$ on $G(x)$ from $g_{0,\alpha}$, without solving the regularized integral equation (8.11), by a simple multiplication with a complex factor :

$$g_{x,\alpha}(d) = e^{-i\kappa x\cdot d} g_{0,\alpha}(d), \qquad \text{for } d \in \mathbb{S}^2. \tag{8.13}$$

Finally, we obtain a complete reconstruction by repeating this procedure with different configurations of the approximation domain : $G^{(j)}(0) = R^{(j)}(G(0))$, for $j = 1, ..., n$. Then, for each configuration $(0, G^{(j)}(0))$, we calculate the densities $g^{(j)}_{x,\alpha}$ in Ω as explained above by setting $G^{(j)}(x) = x + G^{(j)}(0)$.

In the post-processing step, we restrict the reconstructed field (8.8), to some illuminated area $\mathcal{E}$ since we expect a valid approximation of the point source only in this special region. We use the indicator function

$$\mathcal{I}_{\text{enl}}(x) = u_{\text{rec},1}(x) - u_{\text{rec},2}(x)\ , \quad x \in \mathbb{R}^3, \tag{8.14}$$

which is the difference of two reconstructed fields obtained with two different regularization parameters. We choose some cut-off parameter c and set $u_{\text{rec}} = 0$ if $|\mathcal{I}_{\text{enl}}(x)| > c$, i.e. when x does not belong to $\mathcal{E}_c = \{x : |\mathcal{I}_{\text{enl}}(x)| < c\}$, where $\mathcal{E}_c$ is an approximation of the illuminated area.

8.3.3 Numerical implementation of the point source method

We study shape reconstructions for scattering by a sound-soft obstacle.
To produce the input data, given by the far field pattern, we solve the forward problem by the Nyström's method ignoring the singularities of the kernel (by introducing a cut-off scheme).
Figure 8.1 illustrates the reconstruction of the total field due to the scattering of the incident point source with wave number $\kappa = 2$, by the ring of radii $r_i = 0.3$ and $r_o = 0.6$. For the reconstruction, we used the approximation domains

$$G^{(j)}(0) := \mathbb{B}_3 + 1.1 n_j, \quad j = 1, \ldots, 26.$$

The 26 directions n_j are the 6 face normals of the unit cube, its 8 normalized diagonals and the 12 normalized diagonals of the cube's faces. The illuminated area is computed with the regularization parameters $\alpha_1 = 10^{-8}$ and $\alpha_2 = 2\alpha_1$.
To reconstruct the scatterer, we extracted the iso-surface of level 0.004. We obtain a good reconstruction of the sound-soft ring as illustrated in Figure 8.2.

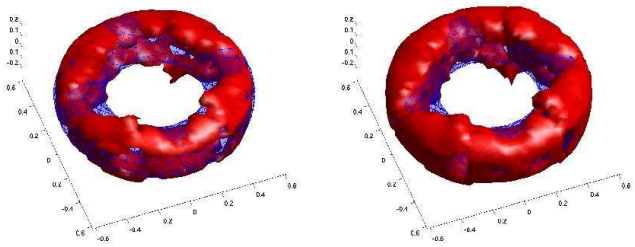

Figure 8.2: *The iso-surface of level* 0.004 *of the total field due to the scattering of a point source by the ring for balls and ellipsoidal approximation domains.*

8.4 The singular sources method

The main idea of the SSM is to reconstruct the scattered field $\Phi^s(\cdot, z)$ in z, due to an incident point source, from the far field pattern $u^\infty(\cdot, d)$, $d \in \mathbb{S}^2$, associated to a scattering of an incident plane wave of direction d. The boundary ∂D of an obstacle D can be identified as the set of points where the scattered field $\Phi^s(z, z)$ becomes singular. The behaviour of $\Phi^s(z, z)$ is explicitly given by Theorem 2.1.15 in [4]. It proves that the function

$$I(z) := |\Phi^s(z, z)| , \quad z \in \Omega \setminus \overline{D} \tag{8.15}$$

is bounded in every set Ω_τ of the form $\Omega_\tau := \{z \in \Omega \setminus \overline{D} : d(z, D) > \tau > 0\}$, where $d(z, D)$ denotes the Hausdorff distance, but unbounded when z tends to the boundary of the obstacle, i.e.

$$\lim_{z \to \partial D} I(z) = \infty \tag{8.16}$$

holds. Thus I may serve as an indicator function for the reconstruction of the obstacle D. However, we can not calculate the indicator function $I(z) = \Phi^s(z, z)$ directly without the knowledge of the obstacle D and the boundary condition on ∂D. Therefore we will compute an approximation of the scattered field $\Phi^s(\cdot, z)$ in the source point $z \in \Omega \setminus \overline{D}$ based on ideas from the PSM. This is given by the following Theorem:

Theorem 8.2 (SSM for inverse acoustic scattering problem) *Let M be a compact subset of the illuminated area $\mathcal{E}$ and let $\mathcal{G}$ be a strategy for the choice of the approximation domain. Then, the backprojected far field pattern*

$$(Q_\varepsilon u^\infty)(x, z) = 4\pi \int_{\mathbb{S}^2} \int_{\mathbb{S}^2} u^\infty(-d, \hat{x}) \tilde{g}_{x,\tilde{\varepsilon}}(d)\, ds(d)\, g_{z,\varepsilon}(\hat{x})\, ds(\hat{x}) \tag{8.17}$$

converges uniformly towards $\Phi^s(x, z)$ on $M \times M$. The densities $g_{z,\varepsilon}$ and $\tilde{g}_{x,\tilde{\varepsilon}}$ are obtained by solving the ill-posed linear integral equation (8.11) with an approximation error ε and $\tilde{\varepsilon} := \frac{\varepsilon}{\|g_{z,\varepsilon}\|}$, respectively.

In particular, the approximating indicator function $\tilde{I}(z)$ given by the backprojected far field pattern $Q_\varepsilon u^\infty$ evaluated in $(z, z) \in \Omega \times \Omega$, approximates the true indicator function $I(z) = \Phi^s(z, z)$ whenever $z \in \mathcal{E}$. Then, we obtain an approximation to the unknown scatterer D as the set of points where $\tilde{I}(z)$ becomes larger than a predefined cut-off value c_0. This threshold value c_0 can be chosen empirically by investigating some reference obstacle D_0 with known boundary

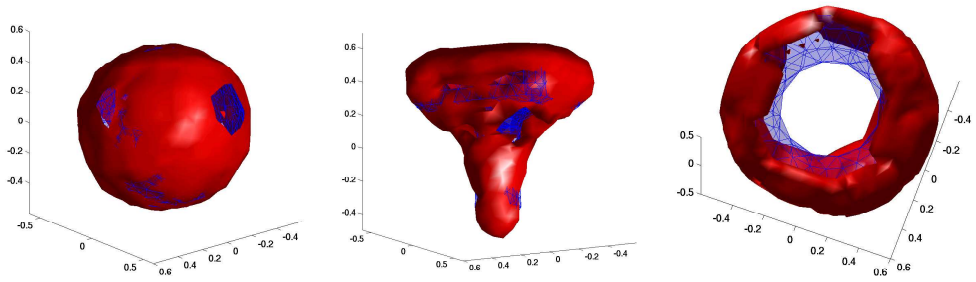

Figure 8.3: *Boundary reconstructions of impenetrable obstacles using SSM*

and simulated far field pattern u_0^∞. In contrast to the point source method the singular sources method needs to know the full far field pattern for all incident waves as input data. This means that we must have more information available than in the single wave setting but we also expect a better quality of the reconstructions due to the increase in information. On the other hand, the SSM reconstructs a scatterer without the knowledge of the boundary condition on ∂D while PSM essentially needs this information in the reconstruction algorithm. Hence SSM is applicable in a more general setting.

Finally, since the singular sources method is based on the point source approximation, we can apply the same techniques that have already been developed in sections 8.3.2 and 8.3.3 to implement the SSM. Figure 8.3 shows boundary reconstructions of a ball with an impedance boundary condition, a sound hoft T-shaped obstacle and a sound hard ring using SSM for $\kappa = 2$.

Acknowledgments. The LAMSIN's researche's work is supported by the Ministère de la Recherche Scientifique, de la Technologie et du Développement des Compétences (MRSTDC, TUNISIA) under the LAB-STI-02 program.

Bibliography

[1] David Colton and Rainer Kress. *Inverse Acoustic and Electromagnetic Scattering Theory* Berlin: Springer-Verlag, 1998.

[2] Roland Potthast. *A fast new method to solve inverse scattering problems.* Inverse Problems, 12, 1996.

[3] Roland Potthast. *Habilitation thesis* University of Göttingen, 1999.

[4] Roland Potthast. *Point Sources and Multipoles in Inverse Scattering Theory.* Boca Raton, FL: Chapman & Hall, 2001.

On the determination of thin elastic inclusions from boundary measurements

Elena Beretta[1] *Elisa Francini* [2]

Let $\Omega \subset \mathbb{R}^2$ be a bounded smooth domain representing the region occupied by an elastic material.

Let $\sigma_0 \subset \Omega$ be a simple smooth curve and define, for a positive small ϵ, the set

$$\omega_\epsilon = \{x \in \Omega \ : \ d(x, \sigma_0) < \epsilon\},$$

which represents an inclusion of small size made of a different elastic material.

Let $\mathbb{C}_0$ and $\mathbb{C}_1$ be the elastic tensor fields in $\Omega \setminus \overline{\omega}_\epsilon$ and ω_ϵ respectively.

Given a traction field g on $\partial\Omega$, the displacement field u_ϵ, generated by this traction in the body containing the inclusion ω_ϵ, solves the following system of linearized elasticity

$$\begin{cases} \operatorname{div}\left(\mathbb{C}_\epsilon \widehat{\nabla} u_\epsilon\right) &= 0 \quad \text{in} \quad \Omega \\ (\mathbb{C}_\epsilon \widehat{\nabla} u_\epsilon) \cdot \nu &= g \quad \text{on} \quad \partial\Omega, \end{cases} \tag{9.1}$$

where $\mathbb{C}_\epsilon = \mathbb{C}_0 \chi_{\Omega \setminus \omega_\epsilon} + \mathbb{C}_1 \chi_{\omega_\epsilon}$, $\widehat{\nabla} u_\epsilon = \frac{1}{2}\left(\nabla u_\epsilon + (\nabla u_\epsilon)^T\right)$ is the symmetric deformation tensor and ν denotes the outward unit normal to $\partial\Omega$.

Let us also introduce the background displacement u_0, namely the solution of

$$\begin{cases} \operatorname{div}\left(\mathbb{C}_0 \widehat{\nabla} u_0\right) &= 0 \quad \text{in} \quad \Omega \\ (\mathbb{C}_0 \widehat{\nabla} u_0 \cdot \nu &= g \quad \text{on} \quad \partial\Omega. \end{cases} \tag{9.2}$$

The goal of this talk is to present first the derivation of a rigorous asymptotic expansion for $(u_\epsilon - u_0)_{|\partial\Omega}$ as $\epsilon \to 0$. An analogous expansion has been already derived for the case of thin conductivity inclusions. These expansions represent a powerful tool to solve the inverse problem of identifying the inclusions, given boundary measurements for the case of conductivity inclusions. In the second part of the talk I will show how to use the formula in order to detect the elastic inclusions presenting some preliminary results concerning the case of inclusions which are thin neighborhoods of segments.

[1]Dipartimento di Matematica "G. Castelnuovo" Università di Roma "La Sapienza", Piazzale Aldo Moro 5, 00185 Roma, Italy (Email: beretta@mat.uniroma1.it).

[2]Universita' di Firenze , Italy (Email: elisa@fi.iac.cnr.it).

Locating an obstacle in a 3D finite depth ocean using the convex scattering support

Laurent Bourgeois[1] *Colin Chambeyron*[2] *Steven Kusiak*[3]

10.1 Introduction

Imaging a scatterer in a shallow ocean is a classical inverse problem which has been considered by many authors. Furthermore, it is well known that the inverse scattering problem associated with a 3D waveguide as such is more difficult than in free space. Actually, because of the physical presence of the top and bottom elements of the waveguide, only a finite number of modes can propagate at long distance. The remainder of the modes are said to be evanescent, which means they decay exponentially as a function of distance. This fact increases the so-called ill-posedness of the inverse problem.

The most interesting inversion techniques are those for which no *a priori* assumption is made concerning the physical nature of the scatterer. For example the linear sampling method (see an overview in [2]) has been adapted to the 2D ocean [8]. The main drawback of such a method is that many incident waves are required. Recently, in [3, 5], a theory based on the so-called convex scattering support was developed and implemented. This theory provides the same advantage as the linear sampling method concerning *a priori* knowledge of boundary conditions. Additionally, it allows one to use but one incident wave to deduce information concerning the location, size and shape of the scatterer.

Here we show how this method can be adapted to approximate the convex hull of the vertical projection of an obstacle in a 3D ocean by using the far field patterns generated by single fixed-frequency illumination of the scatterer. Details and proofs are given in [1].

Our waveguide is the open domain W included between the two horizontal boundaries $z = 0$ (called 'top' or Γ_0) and $z = h$ (called 'bottom' or Γ_h) in the Cartesian coordinates (x, y, z). The boundary conditions at $z = 0$ and $z = h$ are of the Dirichlet and Neumann types respectively, and the waveguide can therefore be considered as a model of a finite depth ocean in contact with an acoustically-soft medium (such as air) at the top and with an acoustically-hard medium (such as rock) at the bottom.

We suppose that $\mathcal{O}$ is a sound hard or soft obstacle, which is embedded in W. We define Ω to be the open domain of W complementary to $\mathcal{O}$. A monochromatic acoustic wave scatters due to the presence of the obstacle. Let k denote the wavenumber, and let u^i, u^s and u respectively

[1]bourgeois@ensta.fr
[2]chambey@ensta.fr
[3]kusiak@ll.mit.edu

denote the incident, scattered and total fields ($u = u^i + u^s$). The governing equations for u^s in Ω are

$$\left\{\begin{array}{l} (\Delta_3 + k^2)u^s = 0 \text{ in } \Omega \\ u^s|_{\Gamma_0} = 0, \quad \dfrac{\partial u^s}{\partial z}|_{\Gamma_h} = 0 \quad \text{(referred by (BC) from now on)} \\ \dfrac{\partial u^s}{\partial \nu}|_{\partial\mathcal{O}} = f \text{ or } u^s|_{\partial\mathcal{O}} = g \\ \qquad (RC). \end{array}\right. \tag{10.1}$$

Here, Δ_3 is the three dimensional Laplacian, ν is the outward unit normal on $\partial\mathcal{O}$, $f = -(\partial u^i/\partial\nu)|_{\partial\mathcal{O}}$ and $g = -u^i|_{\partial\mathcal{O}}$. Lastly, (RC) is a radiation condition associated with the behavior of u^s when $r = \sqrt{x^2+y^2} \to \infty$. It consists of assuming that the scattered field is a superposition of waves that are either propagating away from the obstacle or decaying exponentially with distance from the obstacle.

We define the three dimensional cylindrical domain $C(R) = B(R) \times (0,h)$, where $B(R)$ is the open ball of radius R in $\mathbb{R}^2$, and define its two dimensional boundary by $\Sigma(R) = \partial B(R) \times (0,h)$. We assume R to be large enough such that $\mathcal{O}$ is included in $C(R)$, and we define the domains $\Omega' = (B(R)/\overline{\mathcal{O}}) \times (0,h)$ and $\Omega'' = (\Omega/\overline{B(R)}) \times (0,h)$ ($\Omega = \overline{\Omega'} \cup \Omega''$). Finally, let S^1 denote the unit sphere in $\mathbb{R}^2$.

It is well known that any field u^s which satisfies the 3D Helmholtz equation in Ω'', the boundary conditions (BC) and the radiation condition (RC), has, in cylindrical coordinates, the following representation in the domain Ω''

$$u^s(r,\theta,z) = \sum_{n\in\mathbb{N}} \sum_{m\in\mathbb{Z}} a_{mn} H_m^{(1)}(k_n r)\psi_m(\theta) w_n(z). \tag{10.2}$$

Here, H_m^1 are the Hankel functions of the first kind, while the functions ψ_m and w_n are defined by

$$\psi_m(\theta) = \frac{e^{im\theta}}{\sqrt{2\pi}}, \quad w_n(z) = \sqrt{\frac{2}{h}} \sin\Big((n+1/2)\frac{\pi z}{h}\Big). \tag{10.3}$$

The sequence of complex numbers k_n is defined by

$$k_n = \sqrt{k^2 - \Big((n+1/2)\frac{\pi}{h}\Big)^2}, \quad \mathrm{Re}(k_n) + \mathrm{Im}(k_n) \geq 0. \tag{10.4}$$

From now on, we assume that k is chosen such that k_n never vanishes.

We note that, in the domain Ω'', we may also write the scattered field as

$$u^s(r,\theta,z) = \sum_{n\in\mathbb{N}} u_n^s(r,\theta) w_n(z), \quad u_n^s(r,\theta) = \sum_{m\in\mathbb{Z}} a_{mn} H_m^{(1)}(k_n r)\psi_m(\theta). \tag{10.5}$$

The modes u_n^s for $n \in [0, N-1]$ having $\mathrm{Im}(k_n) = 0$ correspond to the propagating waves, while the modes for $n \geq N$ having $\mathrm{Re}(k_n) = 0$ correspond to the evanescent ones.

It should be pointed out that the well-posedness of problem (10.1) is not known in general. To the authors' knowledge, the well-posedness has been proved only in the case of the acoustically-soft obstacle (Dirichlet data f), when $\partial\mathcal{O}$ and f are sufficiently smooth (say $\partial\mathcal{O}$ of class C^2 and $f \in H^{\frac{3}{2}}(\partial\mathcal{O})$), and when the scatterer $\mathcal{O}$ satisfies the following convexity condition, referred by (CC) from now on : there exists a point M inside $\mathcal{O}$, such that if the origin of the cartesian coordinates is chosen such a way that $x_M = y_M = 0$, then $\nu.(x,y,0) = \nu_x x + \nu_y y \geq 0$ for all points of $\partial\mathcal{O}$ [6, 7].

In order to compute the simulated far field patterns which form the data of the inverse problem, an auxiliary problem in the bounded domain Ω' is considered, and a finite element method is used (precisely the FE code Melina, *c.f.* [4]). This auxiliary problem involves an appropriate Dirichlet-to-Neumann operator on $\Sigma(R)$.

10.2 The convex scattering support in 2D

In this section, we recall the main definitions and properties which substantiate the theory developed in [3, 5]. It leads to a summability test which characterizes the convex scattering support. From that accurate but unpractical criterion we derive a heuristic but practical one, as well as an identification strategy based on that new criterion.

Definition 10.1 *A test domain D ($D' = \mathbb{R}^2/\overline{D}$) supports the far field pattern $u^\infty \in L^2(S^1)$ iff there exists a field $u^s \in H^1_{loc}(D')$ satisfying $(\Delta_2 + k^2)u^s = 0$ in D', and for which u^∞ is the far field pattern corresponding to u^s.*

Definition 10.2 *The intersection of all convex domains that support u^∞ is a convex domain that supports u^∞. It is called the convex scattering support of u^∞ and is denoted $cS_k supp(u^\infty)$.*

From the two previous definitions, we immediately conclude that if u^∞ is the far field pattern produced by a scatterer $\mathcal{O}$ with convex hull $ch(\mathcal{O})$, then $cS_k supp(u^\infty) \subset ch(\mathcal{O})$. The convex scattering support is then a minimal set included in the convex hull of the obstacle.

Definition 10.3 *Let $S_D^\infty : H^{-1/2}(\partial D) \to L^2(S^1)$ be defined by*

$$(S_D^\infty)\varphi(\hat{x}) = \int_{\partial D} \varphi(y)\, \Phi^\infty(\hat{x}, y)\, dy, \quad \Phi^\infty(\hat{x}, y) = \frac{e^{i\frac{\pi}{4}}}{\sqrt{8\pi k}} e^{-ik\hat{x}.y}.$$

The theory of the scattering support is based in part on the following theorem.

Theorem 10.1 *Assuming that k is such that the homogeneous Dirichlet problem for the Helmholtz equation inside D admits only the trivial solution, S_D^∞ is a compact, injective operator with dense range. Furthermore, D supports $u^\infty \in L^2(S^1)$ iff*

$$\sum_{p\in\mathbb{N}} \frac{|(u^\infty, g_p)|^2}{\sigma_p^2} < +\infty, \tag{10.6}$$

where $\{\sigma_p, f_p, g_p\}$ ($p \in \mathbb{N}$) is a singular system of S_D^∞.

The following corollary enables one to establish criterion (10.6) when D is any ball $B(C, R)$ in $\mathbb{R}^2$ of center C and radius R.

Corollary 10.1 *When $D = B(C, R)$, with $C = (C_x, C_y) \in \mathbb{R}^2$, criterion (10.6) is simply: $B(C, R)$ supports u^∞ iff*

$$\sum_{m\in\mathbb{Z}} \frac{|c_m|^2}{\sigma_m^2} < +\infty, \tag{10.7}$$

with

$$c_m = \frac{1}{\sqrt{2\pi}} \int_0^{2\pi} e^{-im\theta} e^{ik(C_x \cos\theta + C_y \sin\theta)} u^\infty(\theta)\, d\theta, \quad \sigma_m = \sqrt{\frac{\pi R}{2k}} |J_m(kR)|,$$

where the J_m are the classical Bessel functions of the first kind.

A practical and useful implementation of criterion (10.7) is delicate because of the interpretation of $+\infty$. To deal with this issue, we have derived a simplified and heuristic criterion which relies on the fact that, as a function of the index m and for a fixed argument z, the function $|J_m(z)|$ of m is a bounded oscillating function for $|m| \ll z$, and a rapidly decaying one to zero when $|m| \gg z$, exhibiting a region of rapid transition near $m = z$. Similarly, for a real bounded obstacle $\mathcal{O} \subset W$ and for a given C, we observe that the Fourier coefficients $|c_m|$ also possess a similar behavior. Namely, we witness a rapid accumulation to zero when $m \ll -m_-^C$ and $m \gg m_+^C$, the lower and upper bounds $-m_-^C$ and m_+^C being directly read on the $|c_m|$-curve. Criterion (10.7) is then 'equivalent' to: $B(C, R)$ supports u^∞ 'iff'

$$kR \geq \max(m_-^C, m_+^C). \tag{10.8}$$

Criterion (10.8) provides, for a given $C = (C_x, C_y)$, the radius of the smallest ball of center C which supports u^∞.

The identification strategy we have chosen consists of the basic following scheme. First, we assume *a priori* that the obstacle is fully contained within the ball $B(C_0, R_0)$. Next, we select a finite collection of balls $B(C_i, R_i)$ $(i \in I)$, the centers C_i of which are equally distributed on the circle $\partial B(C_0, R_0)$, the radii R_i of which are obtained by computing $R_i = \max(m_-^{C_i}, m_+^{C_i})/k$. Finally, we construct the intersection of the collection $B(C_i, R_i)$ for $i \in I$. This provides an approximation of the convex scattering support $cS_k supp(u^\infty)$, and hence an approximation of the convex hull of $\mathcal{O}$.

10.3 The 3D waveguide inverse problem

We begin this section by a uniqueness result. Let the incident wave u^i be of the form $u^i(x, y, z) = w_n(z)e^{ik_n \tilde{d}.\tilde{x}}$, where $\tilde{d} = (d_x, d_y) \in S^1$ and $\tilde{x} = (x, y)$. We choose $n \in [0, N-1]$ such that u^i is a propagating wave which satisfies $\Delta_3 u^i + k^2 u^i = 0$ in W and the boundary conditions (BC).

Theorem 10.2 *Let us denote by $\mathcal{O}_{1,2}$ two soft obstacles whose boundaries are of class C^2 and satisfy the convexity condition (CC). If for an infinite number of incident waves u_q^i with propagation direction $\tilde{d}_q$, the corresponding total fields u_{1q} and u_{2q} coincide on the cylinder $\Sigma(R)$, then $\mathcal{O}_1 = \mathcal{O}_2$.*

Now we demonstrate how we may adapt the simplified criterion and strategy of identification given in section 10.2 to determine the vertical projection $P_z\mathcal{O}$ of a 3D acoustically-soft or acoustically-hard obstacle $\mathcal{O}$ embedded in the waveguide W. This is done by using the two dimensional far field patterns u_n^∞ which correspond to the u_n^s defined by (10.5), for $n \in [0, N-1]$.

We easily prove that the following system holds :

$$\forall n \in [0, N-1], \quad \left\{ \begin{array}{c} (\Delta_2 + k_n^2) u_n^s = 0 \text{ in } \mathbb{R}^2 / \overline{P_z\mathcal{O}} \\ u_n^s(\tilde{x}) = u_n^\infty(\hat{x}) \dfrac{e^{ik_n r}}{\sqrt{r}} + \mathcal{O}(\dfrac{1}{r^{\frac{3}{2}}}), \quad r \to +\infty. \end{array} \right. \tag{10.9}$$

We also we obtain that, the a_{mn} being the coefficients in (10.2),

$$u_n^\infty(\theta) = \sum_{m \in \mathbb{Z}} c_{mn} \psi_m(\theta), \quad c_{mn} = a_{mn} \sqrt{\frac{2}{\pi k_n}} e^{-i(2m+1)\frac{\pi}{4}}. \tag{10.10}$$

Using definition 1, system (10.9) means precisely that $P_z\mathcal{O}$ supports u_n^∞, for all $n \in [0, N-1]$. Hence,

$$\bigcup_{n=0}^{N-1} cS_{k_n} supp(u_n^\infty) \subset ch(P_z\mathcal{O}). \tag{10.11}$$

We finally conclude that the N convex scattering supports of the far field patterns which are associated with the propagating waves (with wavenumber k_n) enable one to find an approximation of $P_z\mathcal{O}$. In practice, for each $n \in [0, N-1]$, the simplified criterion and the identification strategy described at the end of the previous section are performed in order to approximate the corresponding convex scattering support $cS_{k_n} supp(u_n^\infty)$.

It will turn out in the next section that the numerical results are satisfactory even if one single convex scattering support $cS_{k_n} supp(u_n^\infty)$, *i.e.* for a given $n \in [0, N-1]$, is used.

10.4 Some numerical experiments

In the following experiments, we chose $h = 4$ as the height of the waveguide, and we reconstructed the convex hull of the vertical projection of an acoustically-hard obstacle $\mathcal{O}$ for the following four cases:

Case 1 : a sphere of center $(0, 0, 2)$ and radius 1,
Case 2 : a sphere of center $(0, 0, 2)$ and radius 0.5,
Case 3 : an ellipsoid of center $(0, 0, 2)$ and semi-axes 2, 2, and 1,
Case 4 : two spheres of centers $(0, 1, 2)$ and $(0, -1, 2)$, both of radius 0.5.

The incident field is $u^i(x, y, z) = \sin[(n + 1/2)\frac{\pi z}{h}]e^{ik_n x}$ for $k = 4$ and $n = 0$, k_0 being given by (10.4). Hence, the number of propagating modes is $N = 5$.

Using the computed data u_n^∞, for each $n \in [0, N-1]$ we employ the strategy described in section 10.2. The set $P_z(\mathcal{O})$ is approximated by the intersection of 8 balls $B(C_i, R_i)$ ($i \in \{1, 2, \cdots, 8\}$) such that their centers C_i are equally distributed on the circle $\partial B(C_0, R_0)$ with $C_0 = (7, 4)$ and $R_0 = 12$. It amounts to guessing that $P_z(\mathcal{O})$ lies within that circle.

Figures 10.1 and 10.2 show the xy-projection of the true obstacle within the waveguide and the result of the reconstruction, both inside the circle $\partial B(C_0, R_0)$, for case 1 with either u_0^∞ or u_1^∞. The other cases are described in [1].

These experiments reveal that only one 2D far field u_n^∞ associated to only one incident field u^i enables one to locate the vertical projection of the obstacle and to approximately find its size.

Bibliography

[1] L. Bourgeois, C. Chambeyron, and S. Kusiak. Locating an obstacle in a 3d finite depth ocean using the convex scattering support. *To appear in Journal of Computational and Applied Mathematics*, 2006.

[2] D. Colton, J. Coyle, and P. Monk. Recent developments in inverse acoustic scattering theory. *SIAM Review*, 42(3):369–414, 2000.

[3] S. Kusiak and J. Sylvester. The scattering support. *Communications on Pure and Applied Mathematics*, LVI:1525–1548, 2003.

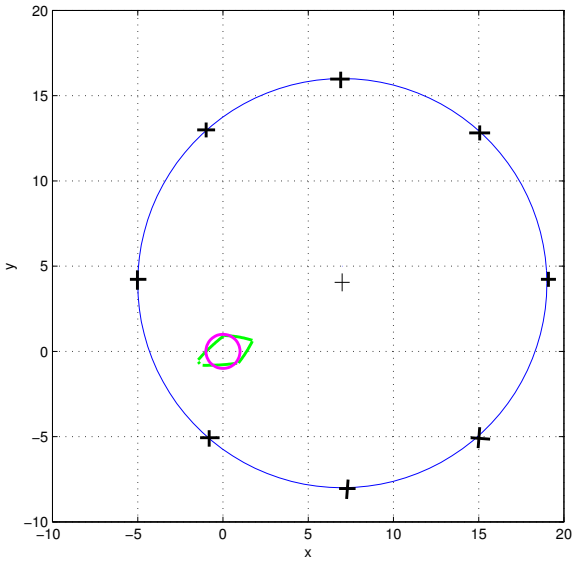

Figure 10.1: *Case 1 :* u_0^∞

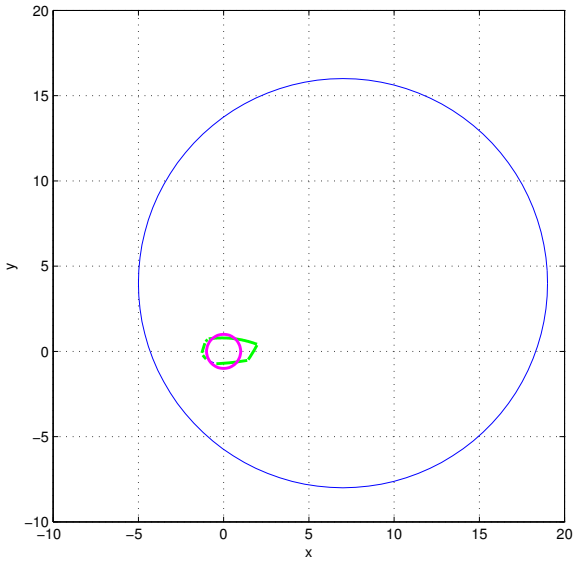

Figure 10.2: *Case 1 :* u_1^∞

[4] D. Martin. *On line documentation of Melina*. http://perso.univ-rennes1.fr/daniel.martin/melina/www/homepage.html, 2004.

[5] R. Potthast, J. Sylvester, and S. Kusiak. A 'range test' for determining scatterers with unknown physical proprieties. *Inverse Problems*, 19:533–547, 2003.

[6] Y. Xu. The propagation solutions and far-field patterns for acoustic harmonic waves in a finite depth ocean. *Applicable Analysis*, 35:129–151, 1990.

[7] Y. Xu. A note on the uniqueness of the propagating solution for acoustic waves in a finite depth ocean. *Applicable Analysis*, 67:201–204, 1997.

[8] Y. Xu, C. Matawa, and W. Lin. Generalized dual space indicator method for underwater imaging. *Inverse Problems*, 16:1761–1776, 2000.

Shape analysis of the crack inverse problem

Dorin Bucur[1]

The talk deals with the uniqueness and stability of the crack identification problem without *a priori* imposing any regularity of the unknown cracks (or cavities). Roughly speaking the problem can be formulated as follows: given a smooth bounded domain $\Omega \subset \mathbb{R}^2$, find a compact set $K \subset \Omega$ knowing the traces on the boundary $w_{i|\partial\Omega}$ of the solutions of

$$\begin{cases} -\Delta w_i = 0 & \text{in } \Omega \setminus K \\ \dfrac{\partial w_i}{\partial n} = 0 & \text{on } \partial K \\ \dfrac{\partial w_i}{\partial n} = \psi_i & \text{on } \partial\Omega \end{cases} \tag{11.1}$$

for *several inputs* ψ_i. It is known that one measure can not uniquely determine even a smooth curve K, and, following [1], two suitably chosen inputs can uniquely determine compact sets K which can be decomposed in a finite union of disjoint continua (see [1, 8]).

As a first purpose of the talk, we discuss the uniqueness of the detection by two boundary measurements for arbitrary compact sets. We prove that unique determination holds in the family of sets satisfying quasi-everywhere a regularity property, called conductivity. This property appears naturally in the study of the boundary behaviour of the conjugates of the solutions of (11.1). Roughly speaking, a set is conductive at a boundary point, if it is "rich" enough in a neighbourhood of that point. This regularity notion does not imply smoothness, and has rather to be compared to the Wiener criterion than to the usual regularity of the boundary. For example, the complement of a compact set composed by an infinite number of cracks (or cavities) of non-zero diameter is conductive at every boundary point. From a practical point of view, this could be interpreted in the following way: in order to be seen, a default should be "enough" thick in the sense of capacity, and this is particularly the case when defects are locally continua. Nevertheless, we give an example of a totally disconnected Cantor set, which is uniquely identifiable. For the proof of the unique identifiability by two boundary measurements we follow the idea of Alessandrini and Diaz Valenzuela based on non-existence of critical points of special holomorphic functions. Compared to the case of a finite number of cracks, two new difficulties appear. First, one has to give a variational sense to the harmonic conjugate of the solution of (11.1) and study its properties on the (non-smooth) boundary of K. Second, this function is not anymore continuous up to the defect K, hence information can not be propagated "across" the defect. For example, suppose that K_1 and K_2 are two compact sets giving the same measures. Contrary to the case of a finite number of cracks, the information given by the unique

[1]bucur@math.univ-metz.fr

continuation property is not exploitable in any connected region of $\overline{\Omega} \setminus (K_1 \cup K_2)$ which does not "touch" $\partial\Omega$.

The second purpose of the talk is to discuss the sequential stability of the detection: *close measures do give close cracks?* We underline the role of this stability result for understanding how geometric approximations of the cracks by finite elements converge (or not) to the real crack.

We refer to [2, 7], where the strong stability is obtained provided that the uniform Lipschitz character of all the cracks (or cavities) is a priori known. Moreover, in [2] the authors prove that their result is, in certain sense, optimal, as soon as the purpose is to give an estimation of the modulus of continuity of the mapping: *measures* $\mapsto$ *cracks*. Without uniform regularity assumptions on the cracks, there is no any estimate for the modulus of continuity of the direct problem.

The general scheme to discuss sequential stability relies on the Tikhonov principle: a continuous one to one functional from a compact set onto a metric space is a homeomorphism. The main difficulty is hidden into the continuity of this functional, which means the continuity of the direct problem: geometrically close defects do give close measures? For non-smooth defects with homogeneous Neumann boundary conditions (like in (11.1)) this is, in general, an open question. Only in two dimensions of the space the stability was recently proved for a similar problem in [4], provided that the number of the connected components of the varying defects is uniformly bounded.

Relying on this result, we prove that if the number of cracks or cavities is uniformly bounded, then sequential stability occurs without any further regularity assumption. This result can also explain how a "dense" curve can give measurements which are close to those given by a cavity (of strictly positive measure) or why two geometries which are *apparently* very different may give close measurements. Within this approach, even though we are not able to estimate the modulus of continuity of the inverse mapping, we can give a formal justification that finite element discretizations provide discretized solutions which are geometrically close to the real defects, regardless their regularity. This result is in a sense similar to the one obtained in [6] for shape optimization problems associated to the Dirichlet-Laplacian.

For more information about the crack identification problem, we refer to a recent survey by Bryan and Vogelius [3], where the reader can find a detailed description of the subject.

The results of presented in this talk were jointly obtained with Z. Belhachmi and N. Varchon.

Bibliography

[1] G. Alessandrini, A. Diaz Valenzuela. Unique determination of multiple cracks by two measurements. *SIAM J. Control Optim.* 34 (1996), no. 3, 913–921.

[2] G. Alessandrini, L. Rondi. Optimal stability for the inverse problem of multiple cavities, *J. Differential Equations*, 176, (2001), 2, 356–386.

[3] K. Bryan, M. Vogelius. A review of selected works on crack identification problem, IMA workshop on Geometric Methods in Inverse Problems and PDE Control 2001.

[4] D. Bucur, N. Varchon. A duality approach for the boundary variation of Neumann problems. *SIAM J. Math. Anal.* 34 (2002), no. 2, 460–477.

[5] D. Bucur, J.-P. Zolésio. N-Dimensional Shape Optimization under Capacitary Constraints. *J. Differential Equations,* **123** (2) (1995), 504–522.

[6] D. Chenais, E. Zuazua. Approximation par éléments finis de problèmes elliptiques d'optimisation de forme. *C. R. Math. Acad. Sci. Paris* 338 (2004), no. 9, 729–734.

[7] F. Friedman, M. Vogelius. Determining cracks by boundary measurements. *Indiana Univ. Math. J.* 38 (1989), no. 3, 527–556.

[8] H. Kim, J.K. Seo. Unique determination of a collection of a finite number of cracks from two boundary measurements. *SIAM J. Math. Anal.* 27 (1996), no. 5, 1336–1340.

Carleman estimates and null controllability properties for degenerate parabolic equations

P. Cannarsa[1] *P. Martinez*[2] *J.-P. Raymond*[3]
J. Vancostenoble[4]

Introduction

Motivated by a boundary layer model and the so-called Crocco equation, we study the controllability properties of some classes of degenerate parabolic equations. Since there are several degeneracies occurring in the Crocco equation, we consider some simplified problems, in order to separate the difficulties.

Because of the degeneracy of the problems, there are some particular behavior with respect to controllability properties that lead us to introduce non standard notions like *regional* null controllability in some cases or to derive new (global) Carleman estimates in some other cases.

12.1 A boundary layer model

The velocity field of a laminar flow on a flat plate can be described by the Prandtl equations [23]. For a two dimensional flow, these equations are stated in an unbounded domain $(0, L) \times (0, \infty)$, where $(0, L)$ represents the part of the plate where the flow is laminar, and $(0, \infty)$ represents the "thickness" of the boundary layer. The matching conditions with the external flow are stated at $+\infty$.

By using the so-called Crocco transformation, these equations are transformed into a nonlinear degenerate parabolic equation (the Crocco equation; see [23]) which is stated in a bounded domain $\Omega = (0, L) \times (0, 1)$. The linearization of the Crocco equation around a stationary solution

[1]cannarsa@mat.uniroma2.it
[2]martinez@mip.ups-tlse.fr
[3]raymond@mip.ups-tlse.fr
[4]vancoste@mip.ups-tlse.fr

is an equation of the form

$$\begin{cases} u_t + bu_x - au_{yy} + cu = g, & (x,y,t) \in \Omega \times (0,T), \\ u(x,0,t) = 0, & (x,t) \in (0,L) \times (0,T), \\ u_y(x,1,t) = \chi_{(x_0,x_1)}(x) f(x,t), & (x,t) \in (0,L) \times (0,T), \\ u(0,y,t) = u_1(y,t), & (y,t) \in (0,1) \times (0,T), \\ u(x,y,0) = u_0(x,y), & (x,y) \in \Omega, \end{cases} \tag{12.1}$$

where g and u_1 depend on the incident velocity of the flow, and where the function f is the control used to stabilize the velocity in the boundary layer. The coefficients a, b, and c are regular, but degenerate at the boundary of the domain [6, 5]. The perturbations of the velocity field in the boundary layer are controlled by a suction velocity f through the plate, localized on a slot (x_0, x_1).

Wellposeness of this model was studied in [5]. Moreover this linearized model has been used to study stabilization problems of boundary layers in [6, 4] where numerical experiments are presented.

12.2 Non degenerate parabolic equations

Before explaining our results, let us recall the main results for nondegenerate parabolic equations. Consider for example the following parabolic equation in $\Omega := (0,1)$:

$$\begin{cases} u_t - (a(x)u_x)_x = f(t,x)\chi_{(\alpha,\beta)}(x), & (t,x) \in (0,T) \times (0,1), \\ u(t,0) = u(t,1) = 0, & t \in (0,T), \\ u(0,x) = u_0(x), & x \in (0,1), \end{cases} \tag{12.2}$$

where $u_0 \in L^2(0,1)$ and $f \in L^2((0,T) \times (0,1))$.

After the pioneering works as [13, 14], there has been substantial progress in understanding the controllability properties of nondegenerate parabolic equations in recent years. A powerful new approach, based on suitable weighted estimates of Carleman type has been developed, see [16, 26]; see also [17] for an other approach of this problem. The theory has also been extended to semilinear problems, see for example [2, 3, 12, 15].

In the non degenerate case (i.e. $a > 0$ on $[0,1]$), (*classical*) null controllability is by now well-known : for all nonempty $(\alpha,\beta) \subset (0,1)$ and for all $T > 0$, there exists $f \in L^2((0,T)\times(0,1))$ such that the solution of (12.2) satisfies

$$u(T) \equiv 0 \ \text{ in the } \textit{whole} \text{ domain } (0,1). \tag{12.3}$$

Notice that there is a large literature on this problem when it is *not degenerate* and when Ω is a *bounded* set. On the other hand, to our knowledge, it seems that no result at all was known concerning a degenerate case.

12.3 A Crocco-type equation (with constant coefficients)

In [18], we first simplify the boundary layer problem by considering only a linearized Crocco-type equation with *constant* coefficients. The problem is described by a degenerate parabolic equation where phenomena of diffusion and transport are coupled :

$$u_t + u_x - u_{yy} = f\chi_\omega, \qquad (x,y,t) \in \Omega \times (0,T), \tag{12.4}$$

where $\Omega = (0, L) \times (0, T)$.

Due to transport phenomenon, the influence domain of the control $\chi_\omega f$ is not the whole domain Ω at time $T > 0$. Thus, we first show that (classical) null controllability does not occur.

For this reason, we introduce the notion of *regional* null controllability. More precisely, we study the following question: *for* $u_0 \in L^2(\Omega)$, $u_1 \in L^2((0,1) \times (0,T))$, *does there exist* $f \in L^2(\omega \times (0,T))$ *such that the solution* u *of* (12.4) *satisfies* $u(x, y, T) = 0$ *for* $(x, y) \in \Omega_C(T)$, *where* $\Omega_C(T)$ *denotes a part of* Ω*?*

As a first step, we give a geometric characterization of the influence domain of the control $\chi_\omega f$ in order to determine the region $\Omega_C(T)$ of Ω on which it will be possible to control $u(\cdot, T)$. Then we prove *regional* null controllability on the domain $\Omega_C(T)$.

12.4 A class of degenerate heat equation

Next we turn to a class of degenerate heat equations :

$$u_t - (a(x)u_x)_x = 0, \quad (t, x) \in (0, T) \times (0, 1), \tag{12.5}$$

Here the degeneracy comes from the fact that the coefficient a vanishes at a point of the boundary, since we assume

$$a > 0 \text{ on } (0, 1] \quad \text{and} \quad a(0) = 0.$$

We will see that the *degree of degeneracy* of the coefficient $a(x)$ plays a crucial role in the controllability properties : even if *(classical)* null controllability is in general false for the previous class of degenerate heat equations, it may be true in some cases depending on the degree of degeneracy of the coefficient.

Lack of (classical) null controllability for strong degeneracies

First we remark that the problem of null controllability for the *degenerate* heat equation (in bounded domain) is closely related to the same problem for the (non degenerate) heat equation in *unbounded* domain.

Consider the typical case $a(x) = x^\alpha$ with $\alpha > 0$, $\alpha \neq 2$. Then a standard change of variable transforms the degenerate parabolic equation

$$u_t - (au_x)_x = f\chi_\omega, \qquad x \in (0, 1), \tag{12.6}$$

set in the bounded space domain $(0, 1)$ into a (non degenerate) heat equation with a potential term:

$$U_t - U_{XX} + b(X)U = F\chi_{\tilde{\omega}}, \qquad x \in D, \tag{12.7}$$

set in the space domain $D := (0, 1/(1 - \alpha/2))$ if $\alpha < 2$ or $D := (0, +\infty)$ if $\alpha > 2$. The term $b(X)$ is *singular* if $\alpha < 2$ and *bounded* if $\alpha > 2$.

In particular, the *degenerate* heat equation (in bounded domain) is equivalent to a (non degenerate) heat equation in *unbounded domain* with a (regular) potential term in the case $\alpha > 2$.

Using a result of Escauriaza, Seregin and Šverák [10, 11], that generalizes a result of Micu and Zuazua [20, 21], we deduce from the previous remark that (classical) null controllability fails in general, at least for $a(x) = x^\alpha$ with $\alpha > 2$. (In this case however, one still can provide some results of *regional* null controllability [8]).

Classical controllability for "weakly" degenerate problems

Finally, we study the *classical* null controllability of the degenerate heat equation (12.5) when the degeneracy is not "too strong".

In the case $a(x) = x^\alpha$ with $\alpha < 2$, we prove that the degenerate parabolic equation that we consider is null controllable [9].

This result extends to general coefficients [19], under some weak assumption on the behavior of the function a near the point where it vanishes:

$$\frac{xa'(x)}{a(x)} \to \alpha \in [0, 2) \quad \text{as } x \to 0^+.$$

The proof follows from new Carleman estimates that take into account the fact that the operator $-(au_x)_x$ that we consider is not uniformly elliptic in the space domain $(0, 1)$. We derive these Carleman estimates using in particular Hardy type inequalities.

Bibliography

[1] P. Albano, P. Cannarsa. *Lectures on Carleman estimates for elliptic and parabolic operators and applications*, in progress.

[2] S. Anița, V. Barbu. *Null controllability of nonlinear convective heat equations*, ESAIM: Control, Optim, Calc. Var., Vol. 5, p. 157-173, 2000.

[3] S. Anița, D. Tataru. *Null controllability for the dissipative semilinear heat equation*, Appl. Math. Optim. 46 (2002), 97-105.

[4] J.-M. Buchot. *Stabilisation et contrôle optimal des équations de Prandtl*, Ph.D. thesis, E.N.S.A.E. Toulouse, Toulouse, France, 2002.

[5] J.-M. Buchot, J.-P. Raymond. *A linearized model for boundary layer equations*, in Optimal Control of Complex Structures, Internat. Ser. Numer. Math. 139, Birkhäuser, Basel, 2002, pp. 31–42.

[6] J.-M. Buchot, P. Villedieu. *Construction de modèles pour le contrôle de la position de transition laminaire-turbulent sur une plaque plane*, Technical report, 1/3754.00 DTIMT/T, 1999.

[7] M. Campiti, G. Metafune, D. Pallara. *Degenerate self-adjoint evolution equations on the unit interval*, Semigroup Forum, Vol. 57 (1998), 1-36.

[8] P. Cannarsa, P. Martinez, J. Vancostenoble. *Persistent regional null controllability for a class of degenerate parabolic equations*, Commun. Pure Appl. Anal. 3 (2004), no. 4, 607–635.

[9] P. Cannarsa, P. Martinez, J. Vancostenoble. *Carleman estimates for a class of degenerate parabolic operators*, SIAM J. Control Optim., to appear.

[10] L. Escauriaza, G. Seregin, V. Šverák. *Backward uniqueness for parabolic equations*, Arch. Ration. Mech. Anal. 169 (2003), no. 2, 147–157.

[11] L. Escauriaza, G. Seregin, V. Šverák. *Backward uniqueness for the heat operator in half-space*, St. Petersburg Math. J. 15 (2004), no. 1, 139–148.

[12] C. Fabre, J. P. Puel, E. Zuazua. *Approximate controllability for the semilinear heat equation*, Proceedings of the Royal Society of Edinburgh 125A (1995), 31-61.

[13] H. O. Fattorini, D. L. Russell. *Exact controllability theorems for linear parabolic equations in one space dimension*, Arch. Rat. Mech. Anal. 4 (1971), 272-292.

[14] H. O. Fattorini, D. L. Russell. *Uniform bounds on biorthogonal functions for real exponentials with an application to the control theory of parabolic equations*, Quarterly of Applied Maths, Vol. 32, p. 45-69, 1974.

[15] E. Fernández-Cara, E. Zuazua. *Null and approximate controllability for weakly blowing-up semilinear heat equations*, Annales de l'IHP, Analyse non-linéaire 17 (2000), 583-616.

[16] A. V. Fursikov, O. Yu. Imanuvilov. *Controllability of evolution equations*, Lecture Notes Series # 34, Research Institute of Mathematics, Global Analysis Research Center, Seoul National University, 1996.

[17] G. Lebeau, L. Robbiano. *Contrôle exact de l'équation de la chaleur*, Comm. P.D.E. 20 (1995), 335-356.

[18] P. Martinez, J.-P. Raymond, J. Vancostenoble. *Regional null controllability of a linearized Crocco type equation*, SIAM J. Control Optim., Vol. 42, no. 2, 709-728.

[19] P. Martinez, J. Vancostenoble. *Carleman estimates for degenerate heat equations*, Journal of Evolution Equations, to appear.

[20] S. Micu, E. Zuazua. *On the lack of null controllability of the heat equation on the half-line*, Trans. Amer. Math. Soc. 353 (2001), p. 1635-1659.

[21] S. Micu, E. Zuazua. *On the lack of null controllability of the heat equation on the half-space*, Portugaliae Math. Vol. 58, p. 1-24, 2001.

[22] L. Miller. *On the null-controllability of the heat equation in unbounded domains*, Bull. Sci. Math. 129 (2005), no. 2, 175–185.

[23] O. A. Oleinik, V. N. Samokhin. Mathematical Models in Boundary Layer Theory, Applied Mathematics and Mathematical Computation 15, 1999, Chapman and Hall/CRC, Boca Raton, London, New York.

[24] D. Tataru. *A-priori estimates of Carleman's type in domains with boundary*, Journal de Maths. Pures et Appliquées, 73 (1994), p. 355-387.

[25] D. Tataru. *Carleman estimates and unique continuation near the boundary for P.D.E.'s*, Journal de Maths. Pures et Appliquées, 75 (1996), p. 367-408.

[26] D. Tataru. *Carleman estimates, unique continuation and controllability for anizotropic PDE's*, Contemporary Mathematics 209 (1997), 267-279.

Inverse problems in electroencephalography

Maureen Clerc[1] *Théo Papadopoulo*[2] *Juliette Leblond*[3]

Introduction

Electroencephalography (EEG) allows the measurement of an electric potential due to brain activity, by means of electrodes placed on the scalp. The variations of potential are measured with a time resolution of the order of one millisecond. The ultimate goal of EEG analysis is to recover the spatiotemporal evolution of the brain activity. This activity can be modelled as a distribution of current dipoles $\mathbf{J}^{\mathrm{p}}$, located in the cortex, a thin layer of gray matter at the surface of the brain, and oriented perpendicularly to the cortical sheet. The relationship between the measured potential V and the cortical activity is given by the Poisson equation

$$\nabla \cdot (\sigma \nabla V) = \nabla \cdot \mathbf{J}^{\mathrm{p}} \ . \tag{13.1}$$

inside the head, with a vanishing Neumann boundary condition on the scalp, because the air around the head is non-conducting.

After presenting the solution of the forward EEG problem in Section 13.1, we describe three inverse problems arising in EEG analysis. Section 13.2 presents a conductivity estimation problem, which for the piecewise constant conductivity model can be regarded as a parameter calibration problem. Section 13.3 presents a Cauchy continuation problem, called *cortical mapping* in the context of brain imaging, which is an important first step for several methods of source localization. Section 13.4 presents a source estimation problem, for the particular case when the source is distributed on a surface. We conclude with a comment concerning the validation of the source localization problem.

13.1 The forward EEG problem

When the conductivity σ and the sources $\mathbf{J}^{\mathrm{p}}$ are known, the potential V solution of (13.1) is computed by solving a *forward EEG problem*, a well-posed problem, whose numerical solution relies on one of three types of methods: analytical, surface-based or volume-based.

- Analytical methods can be used for simple geometries, such as planes, spheres. Because of its simplicity, a head model which is often used in practice is a three-sphere head model, the inner (resp. middle, outer) sphere representing the brain (resp. skull, scalp).

[1]CERTIS-ENPC, Odyssée team, email: Maureen.Clerc@sophia.inria.fr
[2]INRIA Sophia Antipolis, Odyssée team
[3]INRIA Sophia Antipolis, APICS team

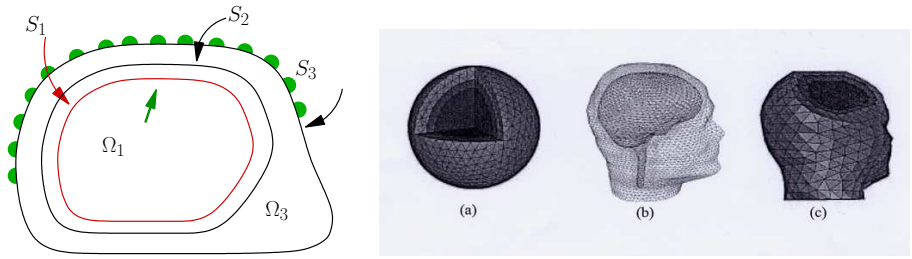

Figure 13.1: **Left:** *a slice through a three-layer model: the brain compartment is* Ω_1*, the skull is between surfaces* S_1 *and* S_2*, and the scalp between surfaces* S_2 *and* S_3*.* **Right:** *different geometries for discretizing the EEG problem (a) nested spheres (b) surface meshes (c) volume meshes.*

- Boundary Element Methods (BEM) are surface-based methods. Assuming a piecewise-constant conductivity, the unknowns are discretized on interfaces between volumes of constant conductivity [7, 8].
- Volume-based methods comprise the Finite Element and the Finite Difference methods (FEM, FDM). They are the most versatile of the three types of methods, since they do not impose a specific model for conductivity. The conductivity value can be defined element per element, and can even be tensor-valued in tissues with anisotropic conductivity. The white matter of the brain is an example of a tissue with anisotropic conductivity, due to many elongated fibers [9].

The major difficulty associated with the forward EEG problem is of a geometrical nature. Realistic head models are constructed by segmenting a Magnetic Resonance Image (MRI) of the subject. The meshing process involved is far from trivial, because it must accommodate for very intricate surfaces, and nevertheless have a high quality in terms of aspect ratio of its elements, and of topology, in order to be comply with numerical computations.

13.2 Conductivity estimation

Due to the gradually increasing precision of the EEG forward problem, and with the widespread use of realistic head models instead of the nested spheres, there is growing interest for a calibration of the head tissue conductivities. The relationship (13.1) suggests that the conductivity may be estimated by imposing a known source term $\mathbf{J}^{\mathrm{p}}$ and measuring the corresponding potential. If the source is localized inside the brain, its spatial characteristics must be estimated independently. Magnetoencephalography (MEG) offers the possibility of localizing the source independently from the EEG, and with less dependence on the conductivity parameters [6]. Rather than imposing a source inside the brain, it is simpler to impose a current on the scalp, a technique known as *Electrical Impedance Tomography*. In the particular case of head conductivity estimation, the boundaries between constant conductivity tissues can be extracted from the segmentation of an MRI. Suppose a scalar conductivity in each tissue, we have developed an iterative estimation procedure based on a Boundary Element discretization of the forward EIT problem:

$$\nabla \cdot (\sigma \nabla V) = 0 \tag{13.2}$$

and $\sigma \frac{\partial V}{\partial n} = j$ on the scalp, where j is the impressed current. Using a gradient descent approach, the scalp-to-skull conductivity ratio can be estimated [5].

13.3 The Cauchy problem in EEG

Several source reconstruction methods for EEG [2, 3] assume the knowledge of Cauchy data on the boundary of the innermost volume containing the sources - the surface denoted S_1 in Figure 13.1 (*left*). This implies the propagation to S_1 of Cauchy data which is only partially known on the scalp S_N: indeed, $\partial_{\mathbf{n}} V = 0$ on all of S_N, but V is only known at the discrete positions of the scalp electrodes. We have recently proposed two different methods to tackle the EEG Cauchy continuation problem from the scalp to the cortical surface: one using the Boundary Element Method, and the second one using a Bounded Extremal Problem [4].

13.4 Source estimation

The sources of electrical activity in the brain can be modeled either as a linear combination of dipolar sources, or as a volume or surface distributions. We restrict our analysis to sources distributed on a prescribed surface, and oriented perpendicularly to it. For exact measurement of V over a dense region on the scalp, this inverse problem has a unique solution, up to a constant normal distribution.

We have developed a source estimation procedure which works directly with measurements on the scalp, and does not require an initial Cauchy data propagation step as in Section 13.3. A natural approach to find the source distribution is to minimize a cost function $C(\mathbf{J}^{\mathrm{p}}) = \|V_{\mathrm{meas}} - V(\mathbf{J}^{\mathrm{p}})\|$, where V_{meas} represents the measured potential, and $V(\mathbf{J}^{\mathrm{p}})$ represents the solution of (13.1) with a vanishing Neumann boundary condition on the scalp. The instability of the inverse problem however imposes a regularization in the source reconstruction, either by requiring the source $\mathbf{J}^{\mathrm{p}}$ to belong to a subspace, or by adding a regularizing term to the cost. A disadvantage of many regularization methods, such as Tikhonov or Minimum Norm solutions, is that they tend to produce very blurred solutions, and are unable to cope with sharp discontinuities. In image processing, a remedy is to penalize the cost with a L^p norm of the image gradient. Incorporating such a regularization in the EEG inverse problem, by controlling a L^1 norm of the source distribution gradient indeed provides a solution with an enhanced spatial resolution [1].

13.5 Validation

The validation of the source localization problem is a difficult task, because very little is known on the actual spatio-temporal behavior of the electrical sources of the brain. Phantom models can help validate algorithms, but their electrical properties are rather far from reality. Simultaneous intracranial and extracranial recordings are sometimes performed in pathological cases. Such recordings are very useful to validate localization methods, with a limit however due to the scarceness of the spatial sampling. Perhaps the most promising strategy for validation is a multimodal approach, combining different brain imaging modalities – EEG, MEG, PET, MRI, with neurophysiologists and neuropsychologists' expertise.

Bibliography

[1] G. Adde. *Méthodes de traitement d'image appliqués au problème inverse en Magnéto-Electro-Encéphalographie*. PhD thesis, Ecole Nationale des Ponts et Chaussées, 2005.

[2] A. El Badia and T. Ha-Duong. An inverse source problem in potential analysis. *Inverse Problems*, 16:651–663, 2000.

[3] L. Baratchart, J. Leblond, and J.-P. Marmorat. Inverse source problem in a 3D ball from best meromorphic approximation on 2D slices. *Electronic Transactions in Numerical Analysis*, 2006. to appear.

[4] M. Clerc, B. Atfeh, J. Leblond, L. Baratchart, J.-P. Marmorat, T. Papadopoulo, and J. Partington. The cauchy problem applied to cortical imaging: comparison of a boundary element and a bounded extremal problem. In Christoph Michel D. Brandeis, T. Koenig, editor, *Brain Topography*, volume 18. Springer Science and Business Media B.V., October 2005.

[5] M. Clerc, J.-M. Badier, G. Adde, J. Kybic, and T. Papadopoulo. Boundary element formulation for electrical impedance tomography. In *ESAIM: Proceedings*, volume 14, pages 63–71. EDP Sciences, September 2005.

[6] S. Gonçalves, J.C. de Munck, J.P. Verbunt, R.M. Heethaar, and F.H. Lopes da Silva. In vivo measurement of the brain and skull resistivities using an EIT-based method and the combined analysis of SEF/SEP data. *IEEE Transactions on Biomedical Engineering*, 50(9):1124–8, September 2003.

[7] J. Kybic, M. Clerc, T. Abboud, O. Faugeras, R. Keriven, and T. Papadopoulo. A common formalism for the integral formulations of the forward EEG problem. *IEEE Transactions on Medical Imaging*, 24(1):12–28, January 2005.

[8] J. Kybic, M. Clerc, O. Faugeras, R. Keriven, and T. Papadopoulo. Generalized head models for MEG/EEG: boundary element method beyond nested volumes. *Phys. Med. Biol.*, 51:1333–1346, 2006.

[9] D.S Tuch, V.J. Wedeen, A.M. Dale, J.S. George, and J.W. Belliveau. Conductivity tensor mapping of the human brain using diffusion tensor MRI. In *Proceedings of the National Academy of Sciences*, volume 98, pages 11697–11701, 2001.

A soliton-based analysis of the arterial blood pressure

E. Crépeau[1] *T.M. Laleg*[2] *M. Sorine*[3]

Abstract

A model-based signal analysis of the arterial blood pressure (ABP) is proposed. The objective is to estimate some characteristics of the ABP pulse waveform from non-invasive measurements for clinical interpretations. The blood is considered as an incompressible fluid in an elastic vessel modelled by some one-dimensional Navier-Stokes equations. Analysis of the pressure pulse waveform consists in identifying the parameters of a reduced model of the ABP based on an integrable approximation of these Navier-Stokes Equations. This ABP model is a superposition of a forward N-soliton of a Korteweg de Vries equation with a windkessel flow. The soliton takes into account fast phenomena which predominate during the systolic phase and the windkessel model represents slow phenomena during the diastolic phase. Some promising results obtained with this model-based signal processing method are presented.

14.1 Introduction

The cardiovascular system is composed of the heart and of a complex vascular network, organised into vascular compartments. It supplies tissues with oxygen, nutrients and to remove carbon dioxide and other catabolits. Pressure and flow waves are created by the beating heart and propagate through the aorta and the major arteries to the periphery. The pulse pressure (PP) plays an important role in the circulatory system. It undergoes an increase in its amplitude and a decrease in its width when it propagates along the arterial tree as it is shown in Figure 14.1. These observed phenomena which are called respectively "Peaking" and"Steepening", are often explained by the existence of reflected waves so that the PP is usually decomposed into forward and backward waves associated to some linearized model [8]. Here, they will be associated to some nonlinear waves. Models proposed to describe the blood pressure in cardiovascular compartments are of two types:
– Lumped models (0D models) [7] are built by analogy with electrical circuits. They are simple and explain the global behavior of the vascular compartment with a small number of parameters having a physiological meaning. They do not explain the propagation phenomena nor the peaking and the steepening.
– Distributed models (1D, 2D and 3D models) [3] use the principles of computational fluid

[1]UVSQ, emmanuelle.crepeau@math.uvsq.fr
[2]INRIA Rocquencourt, Taous-Meriem.Laleg@inria.fr
[3]INRIA Rocquencourt, Michel.Sorine@inria.fr

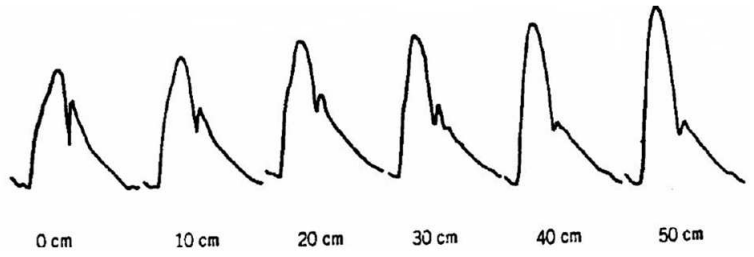

Figure 14.1: *Propagation of a pressure pulse along the arterial tree.*

dynamic. They can explain the observed phenomena but are too complex, especially in 3D, for signal processing applications.

14.2 Governing equations

The blood is considered as an incompressible fluid in a long, straight, circular homogeneous, thin walled elastic tube. The flow is modelled by the following one-dimensional Navier-Stokes equations, T and Z being respectively the time and space variables:

$$A_T + Q_Z = 0, \tag{14.1}$$

$$Q_T + \left(\frac{Q^2}{A}\right)_Z + \frac{A}{\rho}P_Z + \nu\frac{Q}{A} = 0. \tag{14.2}$$

where, $A(T,Z)$ is the cross-sectional area of the vessel, $Q(T,Z)$ is the blood flow and $P(T,Z)$ is the blood pressure. Moreover ρ is the blood density and ν a coefficient of viscosity of blood. Furthermore, the motion of the wall satisfies, (see for example [10])

$$\frac{\rho_w h_0 R_0}{A_0} A_{TT} = P - P_0 - \frac{h_0}{R_0}\sigma \tag{14.3}$$

where, ρ_w is the wall density, P_0 is the pressure outside the tube, taken in the following as a reference value. h_0 and R_0 denote respectively the mean mean thickness of the wall and the mean inner radius of the tube, and $A_0 = \pi R_0^2$. Moreover, σ is the extending stress in the tangential direction. Remark that usually the term $\frac{\rho_w h_0 R_0}{A_0} A_{TT}$, leading to the classical "Laplace law". This system is completed by a model of the local compliance of the vessels, a state equation, where $\Delta A = A - A_0$, E being the coefficient of elasticity.

$$\sigma = E\frac{\Delta A}{2A_0}. \tag{14.4}$$

14.3 A reduced model of the ABP

We first rewrite system (14.1)-(14.4) in non-dimensional variables in order to use some singular perturbation technique to separate slow and fast modes in the pressure. Let

$$Z = Lz,\ T = \frac{L}{c_0}t$$

where L is the typical wave length of the waves propagating in the tube and $c_0 = \sqrt{\frac{Eh_0}{2\rho R_0}}$ is the typical Moens-Korteweg velocity of a wave propagating in an elastic tube, when all nonlinear

terms are neglected. We suppose that $\epsilon = \left(\frac{R_0}{L}\right)^{2/5} << 1$. Let us rescale pressure, blood flow and cross-sectional area:

$$P - P_0 = \rho c_0^2 p, \quad Q = A_0 c_0 q, \quad A = A_0(1+a),$$

We get the following system, where, by hypothesis, $\frac{\rho_w h_0 R_0}{\rho L^2} = O(\epsilon^5) = \lambda\epsilon^5$:

$$a_t + q_z = 0, \tag{14.5}$$

$$q_t + \left(\frac{q^2}{1+a}\right)_z + (1+a)p_z = -\eta\frac{q}{1+a}, \tag{14.6}$$

$$\lambda\epsilon^5 a_{tt} + a = p. \tag{14.7}$$

Fast time behaviour. In fast time, corresponding to the Pulse Transit Time (PTT), we look for a solution with the following asymptotic expansion in terms of ϵ [2],

$$a(t,z) = \sum_{k\geq 1} \epsilon^k [a^k(\frac{t-z}{\epsilon^2}, \frac{z}{\epsilon}, t, z)],$$

$$p(t,z) = \sum_{k\geq 1} \epsilon^k [p^k(\frac{t-z}{\epsilon^2}, \frac{z}{\epsilon}, t, z)],$$

$$q(t,z) = \sum_{k\geq 1} \epsilon^k [q^k(\frac{t-z}{\epsilon^2}, \frac{z}{\epsilon}, t, z)].$$

The following new variables are used in the PTT boundary layer

$$\tau_1 = \frac{t-z}{\epsilon^2}, \; \xi_1 = \frac{z}{\epsilon}.$$

Remark that this choice of variables implies that we consider only waves moving from the left to the right. If we keep both directions, we get a Boussinesq type model as for example in [6]. Remark also that we have chosen $\epsilon = \left(\frac{R_0}{L}\right)^{2/5}$ instead of $\epsilon = \frac{R_0}{L}$ as commonly done [1] so that the acceleration term in (14.7) does not disappear in the sequel. Thus equations (14.5)-(14.7) become (at the second order of ϵ),

$$q^1 = p^1 = a^1, \quad 2q^1_{\xi_1} - 3q^1 q^1_{\tau_1} - \lambda q^1_{\tau_1\tau_1\tau_1} = 0. \tag{14.8}$$

In fast times, and in a boundary layer, p^1 is solution of a Korteweg-de Vries equation. In initial variables, we have the following KdV equation, with Z in the real line, for the fast blood pressure $P^S(T,Z) = \rho c_0^2 p^1(\frac{c_0 T - Z}{L\epsilon^2}, \frac{Z}{L\epsilon})$,

$$P^S_Z + d_0 P^S_T + d_1 P^S P^S_T + d_2 P^S_{TTT} = 0, \tag{14.9}$$

with

$$d_0 = \frac{1}{c_0}, \quad d_1 = -\frac{3}{2}\frac{1}{A_0 c_0^2}, \quad d_2 = -\frac{\rho_w h_0 R_0}{2\rho c_0^3}.$$

Here the superscript S denotes that we are interested in soliton solutions of (14.9). The blood flow, Q^1, and the cross sectional area ΔA^1 are also solutions of Korteweg-de Vries equations in the same boundary layer.

Usually, with the available measurements (e.g. given by a FINAPRES sensor), we get the pressure at a localized point, for example the finger, and as a function of time. Thus, it is useful to get, not a time-evolution equation as usual, but a space-evolution equation as obtained in (14.9).

Slow time behaviour. Equation (14.9) describes rather fast traveling waves (3-10 m/s). After the PTT, these waves have gone across the compartment and there is still a slowly varying flow that appears as some kind of parabolic flow obtained by neglecting, for large time, the acceleration terms in (14.2). As this component will later well approximated by a classical windkessel model, we use the superscript wk for it, leading to the decomposition:

$$P(Z,T) = P^S(Z,T) + P^{wk}(Z,T) \tag{14.10}$$

$$A^{wk}_T + Q^{wk}_Z = 0, \tag{14.11}$$

$$\frac{A_0}{\rho} P^{wk}_Z + \nu \frac{Q^{wk}}{A^{wk}} = 0, \tag{14.12}$$

$$\Delta P^{wk} - \frac{h_0 E}{2A_0\rho_0} \Delta A^{wk} = 0 \tag{14.13}$$

The boundary conditions in (14.1), (14.2) are now necessary: they describe the pressure-flow relationships using the vascular proximal and distal impedances R_H and R_p in $Z = 0$ and $Z = l$. We get the following parabolic equation in P^{wk},

$$P^{wk}_T - \frac{A_0 h_0 E}{2\rho\nu R_0} P^{wk}_{ZZ} = 0, \tag{14.14}$$

$$-R_H(P^S(0,T) + P^{wk}(0,T))_Z + P^S(0,T) + P^{wk}(0,T) = 0, \tag{14.15}$$

$$R_p(P^S(l,T) + P^{wk}(l,T))_Z + P^S(l,T) + P^{wk}(l,T) = 0 \tag{14.16}$$

14.4 N-soliton+windkessel approximation of the ABP

N-soliton approximation of P^S. Let $\xi = t - d_0 z$, $\tau = d_2 z$ and $y = \frac{d_1}{6d_2} P^S$, so that equation (14.9) becomes a normalized KdVE:

$$y_\tau + 6yy_\xi + y_{\xi\xi\xi} = 0, \quad y(\xi, 0) = y_0(\xi). \tag{14.17}$$

The N-soliton solutions of the KdVE (14.17) will be used here. Their analytical expression is given by the Inverse Scattering Technique (see e.g. [9]):

$$y(\xi,\tau) = 2\frac{\partial^2(\ln\det(\mathbf{M}))}{\partial\xi^2}, \tag{14.18}$$

where $\mathbf{M}$ is a $N \times N$ matrix with coefficients given by:

$$M_{mk} = \delta_{mk} + \frac{2a_m}{a_m + a_k} f_m, \quad m,\ k = 1...N \tag{14.19}$$

where δ_{mk} is the Kronecker symbol and

$$f_m(\xi,\tau) = \exp[-a_m(\xi - s_m - a_m^2\tau)], \quad (a_m, s_m) \in \mathbb{R}^+ \times \mathbb{R}$$

We note $P^{NS}(Z,T)$ the corresponding soliton in the original variables.

The solitons have some interesting characteristics for the present application: the velocity of a soliton is proportional to its amplitude; after collision between solitons, their individual

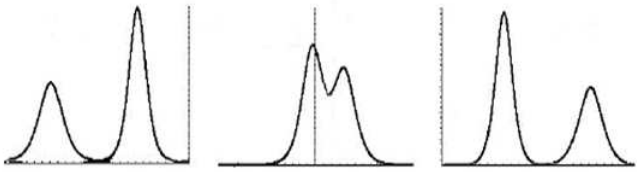

Figure 14.2: *Propagation of a 2-soliton.*

shape and velocity are preserved; a N-soliton has N components of different heights traveling with different velocities while interacting. This is illustrated Figure 14.2.

From real data, it can be noticed that the ABP can be approximated by 2 or 3-solitons.

The introduction of solitons can explain the observed phenomena. The "Peaking" can be explained by the increase in the soliton velocity which leads to an increase in its amplitude. The increase in the velocity results from the changes in the vessel characteristics (the increase in stiffness and the decrease in section). The "Steepening" can be explained by the conservation laws: the increase in the amplitude leads to a decrease in the width.

0D approximation of P^{wk}. A low frequency approximation of (14.14, 14.16) gives a 2 or 3 -element windkessel system for each measurement position, $Z = Z_m$, see for example [4, 5]:

$$\frac{dP_{wk}(t)}{dt} + \frac{P_{wk}(t)}{R_p C} = \frac{P_\infty}{R_p C} + \frac{P^{NS}(Z_m, t)}{R_H C} \tag{14.20}$$

where C and P_∞ are respectively the arterial compliance and the asymptotic pressure (teledi-astolic value).

Therefore, we propose to estimate the measured ABP as the sum of a N-soliton describing fast phenomena and a windkessel model ($P_{wk}(t)$) representing slow phenomena.

$$\hat{P}(Z_m, t) = P^{NS}(Z_m, t) + P_{wk}(t) \tag{14.21}$$

14.5 Numerical results

The identification is done for a 2 or 3-solitons and a 2-element windkessel. Identifiability of 2 and 3 solitons has been studied in [2]. The Figure 3 illustrates the rather good results obtained from real ABP data measured at the finger level with a FINAPRES.

Conclusion

We have proposed a reduced model of ABP based on an integrable approximation of Navier-Stokes equations. The ABP is estimated as the sum of a 2 or 3-soliton and a 2-element windkessel model. Unlike the linear approach which necessitates simultaneous blood pressure and flow measurements, the proposed model requires only pressure measurements. Its depends on few number of parameters and it seems that these results on ABP waveform analysis can lead to some interesting clinical applications, in particular in the systolic phase, where a new description of the pressure pulse contour has been given.

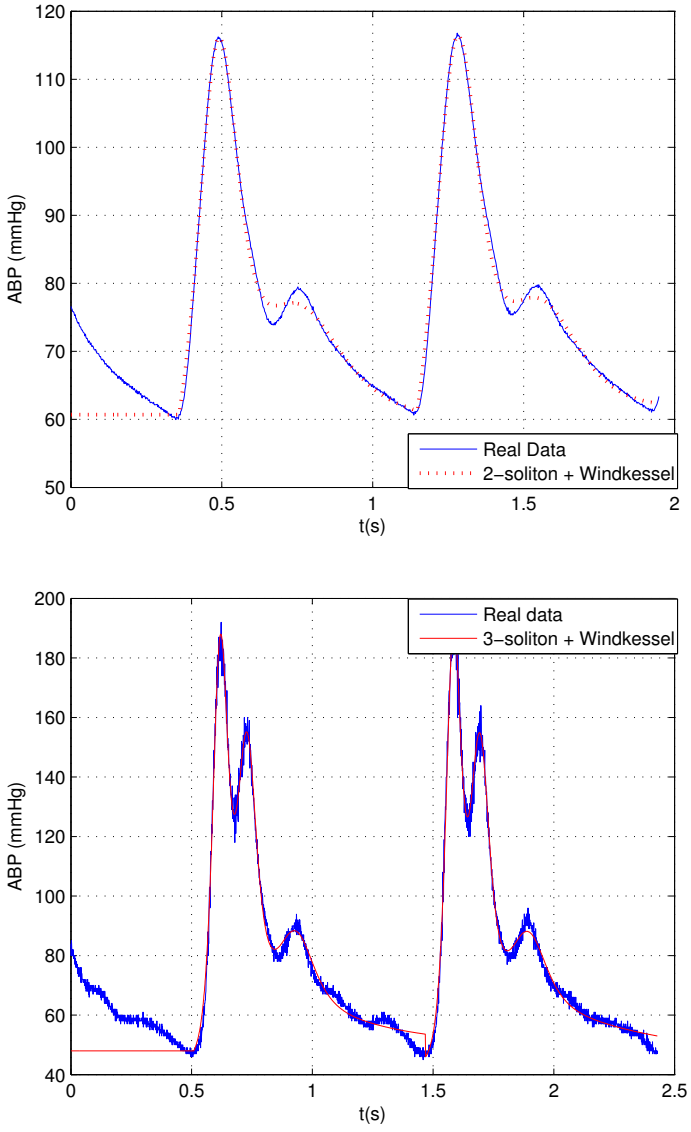

Figure 14.3: *Pressure at the finger: real and estimated data.*

Bibliography

[1] S. Canic and A. Mikelic. Effective equations modeling the flow of a viscous incompressible fluid through a long elastic tube arising in the study of blood flow through small arteries. *SIAM J. Applied Dynamical Systems*, 2:431–463, 2003.

[2] E. Crépeau and M. Sorine. Identifiability of a reduced model of pulsatile flow in an arterial compartment. *IEEE CDC and ECC*, 2005.

[3] D.A. McDonald. *Blood flow in arteries*. Edward Arnold, 2nd edition, 1974.

[4] A. Monti, C. Médigue, and M. Sorine. Short-term modelling of the controlled cardiovascular system. *ESAIM: Proceedings*, 12:115–128, 2002.

[5] M.S. Olufsen and A. Nadim. On deriving lumped models for blood flow and pressure in the systemic arteries. *Mathematical Biosciences and Engineering*, 1:61–80, 2004.

[6] J.F. Paquerot and M. Remoissenet. Dynamics of nonlinear blood pressure waves in large arteries. *Physics Letters A*, 194:77–82, 1994.

[7] N. Stergiopulos, B.E. Westerhof, and N. Westerhof. Total arterial inertance as the fourth element of the windkessel model. *The American Physiological Society*, pages 81–88, 1999.

[8] N. Westerhof, P. Sipkema, G.C. Van Den Bos, and G. Elzinga. Forward and backward waves in the arterial system. *Cardiovascular Research*, 6:648–656, 1972.

[9] G.B. Whitham. *Linear and nonlinear Waves*. J.Wiley & sons, 1999.

[10] S. Yomosa. Solitary waves in large vessels. *Journal of the Physical Society of Japan*, 50(2):506–520, 1987.

On the Mathematical Analysis and Numerical Simulations of Some Direct and Inverse Problems in the Seawater Intrusion

Mohamed El Alaoui Talibi[1] *M.H. Tber*[2]

15.1 Introduction

Coastal aquifers serve as major sources for fresh water supply in many countries around the world, especially in arid and semiarid zones. In these areas, groundwater usually flows into the sea. As the specific gravity of sea water is larger than that of fresh one, the sea water rests under the fresh water like a wedge (see figure 15.1). When the fresh water in confined or unconfined aquifer is overpumped, its hydraulic head may be dropped drastically. Then a series of problems will be generated, the sea water may intrude the land, the fresh water in the wells may be salted, and the aquifers and cultivated horizons may be destroyed. Thus the development and utilization of groundwater in coastal areas must be managed in rational way in order to prevent sea water intrusion. If this intrusion happened, measures should be taken to remedy it, such as the control of water supply, artificial recharge and the building of hydraulic barriers. For this purpose, it is necessary to use mathematical models to simulate the phenomena and make quantitative estimations of the effects of various management decisions and engineering installations.

The main approaches that have been used to analyze salt water intrusion in coastal aquifers are the dispersive model and the sharp interface. While the disperse-interface model accounts for presence of a transition zone of mixed salt and fresh water, the sharp interface idealization simplifies the analysis by assuming that the transition zone is thin relative to the dimension of the aquifer which reproduces the general position, shape, and behavior of the interface.

The sharp-interface model based on the two-fluid approach is widely used in practice, but there is not, in our knowledge, any rigorous mathematical analysis of problems related to this model, especially inverse problems. In fact, although the groundwater parameters estimation has received substantial attention in the water resources literature (see e.g, [4]), a few works have been interested to the intrusion problem where parameters, particularly with discontinuous coefficients, depend on hydraulic head of two fluids (see [3]).

In this talk we present a mathematical and numerical results for some direct and inverse problems issued from the problem of seawater intrusion in a coastal aquifers. Our principal

[1]elalaoui@ucam.ac.ma
[2]tber.hicham@ucam.ac.ma

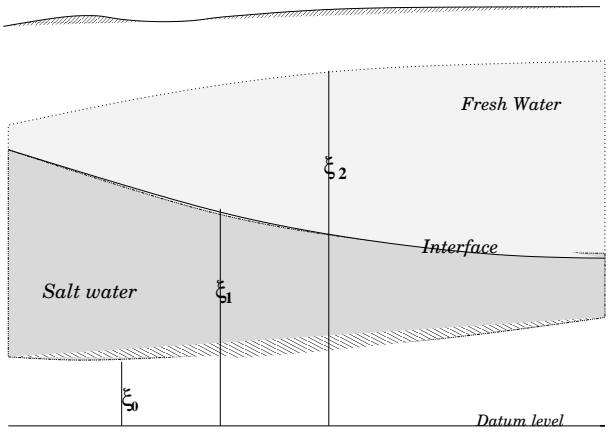

Figure 15.1: *Saltwater intrusion phenomena*

aim is to identify some parameters like hydraulic conductivities and storativity. We consider the sharp interface model and formulate the problem as an optimal control one. The state equations are nonlinear and of degenerate type. We then first give an existence and uniqueness result in the steady state case and an existence result for the unsteady problem. The identification problem is considered and studied in the too cases. Many numerical results, using the gradient method, are presented.

15.2 Steady State Problem

Let us consider the flow of fresh and salt groundwater, separated by sharp interface, in a confined aquifer, bounded by two, approximately horizontal, impermeable layers. Substitution of Darcy's law let us consider the flow of fresh and salt groundwater, separated into the equations of continuity of the two fluids (fresh and salt) leads to the following system of coupled partial differential equations [1]:

$$\begin{cases} -\operatorname{div}(k_f(x)B_f(x,h_f,h_s)\nabla h_f) = Q_f & \text{on } \Omega \\ -\operatorname{div}(k_s(x)B_s(x,h_f,h_s)\nabla h_s) = Q_s & \text{on } \Omega \end{cases} \tag{15.1}$$

where Ω is an open bounded domain of $\mathbf{R}^2$ with piecewise smooth boundary Γ; h_f is the fresh-water head; h_s is the salt water head; Q_f and Q_s are supply functions representing a distributed surface supply of salt and fresh water into the aquifer; k_f and k_s are two positive functions representing the hydraulic conductivities or transmissivities; $B_f(x,h_f,h_s)$ and $B_s(x,h_f,h_s)$ represent the thicknesses of fresh-water and salt-water respectively, such that:

$$B_f(x,h_f,h_s) = \xi_2(x) - \xi_1(x), \tag{15.2}$$

$$B_f(x,h_f,h_s) = \xi_1(x) - \xi_0(x), \tag{15.3}$$

where ξ_0 and ξ_2 are the depths of the lower and the upper surfaces of the aquifer, respectively; ξ_1 is the interface depth given by the following relation:

$$\xi_1(x) = (1+\delta)h_s - \delta h_f, \tag{15.4}$$

where $\delta = \dfrac{\rho_f}{\rho_s - \rho_f}$ is the relative density with ρ_f and ρ_s are the fresh and salt water densities.

Two approximations that are commonly used in groundwater and salt water intrusion studies have been made here. Firstly, the Dupuit hydraulic assumption is employed to vertically integrate the flow equation, reducing it from three-dimensional geometry to two-dimensional. Secondly the aquifer storativity is ignored such that the governing equations becomes time independent [3].

To resolve the system we consider the nonhomogeneous Dirichlet boundary conditions as follows:

$$\begin{cases} h_f = g_f & \text{on } \Gamma \\ h_s = g_s & \text{on } \Gamma \end{cases}$$

We suppose that $Q = (Q_f, Q_s) \in L^4(\Omega)^2$, $(\xi_0, \xi_2) \in L^2(\Omega)^2$ and $g = (g_f, g_s) \in H^1(\Omega)^2$. We also set $V_g = V_g^f \times V_g^s$, where $V_g^t = H_0^1(\Omega) + g_t$ $(t = f, s)$.

The variational formulation of the problem can then be written as follows:

$$\begin{cases} \text{Find } \ h = (h_f, h_s) \in V_g \text{ such that} \\ \displaystyle\int_\Omega k_f(x) B_f(x, h_f, h_s) \nabla h_f \nabla \varphi_f \ = \int_\Omega Q_f \varphi_f \qquad \forall \varphi_f \in H_0^1(\Omega) \\ \displaystyle\int_\Omega k_s(x) B_s(x, h_f, h_s) \nabla h_s \nabla \varphi_s \ = \int_\Omega Q_f \varphi_s \qquad \forall \varphi_s \in H_0^1(\Omega) \end{cases} \tag{15.5}$$

Thus to identify the transmissivities k_f and k_s from the water-head observations, we introduce the following optimization problem:

$$(O) \begin{cases} \text{Find} \quad (k_f^*, k_s^*) \in U_{ad} \qquad \text{such that} \\ J(k_f^*, k_s^*) = \inf\limits_{(k_f, k_s) \in U_{ad}} J(k_f, k_s) \end{cases}$$

where

$$J(k_f, k_s) = \frac{1}{2} \| h_f(k_f, k_s) - \overline{h}_f \|^2_{L^2(\Omega)} + \frac{\text{Index}}{2} \| h_s(k_f, k_s) - \overline{h}_s \|^2_{L^2(\Omega)}$$

with (h_f, h_s) is the solution of the problem (15.5), $(\overline{h}_f, \overline{h}_s)$ is the observed data, and $Index \in \{0, 1\}$. We set $Index$ equal zero when we have no salt-water informations. In fact, it is practically expensive to obtain salt water head observations since it requires extra wells that penetrate deeper into the salt water region.

U_{ad} is closed bounded set of the space of the functions of bounded variation in Ω defined by

$$U_{ad} = \left\{ (k_f, k_s) \in (BV(\Omega) \cap L^\infty(\Omega))^2, \alpha \le k_t \le \beta \text{ and } TV(k_t) \le c \ (t = f, s) \right\}$$

with α, β and c are positive constants, $(BV(\Omega), \|.\|_{BV(\Omega)})$ is the Banach space of bounded variation functions and $TV(k_t)$ is the total variation of k_t.

Using a fixed point argument, we prove an existence result of a weak solution. The L^∞ estimates were obtained via a maximum principle established by Stampacchia's technique. The uniqueness of the solution is shown by the transposition method. Thanks to the properties of the space of functions with bounded variation, we show the existence of an optimal control. The optimality conditions are derived by the classical Lagrangian method. From a numerical point of view, the ill posedness of the problem and the multiple minima difficulties are addressed through a combination of Thikhonov or total variation regularization with an hierarchical parametrization procedure.

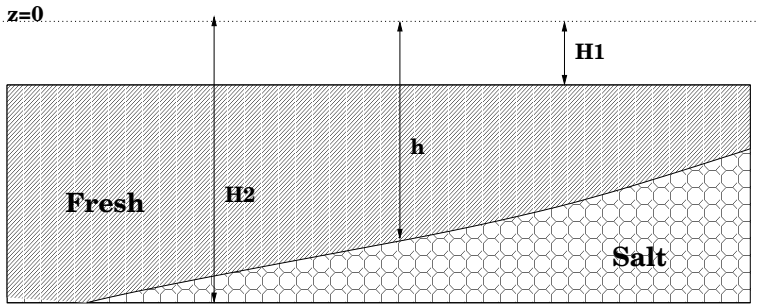

Figure 15.2: *Saltwater intrusion phenomena*

15.3 Unsteady problem

We consider the flow of fresh and salt groundwater, separated by a sharp interface, in a confined aquifer. The aquifer is bounded by two approximately horizontal and impermeable layers (Figure 15.2). The lower and upper surfaces of the aquifer are described by $z = -H_2$ and $z = -H_1$, respectively.

For this problem we introduce the practical change of functions and notations of [2] lead to the following system of coupled partial differential equations :

$$\begin{aligned} S(x)\partial_t h - \operatorname{div}(\alpha k(x) T_s(h)\nabla h) + \operatorname{div}(k(x)T_s(h)\nabla\varphi) &= -Q_s \\ -\operatorname{div}(k(x)T_a\nabla\varphi) + \operatorname{div}(\alpha k(x)T_s(h)\nabla h) &= Q_f + Q_s \end{aligned} \tag{15.6}$$

for $(x,t) \in \Omega_T := \Omega \times J$ with $J =]0,T[$ and Ω is an open bounded domain of $\mathbb{R}^2$, describing the projection of the porous medium on the horizontal plane $z = 0$, with a smooth boundary $\Gamma = \Gamma_D \cup \Gamma_N$. Here $T_a = H_2 - H_1$ is the thickness of the aquifer, $T_s = H_2 - h$ is the thickness of saltwater zone, k is the hydraulic conductivity, S is the storativity of the aquifer, α is a positive constant representing the relative density difference, φ is the freshwater hydraulic head, h is the depth of the interface and where I_f and I_s are supply functions, representing distributed surface supply of fresh and saline water into the aquifer.

Introducing the new variables $f = \dfrac{\varphi}{\alpha}$ and $K = \alpha k$ leads to the following system:

$$\begin{aligned} S(x)\partial_t h - \operatorname{div}(K(x) T_s(h)\nabla h) + \operatorname{div}(K(x)T_s(h)\nabla f) &= -Q_s \\ -\operatorname{div}(K(x)T_a\nabla f) + \operatorname{div}(K(x)T_s(h)\nabla h) &= Q_f + Q_s \end{aligned} \tag{15.7}$$

The boundary conditions are

$$\begin{aligned} h = h_D,\, f = f_D \quad &\text{on } \Gamma_D \\ (K(x)T_s(h)\nabla h - K(x)T_s(h)\nabla f)\cdot\overrightarrow{n} = 0 \quad &\text{on } \Gamma_N \\ (K(x)T_a\nabla f - K(x)T_s(h)\nabla h)\cdot\overrightarrow{n} = 0 \quad &\text{on } \Gamma_N \end{aligned} \tag{15.8}$$

where f_D and h_D are given functions, and $\overrightarrow{n}$ is the outward unit normal to Γ. The initial condition is

$$h(x,0) = h_0(x), \quad x \in \Omega. \tag{15.9}$$

Under physical assumptions, we prove an existence result of a weak solution for the parabolic-elliptic system (15.7). The difficulty of the degeneracy, due to the possibility to have no salt water in some zone of the aquifer, is handled using a regularization technique. The adoption of the freshwater head and the interface depth as unknown variables enabled us to find a relation

between the diffusion coefficients and consequently to draw up the necessary estimates in spite of the strong coupling between the two system equations. A numerical code based on this analytical study is developed. In addition, we made a numerical simulation of the simultaneous identification of the hydraulic conductivity and the effective porosity.

Bibliography

[1] J. Bear, A. H-D. Cheng, S. Sorek, D. Ouazar and I. Herrera (Eds.). *Seawater Intrusion in Coastal Aquifers - Concepts, Methods and Practices*, Kluwer Academic Publishers, Netherlands, 1999.

[2] J. Bear, A.Verruijt. *Modelling groundwater flow and pollution, D.Reidel Publishing Company*, Dordecht, Holland, 1987.

[3] K. El Harouni, D. Ouazar and A.H.-D. Cheng. Salt-/Fresh-Water interface model and GAs for parameter estimation, Natururwet. Tijdschr Vol.79 (1999), p.43-47, 2 tabs.

[4] N.-Z. Sun. Inverse problems in groundwater modelling, Kluwer Academic Publishers, Dordrecht, Netherland, (1994).

Stabilization of parabolic equation and Navier-Stokes system in a bounded domain Ω by feed-back control defined on $\partial\Omega$

Andrei V. Fursikov[1]

16.1 Setting of the problem

We consider the evolutionary Navier-Stokes equations (NSE)

$$\partial_t v(t,x) - \Delta v(t,x) + (v,\nabla)v + \nabla p(t,x) = f(x), \quad \operatorname{div} v = 0 \tag{16.1}$$

defined for $t > 0$ in a bounded domain $\Omega \in \mathbb{R}^3$ with smooth boundary $\partial\Omega$. Suppose that a steady-state solution of (16.1) with velocity component $\hat{v}(x) = (v_1, v_2, v_3), x \in \Omega$ is given and it is not stable. We have an initial condition $v_0(x)$ for NSE:

$$v(t,x)|_{t=0} = v_0(x), \quad x \in \Omega \tag{16.2}$$

where $v_0 \neq \hat{v}$ and v_0 is a small perturbation of $\hat{v}$. Besides

$$v(t,\cdot)|_{\partial\Omega} = u, \tag{16.3}$$

where $u(t,x'), x' \in \partial\Omega$ is a control.

Stabilization problem is formulated as follows: Given a positive number σ, find a control $u(t,x'),\ x' \in \partial\Omega$ such that the solution $v(t,x)$ of boundary value problem (BVP) (16.1), (16.2), (16.3) for NSE tends to $\hat{v}$ with prescribed rate σ:

$$\|v(t,\cdot) - \hat{v}\|_{V^1(\Omega)} \leq ce^{-\sigma t} \text{ as } t > 0 \tag{16.4}$$

where $V^1(\Omega) = \{v \in (H^1(\Omega))^3 : \operatorname{div} v = 0)\}$, $H^1(\Omega)$ is Sobolev space. Moreover, this stabilization should be realized by feedback control which can react on unpredictable fluctuations of velocity $v(t,x)$ damping them.

[1]Department of Mechanics and Mathematics, Moscow State University, 119992 Moscow, Russia. fursikov@mtu-net.ru

16.2 Construction of stabilization

To solve stabilization problem we use the following construction. Let a domain G be such that $\Omega \subset G$. We extend $\hat{v}(x)$ in an arbitrary solenoidal vector field $a(x),\ x \in G$ satisfying $a|_{\partial G} = 0$. We substitute $a(x)$ and extended pressure into the left part of the steady-state NSE and obtain after proper calculations the extension $g(x), x \in G$ of the right-hand side $f(x)$ for NSE (16.1).

To extend (16.1) from Ω to G we forget for a while about boundary condition (16.3), take $g(x)$ as the right-hand side for extended evolutionary NSE, denote extended velocity vector field as $w(t,x)$. As a result we get:

$$\partial_t w(t,x) - \Delta w(t,x) + (w,\nabla)w + \nabla p_1(t,x) = g(x), \quad \operatorname{div} w = 0 \tag{16.5}$$

We impose the following conditions on w:

$$w|_{\partial G} = 0, \quad w(t,x)|_{t=0} = w_0(x) \equiv Ev_0(x) \tag{16.6}$$

Here E is a special nonlinear extension operator from Ω in G. Construction of E is the main part of the proposed stabilization method.

Let $V_0^1(G) = \{w(x) \in V^1(G) : w|_{\partial\Omega} = 0\}$. For a given $\sigma > 0$ we define a stable invariant manifold $M_\sigma(a)$ as a smooth manifold in $V_0^1(G)$ of finite codimension determined in a neighbourhood of a such that for each initial condition $w_0 \in M_\sigma(a)$ the solution $w(t,\cdot)$ of BVP (16.5), (16.6) for every $t > 0$ belongs to $M_\sigma(a)$ and

$$\|w(t,\cdot) - a\|_{V_0^1(G)} \le c\|w_0 - a\|_{V_0^1(G)} e^{-\sigma t} \ \text{ as } t \ge 0 \tag{16.7}$$

Lemma 16.1 *For each $\sigma > 0$ except, maybe, a finite set θ there exists a unique stable invariant manifold $M_\sigma(a)$ of minimal possible codimension.*

Theorem 16.1 *Let $\sigma \in \mathbb{R}_+ \setminus \theta$. For sufficiently small ε there exists an operator E of extension of vector fields from Ω in G such that $E : \mathcal{O}^\varepsilon(\hat{v}) \to M_\sigma(a)$ where $\mathcal{O}^\varepsilon(\hat{v}) = \{v \in V^1(\Omega) : \|v - \hat{v}\|_{V^1(\Omega)} < \varepsilon\}$.*

Define now a solution (v,u) of initial stabilization problem (16.2), (16.3), (16.4):

$$(v(t,\cdot), u(t,\cdot)) = (\gamma_\Omega w(t,\cdot), \gamma_{\partial\Omega} w(t,\cdot)) \tag{16.8}$$

where $\gamma_\Omega, \gamma_{\partial\Omega}$ are restriction operators to $\Omega, \partial\Omega$ respectively, $w(t,x)$ is the solution of BVP (16.5), (16.6) with $w_0 = Ev_0$ where v_0 is initial condition from (16.2). Note that estimate (16.4) follows from (16.7).

Complete description of the stabilization construction including the proof of Theorem 16.1 one can find in [2], [3]. Note, that analogous results can be obtained also for quasilinear parabolic equations (see [1])

16.3 Real process

Invariant manifold $M_\sigma(a)$ introduced in Lemma 16.1 is repelling set: if at instant t_0 a solution $w(t_0,\cdot) \in M_\sigma(a)$ leaves $M_\sigma(a)$ being subjected by certain perturbation, it will recede from $M_\sigma(a)$ as $t \to \infty$. To construct a stabilization theory for NSE that can be used for justification of numerical simulation we introduce the notion of real process $\tilde{v}(t,x)$. By definition, $\tilde{v}(t,x) = v(t,x) + \varphi(t,x),\ t > 0, x \in \Omega$ where $v(t,x)$ is the exact solution of the stabilization problem

and discrepancy $\varphi(t,x)$ is called fluctuation. To describe evolution of $\tilde{v}(t,x)$ we have worked out an axiomatics for real processes simulating situation in numerical calculations. To stabilize $\tilde{v}$ we consider real process $\tilde{w}(t,x), x \in G$ corresponding to a solution w of BVP (16.5),(16.6) for NSE. Suppose that corresponding fluctuation ψ arise at discrete moments of time $\{t_j = j\tau\}$ where $\tau > 0$ is a fixed small number and $j \in \mathbb{N}$. Just at these moments we stabilize $\tilde{w}$ applying to it operator P of projection on $M_\sigma(a)$ ($P\tilde{w}(j\tau,\cdot) \in M_\sigma(a)$), such that $P\tilde{w}(t,\cdot)|_\Omega = \tilde{w}(t,\cdot)|_\Omega$. After that real process evolves in accordance with NSE till the next time moment $(j+1)\tau$ when we repeat our algorithm. It is easy to show that stabilized real process $\tilde{w}(j\tau,\cdot)$ defined above satisfies the equation

$$w_j = Sw_{j-1} + P\psi_j \quad \text{with} \quad w_j = \tilde{w}(j\tau,\cdot),\ \psi_j = \psi(j\tau,\cdot), \tag{16.9}$$

where $S = S(\tau)$ and $S(t)$ is resolving operator for BVP (16.5),(16.6): $S(t)w_0 = w(t,\cdot)$. We obtain the stabilized real process $\tilde{v}$ for initial stabilization problem and corresponding feedback control $\tilde{u}$ by the formula: $(\tilde{v}(t,\cdot), \tilde{u}(t,\cdot)) = (\gamma_\Omega \tilde{w}(t,\cdot), \gamma_{\partial\Omega}\tilde{w}(t,\cdot))$

Theorem 16.2 (See [3],[4]) *Let $0 < \tau < \infty$, and fluctuations $\psi(j\tau,x)$ satisfy inequality* $\|\psi(j\tau,\cdot)\|_{V_0^1(G)} < \varepsilon_0$ *where ε_0 is sufficiently small. Then stabilized real process $\tilde{v}$, satisfies the estimate*

$$\|\tilde{v}(t,\cdot) - \hat{v}\|_{V^1(\Omega)} \le c_1(e^{-\sigma t}\|v_0\|_{V^1(\Omega)} + c_2\varepsilon_0) \tag{16.10}$$

where constant c_1 is defined by operators E, P, and c_2 is an absolute constant.

16.4 Retaining stabilized flow near unstable steady-state solution

The estimate (16.10) for real process differs from bound (16.4) with term $c_2\varepsilon_0$ that arised because of unpredictable fluctuations $\psi_j = \psi(j\tau,x)$. Therefore, estimate (16.10) is effective only when real process is far enough from stabilized steady-state solution $\hat{v}$. It is clear that to improve estimate (16.10) by eliminating term $c_2\varepsilon_0$ is impossible if only conditions of Theorem 16.2 are imposed. Nevertheless, to investigate behaviour of $\tilde{v}$ near $\hat{v}$ became possible if we impose additional conditions on unpredictable fluctuations ψ_j. In fact these investigations solve the problem of retaining the controlled flow near unstable steady-state solution. This problem has been solved for linearized Navier-Stokes equations

$$\partial_t z(t,x) - \Delta z(t,x) + (\hat{v},\nabla)z + (z,\nabla)\hat{v} + \nabla q(t,x) = 0, \quad \mathrm{div} z = 0 \tag{16.11}$$

This equation we get making change of variable $v = z + \hat{v}$ in (16.1), subtracting from it steady-state equation (16.1) with solution $\hat{v}$ and throwing off nonlinear term in obtained equation. It is clear that after this operation we have to stabilize (16.11) near steady-state solution 0.

We apply to BVP (16.11), (16.2), (16.3) (with v changed on z in last two equations) the stabilization construction from section 16.2 and after that we construct the corresponding controlled real process $\tilde{w}(j\tau,\cdot) = w_j$. Then w_j satisfies equation (16.9) with operator S, P corresponding to equation (16.11).

We assume now that unpredictable fluctuations $\psi_j = \psi(j\tau,\cdot)$ are random variables defined on probability space $\{\widehat{\Omega}, \mathcal{A}, \mathbb{P}\}$ and taking values in $V_0^1(G)$. Moreover, we suppose that random variables ψ_j are independent identically distributed random variables with distribution μ. Here μ is probability measure that is defined on the Borel σ-algebra $\mathcal{B}(V_0^1(G))$ of the space $V_0^1(G)$ and is supported in an neighborhood of origin:

$$\mathrm{supp}\ \mu \subset \{v \in V_0^1(G) : \|w\|_{V_0^1(G)} \le \varepsilon_0\}$$

Then (16.9) defines a family of Markov chains (FMC) in $M_\sigma(0)$ with transition function

$$P(j, w_0, \Gamma) = \mathbb{P}\{w_j(w_0) \in \Gamma\}, \quad \Gamma \in \mathcal{B}(M_\sigma(0)) \tag{16.12}$$

where $w_j(w_0)$ is the solution of (16.9) with initial condition w_0, and $\mathbb{P}$ is probability measure on probability space $\widehat{\Omega}$.

Theorem 16.3 (See [6]) *The family of Markov chains (16.9) is ergodic, i.e. it possess unique steady-state statistical solution $\hat{\mu}$. Moreover, there exists a constant $\gamma \in (0,1)$ such that*

$$\left| \int f(z) P(j, w_0, dz) - \int f(z) \hat{\mu}(dz) \right| \le c\gamma^j, \quad j = 1, 2, 3, \dots, \tag{16.13}$$

for every Lipschitz function f on $M_\sigma(0)$ such that $\|f\|_{C_b(M_\sigma)(0)} \le 1$ and $Lipf \le 1$.

Note that uniqueness of stationary measure $\hat{\mu}$ means that FMC (16.9) is ergodic. The exponential convergence (16.13) means that FMC (16.9) possesses the property of exponential mixing.

Theorem 16.3 provides us the possibility of calculating the probability characteristics of FMC (16.9), i.e of real process connected with (16.11). For instance, in numerical simulation we actually obtain certain realization $w_j = w_j(\omega),\ \omega \in \widehat{\Omega}$ of FMC (16.9), and by the strong law of large numbers we get

$$\lim_{N\to\infty} \frac{1}{N} \sum_{k=0}^{N} w^k(\omega) \to \int w \mu(dw), \text{ as } N \to \infty, \tag{16.14}$$

Thus, by formula (16.14) we can calculate mathematical expectation of $\hat{\mu}$.

16.5 Analyticity of stable invariant manifold

One of the main goal we want to achieve by creation the theory of stabilization is to develop a skilled numerical methods for calculation of stabilization problems. One of the main problem on this way is how to calculate stable invariant manifold $M_\sigma(a)$. In the case of linear equation (16.11) this invariant manifold is a linear subspace of $V_0^0(G)$ which we denote as X_σ. To describe it we introduce the spatial part of operator from the left side of (16.11):

$$A : V_0^0(G) \to V_0^0(G) : \quad Az = \pi(-\Delta z(x) + (\hat{v}(x), \nabla)z + (z, \nabla)\hat{v}) \tag{16.15}$$

where $V_0^0(G) = \{v \in (L_2(G))^3 : \mathrm{div} v = 0)\}$, $\pi : (L_2(G))^3 \to V_0^0(G)$ is orthoprojection. Denote by $X_\sigma^+(A^*)$ the subspace of $V_0^0(G)$ generated by all eigen and associated functions of operator A^* conjugate to operator (16.15) corresponding to eigen-values λ_k with $\mathrm{Re}\ \lambda_k > \sigma$. Let $X_\sigma^-(A)$ be orthogonal complement of $X_\sigma^+(A^*)$ in $V_0^0(G)$. Then it is easy to show (see [1], [2]) that

$$X_\sigma = V_0^1(G) \cap X_\sigma^-(A) \tag{16.16}$$

It follows from definition (16.16) that projection operator on X_σ can be calculated by solving a system of linear algebraic equations ([1],[2],[3]).

Let define the stable invariant manifold $M_\sigma(a)$ in neighborhood of steady-state solution a for nonlinear system (16.5), (16.6). Denote by $X_\sigma^+ = X_\sigma^+(A)$ the subspace of $V_0^1(G)$ generated by all eigen and associated functions of operator (16.15) corresponding to eigen-values λ_k with

Re $\lambda_k > \sigma$. Let $P_+ : V_0^1(G) \to X_\sigma^+, P_- : V_0^1(G) \to X_\sigma$ be projectors. Then $V_0^1(G) = X_\sigma^+ + X_\sigma$ and therefore $V_0^1(G) \ni z = z_+ + z_-$ where $z_+ = P_+ z,\ z_- = P_- z$. Manifold $M_\sigma(a)$ is defined usually as follows:

$$M_\sigma(a) = a + \{z = z_- + F(z_-), \quad z_- \in \mathcal{O}(X_\sigma^-) \tag{16.17}$$

where $\mathcal{O}(X_\sigma)$ is a neighborhood of origin in X_σ and $F : \mathcal{O}(X_\sigma) \to X_\sigma^+$ is a map. Existence of corresponding map F is well-known. The problem is how to make skilled calculation of F, defined on infinite-dimensional space. We propose to look for F in class of analytic maps, i.e. of maps that admit the decomposition

$$F(z_-) = \sum_{k=2}^{\infty} F_k(z_-), \quad \text{where} \quad F_k(z_-) = G_k(z_1, \dots, z_k)|_{z_1 = \dots = z_k = z_-} \tag{16.18}$$

and $G_k(z_1, \dots, z_k)$ are k-linear operators. The way to find F in the form (16.18) is as follows. First we derive a differential equation in variational derivatives for maps F that define invariants manifolds in form (16.17). After substitution decomposition (16.18) into this equation and equating terms of identical order of homogeneity with respect to z_- we get recurrent formulae for G_k. Using them we can prove convergence of serie (16.18). Besides, we can calculate numerically sufficiently precise approximations of stable invariant manifolds $M_\sigma(a)$ and use them for calculation of stabilization problem. Up to now theoretical aspects of analyticity of $M_\sigma(a)$ are developed in [7] only in the case of one-dimensional semilinear parabolic equation.

16.6 Calculations of stabilization problem

At last, we do very short review of results on numerical calculations of stabilization problem for semilinear parabolic equation and for 2-D Navier-Stokes system made in Moscow State University.

First calculations of stabilization problem founded on theoretical investigations from [1]–[5] has been made by E.V.Chizhonkov [8] in the case of (linear) one-dimensional heat equation and (semilinear) one-dimensional Chafee-Infante equation.

Calculations of stabilization for 2D Stokes and Navier-Stokes equations with periodic boundary condition in one dimension and boundary Dirichlet control in other dimension were performed by E.V.Chizhonkov and A.A.Ivanchikov in [9].

At last, numerical stabilization of 2D Couette flow from the boundary in the case when Couette flow lost stability and Taylor vortexes became stable has been made by A.A.Ivanchikov in [10].

All of these three papers are full of content and they are very interesting. But in them only first steps in creating numerical methods of stabilization has been made. In particular, for numerical stabilization of nonlinear equations authors of [8]–[10] used only linear approximation X_σ of nonlinear stable invariant manifold $M_\sigma(a)$. Just this circumstance induced myself to study in [7] analyticity property of $M_\sigma(a)$. Formulae from [7] for approximation of $M_\sigma(a)$ were applied by A.B.Kalinina in [11] for numerical calculations of $M_\sigma(a)$. Approximation of $M_\sigma(a)$ obtained in [11] became essentially more precise than linear approximation.

Bibliography

[1] A.V. Fursikov. *Stabilizability of quasi linear parabolic equation by feedback boundary control,* Sbornik: Mathematics, v.192:4 (2001),p.593-639.

[2] A.V. Fursikov. *Stabilizability of two-dimensional Navier-Stokes equations with help of boundary feedback control,* J. of Math. Fluid Mech., v.3 (2001), p.259-301.

[3] A.V. Fursikov. *Stabilization for the 3D Navier-Stokes system by feedback boundary control,* Discrete and Cont. Dyn. Syst., v.10, no 1&2, (2004), p.289-314.

[4] A.V. Fursikov. *Real Process Corresponding to 3D Navier-Stokes System and Its Feedback Stabilization from Boundary,* AMS Translations Series 2, v.206. Advances in Math. Sciences-51. PDE M.Vishik seminar. AMS Providence Rhode Island (2002), p.95-123.

[5] A.V. Fursikov. *Real Processes and Realizability of a Stabilization Method for Navier-Stokes Equations by Boundary Feedback Control,* Nonlinear Problems in Mathematical Physics and Related Topics II, In Honor of Professor O.A.Ladyzhenskaya, Kluwer/Plenum Publishers, New-York, Boston, Dordrecht, London, Moscow, 2002, p.137-177.

[6] J. Duan and A.V. Fursikov. *Feedback stabilization for Oseen fluid equations: a stochastic approach,* J.Math.Fluid Mech. v.7 (2005), p.574-610.

[7] A.V. Fursikov. *Analyticity of stable invariant manifolds of 1D-semilinear parabolic equations,* Proceedings of Summer Research Conference "Control methods of PDE-dynamical systems", AMS Contemporary Mathematics series. Providence, 2006. (to appear)

[8] E.V. Chizhonkov. *Numerical aspects of one stabilization method*, Russ.J.Numer. Anal. Math. Modelling, V.18:5, (2003), p.363-376.

[9] E.V. Chizhonkov and A.A. Ivanchikov. *On numerical stabilization of solutions of Stokes and Navier-Stokes equations by boundary conditions*, Russ.J.Numer. Anal. Math. Modelling, V.19:6, (2004), p.477-494.

[10] A.A. Ivanchikov. *On numerical stabilization of unstable Couette flow by boundary conditions*, Russ.J.Numer.Anal.Math.Modelling (2006) (to appear)

[11] A.B. Kalinina. *Numerical realization of the method of functional-analytic series for projection on a stable manifold*, Numerical methods and programming. (in Russian), (to appear).

Removing holes in topological shape optimization

Philippe Guillaume[1] *Maatoug Hassine*[2]

17.1 Introduction

Topological optimization is concerned with the variation of a cost function with respect to a topology modification of a domain. The most simple way of modifying the topology consists in creating a small hole in the domain. Usually, the cost function involves the solution of a p.d.e. defined on this domain. In the case of structural shape optimization, creating a hole means simply removing some material. In the case of fluid dynamics where the domain represents the fluid, creating a hole means inserting a small obstacle. The situation is similar in electromagnetism. The topological sensitivity tools which have been developed by several authors [8, 3] allow to find the place where creating a small hole will bring the best improvement of the cost function. These tools are based on a gradient like expression of the form

$$\begin{aligned} j(\Omega_\varepsilon) &= j(\Omega) + f(\varepsilon)\delta j(x) + o(f(\varepsilon)), \\ f(\varepsilon) > 0 \quad \forall \varepsilon > 0, \quad &\lim_{\varepsilon \to 0} f(\varepsilon) = 0. \end{aligned} \tag{17.1}$$

Here Ω is an open and bounded subset of $\mathbb{R}^d$, $d = 2, 3$, and, for $\varepsilon > 0$ and $x \in \Omega$, $\Omega_\varepsilon = \Omega \backslash (\overline{x + \varepsilon\omega})$ is the subset obtained by removing the subset $\overline{x + \varepsilon\omega}$ from Ω, where $\omega \subset \mathbb{R}^d$ is a fixed open and bounded subset containing the origin. Obviously, if we want to minimize j, the "best" place (in the sense of the steepest descent) where to create an infinitesimal hole is there where $\delta j(x)$ is the most negative. Starting with this observation, topological optimization algorithms can then be constructed [3, 5, 6]. The main problem encountered at this stage is that topological sensitivity only provides information on where to add holes, but not where to remove already existing holes: once a hole has been introduced in the domain, it will remain there during all forthcoming iterations. However, it may happen that after creation of other holes, removing this particular hole would improve the cost function. Hence, there is a need for tools giving an estimate of $j(\Omega)$ when $j(\Omega_\varepsilon)$ is known. An analogy with ordinary differential calculus for a function u is that instead of estimating $u(\varepsilon) \simeq u(0) + \varepsilon u'(0)$, we want to estimate $u(0) \simeq u(\varepsilon) - \varepsilon u'(\varepsilon)$. Thus, the goal of this paper is to provide and estimate of the form

$$j(\Omega) = j(\Omega_\varepsilon) - g(x, \varepsilon) + o(f(\varepsilon))$$

where $g(x, \varepsilon)$ is computed by solving a p.d.e. on the current domain Ω_ε, whereas $\delta j(x)$ in (17.1) was computed by solving a p.d.e. on the current domain Ω. Of course, we have $g(x, \varepsilon) =$

[1] philippe.guillaume@insa-toulouse.fr
[2] maatoug.hassine@enit.rnu.tn

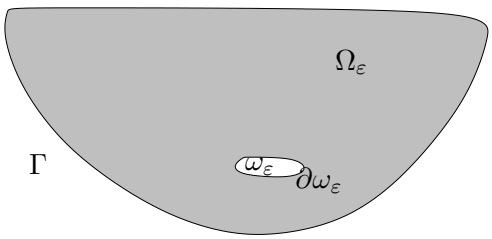

Figure 17.1: *The domain* Ω_ε.

$f(\varepsilon)\delta j(x) + o(f(\varepsilon))$, the only difference being the way of computing this quantity from available data, associated to the current domain during the optimization process. Concerning the hole shape, the theoretical results presented in this paper are valid for any bounded domain $\omega \subset \mathbb{R}^d$ containing the origin and having a connected boundary $\partial\omega$ piecewise of class $\mathcal{C}^1$. However, in order to get an explicit expression of the boundary integral equation, we will choose a simple geometry: the unit ball.

17.2 Formulation of the problem

Let Ω_ε be a bounded domain of $\mathbb{R}^d$, $d = 2, 3$, with smooth boundary Γ_ε, obtained from creating a small hole ω_ε in a fixed and connected domain Ω. The hole is of the form $\omega_\varepsilon = x_0 + \varepsilon\omega$, where $x_0 \in \Omega$, $\varepsilon > 0$ and ω is a given fixed open and bounded domain of $\mathbb{R}^d$, containing the origin, whose boundary $\partial\omega$ is connected and piecewise of class $\mathcal{C}^1$. It is supposed that $\varepsilon \leq \varepsilon_0$ with ε_0 sufficiently small so that $\omega_\varepsilon \subset \Omega$ for all $\varepsilon \leq \varepsilon_0$. The boundary of Ω is denoted Γ, with $\Gamma_\varepsilon = \Gamma \cup \partial\omega_\varepsilon$ and $\Gamma \cap \partial\omega_\varepsilon = \emptyset$ (see Figure 17.1.)

We consider the Stokes equations describing an incompressible fluid flow in Ω_ε. We denote by $(u_D^\varepsilon, p_D^\varepsilon)$ the solution to the problem with a Dirichlet boundary condition on $\partial\omega_\varepsilon$:

$$\left\{\begin{array}{rcl} -\nu\Delta u_D^\varepsilon + \nabla p_D^\varepsilon &= 0 & \text{in } \Omega_\varepsilon \\ \text{div } u_D^\varepsilon &= 0 & \text{in } \Omega_\varepsilon \\ u_D^\varepsilon &= u_d & \text{on } \Gamma_1 \\ \nu\partial_n u_D^\varepsilon - p_D^\varepsilon\, n &= g & \text{on } \Gamma_2 \\ u_D^\varepsilon &= 0 & \text{on } \partial\omega_\varepsilon, \end{array}\right. \tag{17.2}$$

where u_D^ε is the velocity, p_D^ε is the pressure, ν is the kinematic viscosity of the fluid, Γ_1 and Γ_2 are portions of Γ having both a nonnegative Lebesgue measure and satisfy $\Gamma_1 \cup \Gamma_2 = \Gamma$ and $\Gamma_1 \cap \Gamma_2 = \emptyset$, u_d is a given velocity on Γ_1, I is the $d \times d$ identity matrix, g is a given stress vector on Γ_2, and n is the unit normal vector along the boundary Γ. For simplicity, no volume forces are considered.

Topological optimization problem

Consider now a cost function $j(\varepsilon)$ of the form

$$j(\varepsilon) = J_\varepsilon(u_D^\varepsilon), \tag{17.3}$$

where J_ε is defined on $H^1(\Omega_\varepsilon)^d$ and satisfies the following hypothesis.

Hypothesis 17.1 *There exist a linear and continuous form L_ε defined on $\mathcal{V}_\varepsilon$ and a real number δJ (independent of ε) such that*

$$J_\varepsilon(u_N^\varepsilon) - J_\varepsilon(u_D^\varepsilon) = L_\varepsilon(u_N^\varepsilon - u_D^\varepsilon) + f(\varepsilon)\delta J + o(f(\varepsilon)), \tag{17.4}$$

where $u_N^\varepsilon \in \mathcal{V}_\varepsilon$ is the solution to the Stokes equations (17.2) with a Neumann boundary condition: $\nu\partial_n u_N^\varepsilon - p_N^\varepsilon\, n = 0$ on $\partial\omega_\varepsilon$, and the scalar function f is defined in $\mathbb{R}^+$ by

$$f(\varepsilon) = \begin{cases} \varepsilon & \text{if } d = 3, \\ -1/\log(\varepsilon) & \text{if } d = 2. \end{cases}$$

Our aim is to derive an estimate of the cost function j when ε tends to zero.

17.3 Variation of the cost function with respect to a topological perturbation

As mentioned earlier, the aim of this work is to build a new topological optimization algorithm providing the possibility of creating or suppressing holes during the optimization process.

Creating a small hole

We recall here the topological sensitivity results for the Stokes equations when creating a small hole inside the domain with a Dirichlet boundary condition. Cases $d = 2$ and $d = 3$ need to be distinguished. This is due to the fact that the fundamental solutions to the Stokes equations in $\mathbb{R}^2$ and $\mathbb{R}^3$ have an essentially different asymptotic behavior at infinity.

Theorem 17.1 (3D case) *If ω is the unit ball and if Hypothesis 17.1 holds, then function j has the following asymptotic expansion*

$$j(\varepsilon) = j(0) + \varepsilon\left[6\pi\nu\, u_D^0(x_0).v_D^0(x_0) + \delta J\right] + o(\varepsilon), \tag{17.5}$$

where v_D^0 is the solution to the associated adjoint problem in Ω (when $\varepsilon = 0$).

Theorem 17.2 (2D case) *Under the same hypotheses of theorem 17.1, the function j has the following asymptotic expansion*

$$j(\varepsilon) = j(0) + -1/\log(\varepsilon)\left[4\pi\nu\, u_D^0(x_0).v_D^0(x_0) + \delta J\right] + o(-1/\log(\varepsilon)). \tag{17.6}$$

Removing a small hole

In this section we compute the variation of the cost function when removing a small hole ω_ε.

Theorem 17.3 *If Hypothesis 17.1 holds, then we have the following estimate:*

$$j(0) = j(\varepsilon) + \int_{\partial\omega_\varepsilon} (\nu\partial_n v_D^\varepsilon - q_D^\varepsilon\, n).u_N^\varepsilon\, ds + f(\varepsilon)\delta J + o(f(\varepsilon)). \tag{17.7}$$

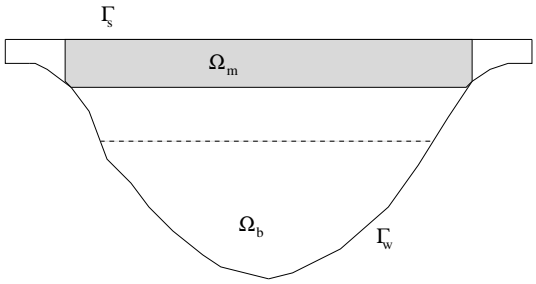

Figure 17.2: *The geometry of the lake.*

17.4 Numerical results

Let Ω be a two dimensional flow domain representing the eutrophized water basin. The boundary Γ of Ω consists in two parts (see Figure 17.2): $\Gamma = \Gamma_w \cup \Gamma_s$.

We suppose that a "good" lake oxygenation can be described by a target velocity $\mathcal{U}_g$. Then, the cost function J which is here considered reads

$$J(u) = \int_{\Omega_m} |u - \mathcal{U}_g|^2 \, dx,$$

where $\Omega_m \subset \Omega$ is the measurement domain (the top layer, see Figure 17.2). We aim to determine the optimal location in Ω_b (the bottom of the lake, see Figure 17.2) of some injector holes ω_k in order to minimize function J. A numerical algorithm is proposed, giving the possibility to create or to suppress holes during the optimization process. It proceeds by iterations. At the $k-$th iteration, δj^k denotes the topological gradient and Ω_k denotes the current domain. We denote by x_p^k, $p = 1, 2, \ldots$, the local minimum of δj^k. The set of holes which are candidates to be inserted in Ω_k is given by $h^k = \{\omega_\varepsilon(x) = x + \varepsilon\omega,\ x \in C_k\}$, where $C_k = \{x_p^k \in \Omega_k,\ 1 \leq p \leq n_k\}$ is the set of the negative local minimum of δj^k in Ω_k and n_k is their number. The holes are ordered in such a way that $\delta j^k(x_p^k) \leq \delta j^k(x_{p'}^k)$ for all $1 \leq p < p' \leq n_k$. Let H^k be the set of N_k holes inserted during all previous iterations: $H^k = \{\omega_\varepsilon(y_l^k) = y_l^k + \varepsilon\omega,\ 1 \leq l \leq N_k\}$.

The variation of the cost function with respect to suppression of hole $y_l^k + \varepsilon\omega$ is denoted by $g_l^k = g^k(y_l^k)$ and the set $\{y_l^k,\ 1 \leq l \leq N_k\}$ is supposed to be arranged in such a way that $g_l^k \leq g_{l'}^k$ if $l < l'$.

Algorithm :

- Initialization: choose $\Omega_0 = \Omega_b$, and set $k = 0$.
- Repeat until $\delta j^k \geq 0$ in Ω_k:
  - Step 1: preparation phase
    - solve direct and adjoint problem in Ω_k,
    - compute the topological sensitivity δj^k,
    - determine the set $h^k = \{\omega_\varepsilon(x_p^k) = x_p^k + \varepsilon\omega,\ 1 \leq p \leq n_k\}$.
  - Step 2: exchange phase
    - compute the variations $\{g_l^k = g^k(y_l^k),\ 1 \leq l \leq N_k\}$,
    - set $q = 1$,
    - while the variation $\delta j^k(x_q^k) + g^k(y_q^k) < 0$:

· remove the hole $\omega_\varepsilon(y_q^k) = y_q^k + \varepsilon\omega$ and add the hole $\omega_\varepsilon(x_q^k) = x_q^k + \varepsilon\omega$,
· increment q,

– Step 3: insertion phase
  * creation of the holes $\{x_{q+i}^k + \varepsilon\omega,\ 1 \le i \le m_k\}$, where q is the number of the holes changed during the second step,
  * set $\Omega_{k+1} = \Omega_k \cup \Big(\cup_{i=1}^{q} \omega_\varepsilon(y_i^k)\Big) \setminus \Big(\cup_{l=1}^{q+m_k} \overline{\omega_\varepsilon(x_l^k)}\Big)$ where $\{\omega_\varepsilon(y_i^k),\ 1 \le i \le q\}$ are the holes removed during the second step,

– increment k.

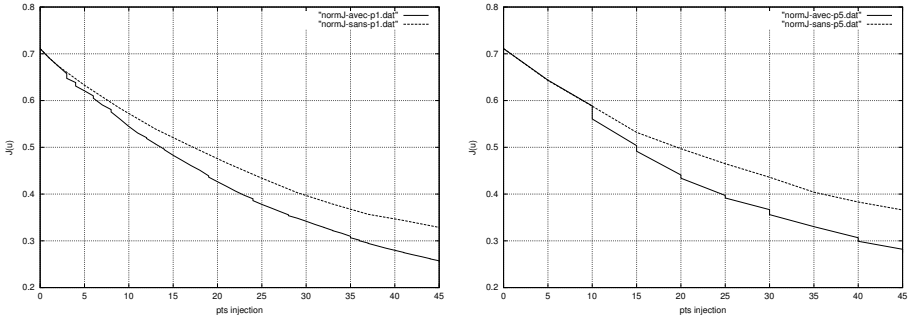

(a) when adding one injector (b) when adding five injectors

Figure 17.3: *Variation of the cost function; without removing injectors (top), with removing (bottom).*

In order to test the advantage of this approach, we have compared the results issued from this technique to those obtained by using a classical version as described in [3, 5, 6], that is, without the second step. The obtained results are presented in figures (17.3)-(17.4). Figure 17.3-(a) describes the variation of the cost function when adding one injector at each iteration. The curve obtained is compared with the one obtained without removing injectors. Figure 17.3-(b) illustrates the variation of the same function when adding five injectors at each iteration. Figure 17.4 presents the wanted velocity $\mathcal{U}_g$ and the obtained velocities in the measurement Ω_m when the optimization process is achieved.

Bibliography

[1] M. Abdelwahed, M. Amara, F. El Dabaghi, M. Hassine. *A numerical modelling of a two phase flow for water eutrophication problems.* ECCOMAS 2000, European Congress on Computational Methods in Applied Sciences and Engineering, Barcelone, 11-14 September 2000.

[2] G. Allaire, F. Jouve, A-M. Toader. *Structural optimization using sensitivity analysis and a level-set method.* J. Comput. Phys. 194 (2004), no. 1, 363-393.

[3] S. Garreau, Ph. Guillaume, M. Masmoudi. *The topological asymptotic for pde systems: the elasticity case*, SIAM J. Control Optim., 39, no.4(2001), 1756-1778.

[4] G. Buttazzo and G. Dal Maso. *Shape optimization for Dirichlet problems: Relaxed formulation and optimality conditions.* Appl. Math. Optim. 23, 17-49, 1991.

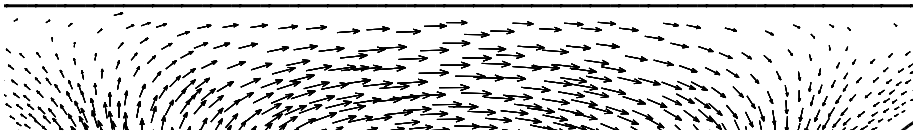

The wanted velocity $\mathcal{U}_g$ in the measurement domain Ω_m.

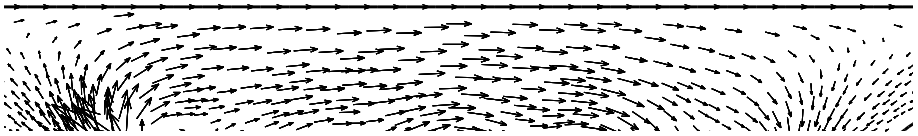

(a) The obtained velocity (without removing), adding one injector at each iteration.

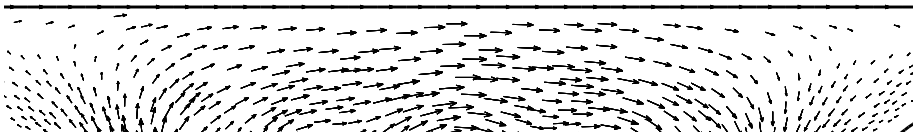

(b) The obtained velocity (with removing), adding one injector at each iteration.

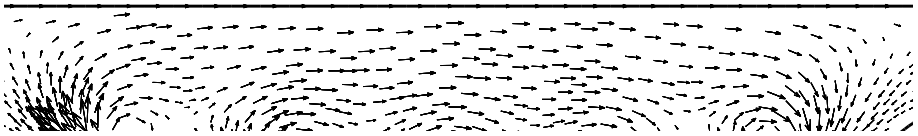

(c) The obtained velocity (without removing), adding five injectors at each iteration.

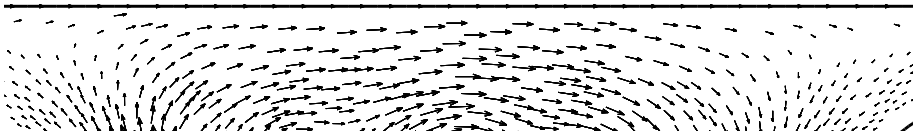

(d) The obtained velocity (with removing), adding five injectors at each iteration.

Figure 17.4: *Velocities fields obtained in Ω_m (measurement domain) at the end of the optimization process.*

[5] Ph. Guillaume and K. Sid Idris. *Topological sensitivity and shape optimization for the Stokes equations*. SIAM J. Control Optim. 43(1), 1-31, 2004.

[6] M. Hassine and M. Masmoudi. *The topological sensitivity analysis for the Quasi-Stokes problem*. ESAIM, COCV J. vol. 10, 478-504, 2004.

[7] M. Masmoudi. *The topological asymptotic*, in Computational Methods for Control Applications, ed. H. Kawarada and J.periaux, International Séries GAKUTO, 2002.

[8] J. Sokolowski and A. Zochowski. *On the topological derivative in shape optimization*. SIAM J. Control Optim., 37, no.4(1999), 1251-1272 (electronic)

Negative results on the controllability of the Burgers equation

Sergio Guerrero[1]

18.1 Introduction

This talk will be structured into two parts. In both of them, we will give several results concerning the controllability of the Burgers equation. Most of these results will be of negative nature.

In the first part, we deal with the Burgers equation where the control acts on the system by its right hand side or one endpoint of the spatial boundary. We will prove that the minimal time one needs for driving the solution of the Burgers equation to zero is positive. We will also give the expression of this time in terms of the L^2-norm of the initial condition. In particular, the previous result implies that the (global) null controllability of the Burgers equation does not hold.

In the second part of the talk, we will control the Burgers equation at both endpoints of the spatial boundary. In this part we will prove two main results. The first one states that the null controllability for small time does not hold, while the second one states that the exact controllability does not hold for large time.

18.2 Controllability of the Burgers equation with one control force

Let $T > 0$ be an arbitrary positive time and let us assume that $\omega \subset (0,1)$ is a nonempty open set, with $0 \notin \overline{\omega}$. In this first part of the talk, we will be concerned with the null controllability of the following system for the Burgers equation:

$$\begin{cases} y_t - y_{xx} + yy_x = v1_\omega, & (x,t) \in (0,1) \times (0,T), \\ y(0,t) = y(1,t) = 0, & t \in (0,T), \\ y(x,0) = y^0(x), & x \in (0,1). \end{cases} \tag{18.1}$$

Here, $v = v(x,t)$ denotes the control and $y = y(x,t)$ denotes the state.

[1]guerrero@ann.jussieu.fr

It will be said that (18.1) is *null controllable at time* T if, for every $y^0 \in L^2(0,1)$, there exists $v \in L^2((0,1)\times(0,T))$ such that

$$y(x,T) = 0 \ \text{ in } \ (0,1). \tag{18.2}$$

Some controllability properties of (18.1) have been studied in [3]. In that reference, it is shown that one cannot reach (even approximately) stationary solutions of (18.1) with large L^2-norm at any time T. In other words, with the help of controls of this kind, the solutions of the Burgers equation cannot go anywhere at any time.

For each $y^0 \in L^2(0,1)$, let us introduce

$$T(y^0) = \inf\{\, T > 0 : (18.1) \text{ is null controllable at time } T \,\}.$$

Then, for each $r > 0$, let us set

$$T(r) = \sup\{\, T(y^0) : \|y^0\|_{L^2(0,1)} \le r \,\}.$$

Our main purpose in this first part is to prove that $T(r) > 0$, with an explicit sharp estimate in terms of r as $r \to 0$. In particular, this will imply that (global) null controllability at any positive time does not hold for (18.1).

More precisely, let us set

$$\phi(r) = \frac{1}{\log \frac{1}{r}}\,.$$

Then we have the following:

Theorem 18.1 *There exist positive constants C_0 and C_1 independent of r such that*

$$C_0\phi(r) \le T(r) \le C_1\phi(r) \ \text{ as } r \to 0. \tag{18.3}$$

Remark 18.1 *The same estimates hold when the control v acts on system (18.1) through the boundary* only *at $x = 1$ (or only at $x = 0$). Indeed, it is very easy to transform the boundary controlled system*

$$\begin{cases} y_t - y_{xx} + yy_x = 0, & (x,t) \in (0,1)\times(0,T), \\ y(0,t) = 0, \quad y(1,t) = w(t), & t \in (0,T), \\ y(x,0) = y^0(x), & x \in (0,1). \end{cases}$$

into a system of the kind (18.1).

Remark 18.2 *Now, let us assume that y^0 is an arbitrary (possibly large) state in $L^2(0,1)$, let us set $R = \|y^0\|_{L^2(0,1)}$ and let us assume that $T \ge T_*(R)$, where*

$$T_*(R) = \frac{1}{\pi}\log R + \frac{2\sqrt{C_1}}{\pi},$$

where C_1 is the constant arising in (18.3). Then there exist controls $v \in L^\infty(\omega\times(0,T))$ and associated solutions of (18.1) such that (18.2) is satisfied.

Indeed, let us first set

$$r = e^{-\sqrt{C_1}\pi}, \quad T_0(R) = \frac{1}{\pi^2}\log\frac{R}{r}$$

and $v(x,t) \equiv 0$ for $0 \leq t \leq T_0(R)$. From the usual energy estimates, we know that the associated state satisfies

$$\|y(\cdot,t)\|_{L^2(0,1)} \leq Re^{-\pi^2 t} \quad \forall t \in [0, T_0(R)]$$

and thus

$$\|y(\cdot, T_0(R))\|_{L^2(0,1)} \leq r.$$

Let us now apply Theorem 1 in the time interval $[T_0(R), T_0(R) + C_1\phi(r)]$, with initial data $y(\cdot, T_0(R))$. We deduce that there exists a control such that

$$y(x, T_0(R) + C_1\phi(r)) = 0 \ \text{ in } \ (0,1).$$

Since $T_0(R) + C_1\phi(r) = T_*(R)$, our assertion follows.

This first part of the talk is inspired in the work [2].

18.3 Controllability of the Burgers equation with two control forces

We consider the following control system associated to the Burgers equation:

$$\begin{cases} y_t - y_{xx} + yy_x = 0 & (t,x) \in Q := (0,T) \times (0,1), \\ y(t,0) = v_1(t), \quad y(t,1) = v_2(t) & t \in (0,T), \\ y(0,x) = y_0(x) & x \in (0,1). \end{cases} \tag{18.4}$$

Here, $T > 0$ is a given final time and $v_1(t)$ and $v_2(t)$ are control functions which are acting over our system at both endpoints of the segment $(0,1)$. Furthermore, y_0 is the initial condition which is supposed to be in $H^1(0,1)$. In the sequel, we will suppose that our control functions v_1 and v_2 belong to the space $H^{1/2}(0,T)$. Under these assumptions, it is classical to see that there exists a solution y of system (18.4) which belongs to the space $X := L^2(0,T;H^2(0,1)) \cap H^1(0,T;L^2(0,1))$ and a continuous function $K_0 > 0$ such that

$$\|y\|_X \leq K_0(\|y_0\|_{H^1(0,1)} + \|v_1\|_{H^{1/2}(0,T)} + \|v_2\|_{H^{1/2}(0,T)}) \tag{18.5}$$

(see, for instance, [5]).

For this system, an *exact controllability* property reads as follows: given $y_0 \in H^1(0,1)$ and $y_1 \in H^1(0,1)$, do there exist controls $v_1 \in H^{1/2}(0,T)$ and $v_2 \in H^{1/2}(0,T)$ such that the corresponding solution of (18.4) satisfies $y(T,x) = y_1(x)$ in $(0,1)$? When $y_1 \equiv 0$, we will refer to this problem as the *exact null controllability*.

For system (18.4), it was shown in [3] that any steady state solution is reachable for a sufficiently large time.

Additionally, in the recent paper [1], the author proved that with the help of two control forces, we can drive the solution of the Burgers equation with null initial condition to large constant states. More precisely, for any time $T > 0$, it is shown the existence of a constant $C_0 > 0$ such that for any $C \in \mathbf{R}$ satisfying $|C| \geq C_0$, there exist two controls $v_1(t)$ and $v_2(t)$ such that the associated solution to (18.4) with $y_0 \equiv 0$ satisfies $y(T,\cdot) = C$ in $(0,1)$. The idea of the proof of this result is based on the Hopf-Cole transformation, which leads to a controllability problem for the heat equation.

In this part of the talk, we have two main objectives. One concerning the exact null controllability for small time and the other one concerning the exact controllability for any time $T > 0$. Both results are of negative nature.

As long as the first one is concerned, we prove that there exists a final time T and an initial condition y_0 such that the solution of (18.4) is far away from zero. That is to say, the global null controllability for the Burgers equation with two control forces does not hold. The precise result says:

Theorem 18.2 *There exists $T > 0$ and $y_0 \in H^1(0,1)$ such that, for any control functions $v_1 \in H^{1/2}(0,T)$ and $v_2 \in H^{1/2}(0,T)$, the associated solution $y \in X$ to (18.4) satisfies*

$$\|y(T,\cdot)\|_{H^1(0,1)} \geq C_1 > 0, \tag{18.6}$$

for some positive constant $C_1(T, y^0)$.

The second main result is a negative exact controllability result:

Theorem 18.3 *For any $T > 0$, there exists an initial condition $y_0 \in H^1(0,1)$ and a target function $y_1 \in H^1(0,1)$ such that, for any $v_1 \in H^{1/2}(0,T)$ and $v_2 \in H^{1/2}(0,T)$, the associated solution $y \in X$ to (18.4) satisfies*

$$\|y(T,\cdot) - y_1(\cdot)\|_{H^1(0,1)} \geq C_2 > 0, \tag{18.7}$$

for some positive constant $C_2(T, y^0, y^1)$.

In order to prove these results, we first show the equivalence of the controllability problem for the Burgers equation (18.4) and some controllability problem for a one-dimensional linear heat equation with positive boundary controls. This is carried out in several steps, by applying Hopf-Cole type transformations.

Then, our controllability results for the Burgers equation (stated in Theorems 2 and 3 above) will be deduced from both results for the corresponding heat equation.

As a consequence of these two theorems, one can easily deduce the following corollaries:

Corollary 18.1 *Let us consider the following control system associated to a semilinear parabolic equation:*

$$\begin{cases} w_t - w_{xx} + \frac{1}{2}|w_x|^2 = \widehat{v}_1(t) & \text{in } Q, \\ w(t,0) = 0, \quad w(t,1) = \widehat{v}_2(t) & \text{in } (0,T), \\ w(0,x) = w_0(x) & \text{in } (0,1), \end{cases} \tag{18.8}$$

with $\widehat{v}_1 \in L^2(0,T)$ and $\widehat{v}_2 \in H^1(0,T)$. Then, the exact controllability of system (18.8) with H^2-data does not hold. That is to say, for any $T > 0$, there exist $w_0 \in H^2(0,1)$ and $w_1 \in H^2(0,1)$ satisfying $w_0(0) = w_1(0) = 0$ such that

$$\|w(T,\cdot) - w_1(\cdot)\|_{H^2(0,1)} \geq C_3,$$

for some $C_3(T, w_0, w_1) > 0$. Furthermore, the exact null controllability does not hold either. That is to say, there exists a time $T > 0$ and an initial condition $w_0 \in H^2(0,1)$ satisfying $w_0(0) = 0$ such that

$$\|w(T,\cdot)\|_{H^2(0,1)} \geq C_4.$$

for some $C_4(T, w_0) > 0$.

Corollary 18.2 *Let us consider the following bilinear-control system associated to a heat equation:*

$$\begin{cases} z_t - z_{xx} = \dfrac{\widehat{v}_3(t) - 1}{2} z & \text{in } Q, \\ z(t,0) = 0, \quad z(t,1) = \widehat{v}_4(t) & \text{in } (0,T), \\ z(0,x) = z_0(x) & \text{in } (0,1), \end{cases} \tag{18.9}$$

with $\widehat{v}_3 \in L^2(0,T)$ and $\widehat{v}_4 \in H^1(0,T)$. Then, equivalently as in the previous corollary, the exact controllability (for large time) and the exact null controllability (for small time) of system 18.9) with H^2-data do not hold.

This second part of the talk is inspired in the recent work [4].

Bibliography

[1] J.-M. Coron. *Some open problems on the control of nonlinear partial differential equations*, in "Perspectives in Nonlinear Partial Differential Equations: In honour of Haïm Brezis", Editors H. Brestycki, M. Bertsch, B. Peletier, L. Véron, Birkaüser.

[2] E. Fernández-Cara and S. Guerrero. *On the controllability of Burgers system*, C. R. Acad. Sci. Paris, Vol 341 (2005), pp 229-232.

[3] A. Fursikov, O. Yu. Imanuvilov. *Controllability of Evolution Equations*, Lecture Notes #34, Seoul National University, Korea, 1996.

[4] S. Guerrero, O. Yu. Imanuvilov. *Remarks on global controllability for the Burgers equation with two control forces*, to appear in Annal. de l'Inst. Henri Poincaré, Analyse Non Linéaire.

[5] J.-L. Lions, E. Magenes. *Non-homogeneous boundary value problems and applications*, Vol. I. Translated from the French by P. Kenneth. Die Grundlehren der mathematischen Wissenschaften, Band 181. Springer-Verlag, New York-Heidelberg, 1972.

An application of conformal mapping to image non perfectly conducting inclusions

Houssem Haddar[1] *Rainer Kress*[2]

19.1 Introduction

In a series of papers Akduman, Haddar and Kress [1, 11, 13] have developed a new simple and fast numerical scheme for solving two-dimensional inverse boundary value problems for the Laplace equation that model non-destructive testing and evaluation via electrostatic imaging. In the fashion of a decomposition method, the reconstruction of the boundary shape Γ_0 of a perfectly conducting or a nonconducting inclusion within a doubly connected conducting medium $D \subset \mathbb{R}^2$ from over-determined Cauchy data on the accessible exterior boundary Γ_1 is separated into a nonlinear well-posed problem and a linear ill-posed problem. The approach is based on a conformal map $\Psi : B \to D$ that takes an annulus B bounded by two concentric circles onto D. In the first step, in terms of the given Cauchy data on Γ_1, by successive approximations one has to solve a nonlocal and nonlinear ordinary differential equation for the boundary values $\Psi|_{C_1}$ of this mapping on the exterior boundary circle of B. Then in the second step a Cauchy problem for the holomorphic function Ψ in B has to be solved via a regularized Laurent expansion to obtain the unknown boundary $\Gamma_0 = \Psi(C_0)$ as the image of the interior boundary circle C_0. In [1, 11, 13] this method is described both for the homogeneous Dirichlet and Neumann condition on the unknown interior boundary Γ_0 and two different convergence results on the successive approximations are presented. The numerical examples in [1, 11, 13] exhibit the feasibility of the scheme.

The more general case to reconstruct a conducting inclusion with a conductivity that is different from the background conductivity of D leads to an inverse transmission problem. For this case, when applying the conformal mapping idea two conformal maps are required. In addition to the mapping $\Psi : B \to D$ also a map taking the interior of C_0 onto the interior of Γ_0 is needed. Furthermore, the simple homogeneous transmission condition on Γ_0 transforms into a more complicated transmission condition on C_0 whereas the homogeneous Dirichlet or Neumann condition on Γ_0 transforms into a homogeneous Dirichlet or Neumann condition on C_0, respectively. Nevertheless, by restriction to the case where the two conformal maps are extensions of each other, and consequently have to coincide with a Moebius transform, in a first attempt Dambrine and Kettab [6] were able to extent parts of the above approach to the inverse transmission problem.

[1] houssem.haddar@inria.fr
[2] kress@math.uni-goettingen.de

In the present work, we follow a different route and develop an analysis of the conformal mapping method for inverse boundary value problems to the case of a homogeneous impedance condition on Γ_0 as an approximation for the transmission problem. In this case, we still need only one conformal map $\Psi : B \to D$. However, unfortunately, the homogeneous impedance condition on Γ_0 transforms into an impedance condition on C_0 that contains the trace of the derivative of the conformal map Ψ on C_0. Therefore, the algorithm does not completely decompose the inverse problem into a well-posed nonlinear ordinary differential equation and an ill-posed Cauchy problem. Consequently its analysis and implementation is more involved and more than a straightforward extension of the algorithm for the Dirichlet or Neumann case.

For applications of nondestructive testing that can be modeled in two dimensions we refer to [4, 5] for the detection of faults in metal plates via applying electric currents and to [9, 10] for monitoring of lung patients and to [7, 14] for the evaluation of wood quality both via electrical impedance tomography in long cylindrical objects. For other work using conformal mapping ideas in the study of inverse problems for the Laplace equation we refer to [2, 3, 4, 8].

19.2 The inverse impedance problem

In order to describe the inverse problem more concisely, assume that D is a doubly connected bounded domain in $\mathbb{R}^2$ with a smooth boundary ∂D that consists of two disjoint closed Jordan curves Γ_0 and Γ_1, that is, $\partial D = \Gamma_0 \cup \Gamma_1$ with $\Gamma_0 \cap \Gamma_1 = \emptyset$ such that Γ_0 is contained in the interior of Γ_1. By ν we denote the outward unit normal to Γ_0 and to Γ_1. For a given function $f \in H^{1/2}(\Gamma_1)$ and a positive constant λ we consider the impedance problem for the Laplace equation

$$\Delta u = 0 \quad \text{in } D \tag{19.1}$$

with boundary conditions

$$\frac{\partial u}{\partial \nu} - \lambda u = 0 \quad \text{on } \Gamma_0 \tag{19.2}$$

and

$$u = f \quad \text{on } \Gamma_1. \tag{19.3}$$

Note that the positivity of λ ensures existence and uniqueness of a solution $u \in H^1(D)$.

The topic of our paper is the inverse problem to determine the shape of the interior boundary curve Γ_0 from a pair of Cauchy data

$$(f, g) = \left(u, \frac{\partial u}{\partial \nu} \right) \Big|_{\Gamma_0}$$

where $u \in H^1(D)$ is harmonic in D and satisfies the impedance condition (19.2) and from the knowledge of the impedance λ.

Let us notice that, as opposed to the inverse Dirichlet or inverse Neumann problem there is no uniqueness for the inverse impedance problem stated above, with one pair of Cauchy data. We refer to [12] where counter examples are constructed in the case of concentric circles. It is also shown that local uniqueness (geometries close to concentric circles) holds when f is constant.

19.3 The conformal mapping method

In the sequel we will identify $\mathbb{R}^2$ and $\mathbb{C}$ in the usual manner. To describe the conformal mapping method we recall the annulus $B := \{z \in \mathbb{C} : \rho < |z| < 1\}$ bounded by the circles $C_0 := \{z \in \mathbb{C} : |z| = \rho\}$ and $C_1 := \{z \in \mathbb{C} : |z| = 1\}$. By the conformal mapping theorem there exists a uniquely determined radius ρ of the annulus and a holomorphic function Ψ that maps B bijectively onto D such that the boundaries C_0 and C_1 are mapped onto Γ_0 and Γ_1, respectively. Denoting by L_1 the length of Γ_1, let

$$\gamma : [0, L_1] \to \Gamma_1$$

be a parameterization of Γ_1 in terms of arc length. Now, we can uniquely characterize the mapping Ψ by prescribing $\Psi(1) = \gamma(0)$.

We define functions $\chi : [0, 2\pi] \to \mathbb{C}$ and $\varphi : [0, 2\pi] \to [0, L_1]$ by setting

$$\chi(t) := \Psi(\rho e^{it}) \quad \text{and} \quad \varphi(t) := \gamma^{-1}(\Psi(e^{it})). \tag{19.4}$$

The function χ is injective and parameterizes the interior boundary curve Γ_0. The function φ is strictly monotonically increasing and bijective and, roughly speaking, it describes how Ψ maps arc length on C_1 onto arc length on Γ_1. Obviously, determining the map χ solves the inverse boundary value problem.

We associate the impedance problem (19.1)–(19.3) in D with an impedance problem posed in the annulus B: For a given function $F \in H^{1/2}(C_1)$ and a positive continuous function μ on C_0 find a harmonic function

$$\Delta v = 0 \quad \text{in } B \tag{19.5}$$

with boundary conditions

$$\frac{\partial v}{\partial r} - \mu v = 0 \quad \text{on } C_0 \tag{19.6}$$

and

$$v = F \quad \text{on } C_1. \tag{19.7}$$

To this end, let u and $\tilde{u}$ be conjugate harmonic functions in D and introduce the conjugate harmonic functions $v := u \circ \Psi$ and $\tilde{v} := \tilde{u} \circ \Psi$ in B. Using polar coordinates (r, t) in the annulus B, from the Cauchy–Riemann equation for v and $\tilde{v}$ we have that

$$\frac{1}{\rho} \frac{\partial \tilde{v}}{\partial t} = \frac{\partial u}{\partial r} \quad \text{on } C_0. \tag{19.8}$$

The chain rule together with the Cauchy–Riemann equation for u and $\tilde{u}$ implies

$$\frac{\partial}{\partial t} \tilde{u}(\chi(t)) = |\chi'(t)| \, \frac{\partial \tilde{u}}{\partial s}(\chi(t)) = |\chi'(t)| \, \frac{\partial u}{\partial \nu}(\chi(t)). \tag{19.9}$$

Therefore, if u satisfies the impedance boundary condition (19.2), combining (19.8) and (19.9) we deduce that

$$\frac{\partial v}{\partial r}(\rho e^{it}) - \frac{\lambda}{\rho} |\chi'(t)| \, v(\rho e^{it}) = 0, \quad 0 \le t \le 2\pi.$$

Therefore, if u solves the impedance problem (19.1)–(19.3) then $v = u \circ \Psi$ solves the impedance problem (19.5)–(19.7) with $F = f \circ \Psi$ and $\mu = \mu_{\rho,\Psi}$ where

$$\mu_{\rho,\Psi}(\rho e^{it}) := \frac{\lambda}{\rho} \left| \frac{d}{dt} \Psi(\rho e^{it}) \right|, \quad 0 \le t \le 2\pi. \tag{19.10}$$

The nonlocal differential equation

Denote by $A_{\rho,\mu} : H^{1/2}(C_1) \to H^{-1/2}(C_1)$ the Dirichlet-to-Neumann operator for the impedance problem (19.5)–(19.7). It maps functions $F \in H^{1/2}(C_1)$ onto the normal derivative $\partial v/\partial\nu$ on C_1 of the solution to (19.5)–(19.7). Note that as opposed to the corresponding operator for the homogeneous Dirichlet or Neumann boundary condition on C_0 in addition to depending on the radius ρ the operator $A_{\rho,\mu}$ also depends on the holomorphic map Ψ via (19.10). As in [1, 11], from the Cauchy–Riemann equations we have the nonlocal differential equation

$$\frac{d\varphi}{dt} = \frac{A(f \circ \gamma \circ \varphi)}{g \circ \gamma \circ \varphi} \tag{19.11}$$

for the boundary map φ which has to be complemented by the boundary conditions

$$\varphi(0) = 0 \quad \text{and} \quad \varphi(2\pi) = L_1. \tag{19.12}$$

In order to rewrite (19.11)–(19.12) as a fixed point equation we introduce an operator V by setting

$$(V\psi)(t) = \frac{L_1}{2\pi}\, t + \psi(t), \quad t \in [0, 2\pi].$$

Then, for any pair of Cauchy data (f, g), after setting

$$U_{\rho,\mu}\psi := \frac{A_{\rho,\mu}(f \circ \gamma \circ V\psi)}{g \circ \gamma \circ V\psi}\ ,$$

we define an operator $T_{\rho,\mu} : H_0^1[0, 2\pi] \to H_0^1[0, 2\pi]$ by

$$(T_{\rho,\mu}\psi)(t) := \int_0^t \left[(U_{\rho,\mu}\psi)(\tau) - \frac{1}{2\pi} \int_0^{2\pi} (U_{\rho,\mu}\psi)(\theta)\, d\theta \right] d\tau, \quad t \in [0, 2\pi]. \tag{19.13}$$

Now, as easily seen, if $\varphi \in H^1[0, 2\pi]$ is a solution of (19.11)–(19.12) then $\psi = V^{-1}\varphi \in H_0^1[0, 2\pi]$ is a fixed point of $T_{\rho,\mu}$, that is,

$$\psi = T_{\rho,\mu}\psi \tag{19.14}$$

is satisfied. Note that if $T_{\rho,\mu}$ is a contraction, then (19.11)–(19.12) and (19.14) are equivalent.

An equation for the radius

To derive an expression for the radius ρ, in terms of the conformal map Ψ we denote by w the solution to the impedance problem (19.5)–(19.7) in B with $F = 1$ and $\mu = \mu_{\rho,\Psi}$ as defined in (19.10). Then we introduce the function $H_\Psi : (0, 1) \to \mathbb{R}$ by

$$H_\Psi(\rho) := \int_{C_1} f \circ \Psi\, \frac{\partial w}{\partial \nu}\, ds. \tag{19.15}$$

Applying Green's theorem to v and w in the annulus B, from the boundary conditions for v and w we obtain that

$$\int_{C_1} f \circ \Psi\, \frac{\partial w}{\partial \nu}\, ds = \int_{C_1} \frac{\partial v}{\partial \nu}\, ds = \int_{\Gamma_1} g\, ds$$

and therefore we have

$$H_\Psi(\rho) = \int_{\Gamma_1} g\, ds \tag{19.16}$$

as a necessary condition for the radius ρ in terms of the data f and g and the holomorphic map Ψ.

We summarize the above results into the following theorem.

Theorem 19.1 *Let (f, g) be a pair of Cauchy data for the impedance boundary condition* (19.2)*. Then, in terms of the holomorphic map $\Psi : B \to D$ and its boundary values φ the function $\psi = V^{-1}\varphi$ is a fixed point of $T_{\rho,\mu}$ where the impedance μ is given via* (19.10) *in terms of Ψ and the radius ρ satisfies equation* (19.16)*.*

For an approximate solution of (19.16) via Newton iterations we need the derivative of H_Ψ. This in turn requires the derivative w' of the solution w of (19.5)–(19.7) for $F = 1$ with respect to the radius ρ.

It is shown in [12] that

$$H'_\Psi(\rho) = \int_{C_1} f \circ \Psi \, \frac{\partial w'}{\partial \nu} \, ds \tag{19.17}$$

where w' is a harmonic function in B satisfying the boundary conditions

$$\frac{\partial w'}{\partial \nu} - \mu w' = \frac{1}{\rho^2} \, \frac{\partial^2 w}{\partial t^2} + \left(\mu^2 + \frac{\mu}{\rho} + \mu' \right) w \quad \text{on } C_0 \tag{19.18}$$

and

$$w' = 0 \quad \text{on } C_1. \tag{19.19}$$

For the numerical evaluation of the derivative $\partial^2 w / \partial t^2$, for example, trigonometric differentiation can be used.

Regularization of the Cauchy problem

Once we determined the boundary function ψ and the radius ρ, finally, we need to solve the Cauchy problem for Ψ in B. To this end we expand $\gamma \circ V\psi$ in a Fourier series

$$\gamma(V\psi(t)) = \sum_{k=-\infty}^{\infty} a_k e^{ikt}, \quad t \in [0, 2\pi],$$

and, in principle, obtain Ψ by the Laurent series

$$\Psi(z) = \sum_{k=-\infty}^{\infty} a_k z^k. \tag{19.20}$$

The series (19.20) exhibits the ill-posedness of the Cauchy problem, since small errors in the Fourier coefficients a_k for $k < 0$ will be amplified by the exponentially increasing factors z^k for $|z| < 1$. Therefore we incorporate a regularization of Tikhonov type and replace (19.20) by

$$\Psi_\alpha(z) = \sum_{k=0}^{\infty} a_k z^k + \sum_{k=1}^{\infty} a_{-k} \, \frac{|z|^{2k}}{\alpha + |z|^{2k}} \, z^{-k}, \quad \rho < |z| < 1, \tag{19.21}$$

where $\alpha > 0$ serves as a regularization parameter. For its choice via a discrepancy principle we refer to [11]. Note that the series (19.21) converges for $|z| < 1$ provided $\gamma \circ V\psi$ is in $L^2[0, 2\pi]$.

19.4 Numerical examples

The system of equations (19.14)-(19.16)-(19.20) is solved using an iterative scheme based on successive approximations. As explained before, the update for the radius is done via a linearization

of (19.16), using (19.17). The following numerical examples illustrate the convergence for different values of the impedance λ, when the exterior boundary is the unit circle and the interior boundary has the parametrization

$$x_1(t) = -0.2 + 0.4\cos t, \quad x_2(t) = 0.4\sin t + 0.2\sin t, \ t \in [0,\, 2\pi].$$

The pair of Cauchy data corresponds to $f = 1$. One observes for instance how the reconstruction quality deteriorates as λ decreases, which is in concordance with the instability of the algorithm for the Neumann problem (see [11]).

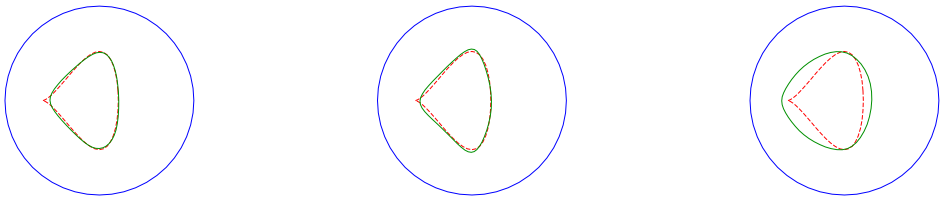

Figure 19.1: *Exact (red-dashed) and reconstructed (green-solid) geometries for* $\lambda = 100$ *(left),* $\lambda = 10$ *(middle),* $\lambda = 1$ *(right). Cauchy data corrupted with 1% added random noise.*

Bibliography

[1] I. Akduman and R. Kress. Electrostatic imaging via conformal mapping. Inverse Problems **18**, 1659–1672 (2002).

[2] G. Alessandrini. Examples of instability in inverse boundary-value problems. Inverse Problems **13**, 887–897 (1997).

[3] G. Alessandrini and L. Rondi. Optimal stability for the inverse problem of multiple cavities. J. Differential Equations **176**, 356–386 (2001).

[4] N.D. Aparicio and M.K. Pidcock. The boundary inverse problem for the Laplace equation in two dimensions. Inverse Problems **12**, 565–577 (1996).

[5] H.T. Bank and F. Kojima. Boundary shape identification in two-dimensional electrostatic problems using SQUIDs. J. Inv. Ill.-Posed Problems **8**, 467–504 (2000).

[6] M. Dambrine and D. Kettab. Conformal mapping and inverse conductivity problem with one measurement. To appear (2006).

[7] V. Dubbel, U. Weihs, F. Krummheuer and A. Just. Die elektrische Widerstandstomographie – Neue Methode zur zweidimensionalen Darstellung von Fäulen an Fichte. Allgemeine Forstzeitschrift/Der Wald **26**, 1422–1424 (1999).

[8] A.R. Elcrat, V. Isakov and O. Neculoiu. On finding a surface crack from boundary measurements. Inverse Problems **11**, 343–351 (1995).

[9] I. Frerichs, J. Hinz, P. Herrman, G. Weisser, G. Hahn, M. Quintel and G. Hellige. Regional lung perfusion as determined by electrical impedance tomography in comparison with electron beam CT imaging. IEEE Trans.Med Imaging **21**, 646–52 (2002).

[10] I. Frerichs, H. Schiffmann, R. Oehler, T. Dudykevych, J. Hinz, G. Hahn and G. Hellige. Distribution of lung ventilation in spontaneously breathing neonates lying in different body positions. Intensive Care Med. **29**, 787–794 (2003).

[11] H. Haddar and R. Kress. Conformal mappings and inverse boundary value problems. Inverse Problems **21**, 935–953 (2005).

[12] H. Haddar and R. Kress. Conformal Mapping and an Inverse Impedance Boundary Value Problem. preprint (2006).

[13] R. Kress. Inverse Dirichlet problem and conformal mapping. Mathematics and Computers in Simulation **66**, 255–265 (2004).

[14] U. Weihs, F. Krummheuer and V. Dubbel. Zerstörungsfreie Baumdiagnose mittels elektrischer Widerstandstomographie. Jahrbuch der Baumpflege 2001, 50-58, Thalacker Medien, Braunschweig.

Inverse modelling in neuro-sciences: what does nature want ?

Antoine Henrot[1] *Yannick Privat*[2]

20.1 Introduction

The observation of the nature and of the "perfection" of most of its mechanisms of living beings drives us to search **a principle of optimality** which governs those mechanisms. If a mathematical model exists for describing a biological phenomenon or component of a living being, there is a temptation to quantify the optimality by finding a functional which leads to the optimality principle. The confrontation between the computed optimum and the real one leads us to validate or invalidate the model and/or the choice of the functional. This inverse modelling method consists in finding the mathematical model starting from observations and theirs consequences. If the optimal shape which is issued from the mathematical model is close to the real shape, we have reasons to believe that the full model (equation and functional) is good. If not, one has to reject it and find another one, or improve it.

To be more precise, we will consider here the example of an axon. What is an axon (see Figure 20.1)?

The part of the nerve cell that contains the nucleus is called *soma*. An *axon* is an extension from the neuron cell body that takes information away from the cell body. The role of an axons is to carry nerve impulses away from the soma to the presynaptic terminals where the impulses are transmitted to other neurons or to muscles in the case of motor neurons. The action potential is an explosive release of charge between a nerve cell (neuron) and its surroundings. It moves along a neuron from a dendrite, through the soma and then the axon. It is part of the mechanism that moves nervous messages (nerve transmissions or impulses) along neurons.

The propagation of an electric impulsion in an axon fiber follows an equation established by W. Rall in the sixties, cf [1], [2], [3]:

$$\left\{\begin{array}{l} \dfrac{1}{2R_a^2}\dfrac{\partial}{\partial x}\left(a^2\dfrac{\partial v}{\partial x}\right) = a\sqrt{1+a'^2}\left(C_m\dfrac{\partial v}{\partial t}+G_m v\right) \\ \dfrac{\pi a^2(0)}{R_a}\dfrac{\partial v}{\partial x}(0,t) = A_s\left(C_m\dfrac{\partial v}{\partial t}(0,t)+G_s v(0,t)\right) - i_0(t) \\ \dfrac{\partial v}{\partial x}(\ell,t) = 0. \end{array}\right. \tag{20.1}$$

where

[1]École des Mines de Nancy et Institut Élie Cartan, Universités de Nancy, CNRS, INRIA, Antoine.Henrot@iecn.u-nancy.fr

[2]Institut Élie Cartan, Universités de Nancy, CNRS, INRIA, Yannick.Privat@iecn.u-nancy.fr

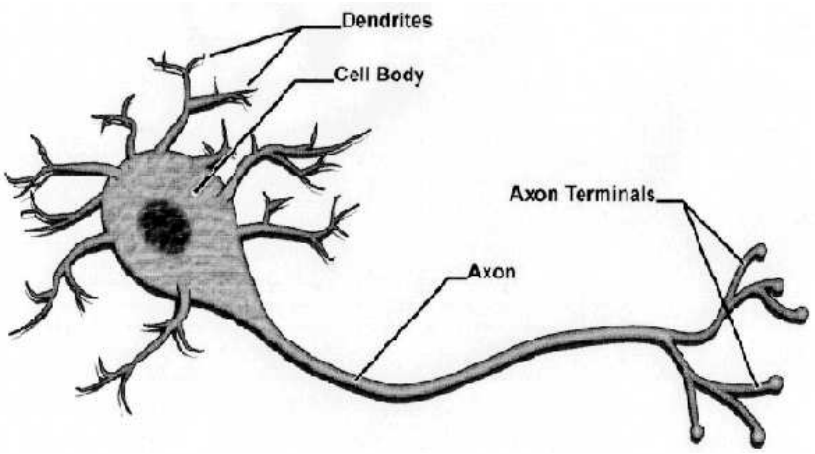

Figure 20.1: *Axon*

- we consider a fiber with a cylindrical symmetry of length ℓ and radius $a(x)$;
- $i(x,t)$ denotes the axial current at point x and time t;
- $v(x,t)$ denotes the difference from rest of the membrane potential;
- R_a denotes the axial resistance (kΩcm);
- C_m denotes the membrane capacitance (μF/cm^2);
- G_m denotes the membrane conductance (mS/cm^2);
- A_s is the surface area of the soma.

By assumption a is a radial function. It is our main unknown. We assume : $a \in W^{1,\infty}([0,\ell])$ and $\min_{x\in[0,\ell]} a(x) \geq a_0$, where a_0 depends on the constants A_s, γ and ℓ. We suppose that at $t=0$, the fiber receives an impulsion. We choose $i_0(t) = \delta_{\{t=0\}}$ (Dirac operator). Expanding the solution of (20.1) in the spectral basis leads us to consider the eigenvalue problem:

$$\begin{cases} -(a^2\varphi_n')' = \lambda_n(a)\, a\sqrt{1+a'^2}\,\varphi_n & x \in [0,\ell] \\ \dfrac{2\pi}{A_s}\, a^2(0)\varphi_n'(0) + (\lambda_n+\gamma)\varphi_n(0) = 0 & \\ \varphi_n'(\ell) = 0 & \end{cases} \tag{20.2}$$

with $\gamma := 2R_a(G_m - G_s)$.

20.2 The optimization problem

We look for the shape of an axon which minimizes **the attenuation in time** of the signal. A good criterion should be the first eigenvalue of (20.2). We must assume some bounds on the possible radius $a(x)$ of the axon and also a total surface constraint. The surface area is clearly given by $S := 2\pi \int_0^\ell a(x)\sqrt{1+a'^2(x)}dx$. So our problem is:

Optimization problem:
Let S_0, ρ_0, ρ_1 be three positive numbers such that $\rho_0 < \rho_1$ and let us define the class:

$$\mathcal{A}_{\rho_0,\rho_1,S_0} := \{a \in W^{1,\infty}(0,\ell) : \rho_0 \leq a^3\sqrt{1+a'^2} \leq \rho_1, \int_0^\ell a(x)\sqrt{1+a'^2(x)}dx = S_0\}.$$

We want to find $a^* \in A_{\rho_0,\rho_1,S_0}$ which minimizes $\lambda_1(a)$ (the first eigenvalue of (20.2)).

We introduce the change of variable $y = \displaystyle\int_0^x \frac{dt}{a^2(t)}$, and the following notations :

- $b(y) := a(x)$ and $v(y) := u(x)$;
- $\rho(y) = b^3(y)\sqrt{1+\dfrac{b'^2(y)}{b^4(y)}} = a^3(x)\sqrt{1+a'^2(x)}$.
- $\ell_1 := \displaystyle\int_0^\ell \frac{dt}{a^2(t)}$.

The eigenvalue problem (20.2) becomes:

$$\begin{cases} -v'' = \lambda(\rho)\,\rho v & y \in [0,\ell_1] \\ v'(0) + A(\lambda+\gamma)v(0) = 0 & \\ v'(\ell_1) = 0. & \end{cases} \tag{20.3}$$

Moreover, we have that :

(i) $\rho_0 \leq \rho(y) \leq \rho_1$

(ii) $\int_0^{\ell_1} \rho(y)dy = S_0$.

Now, the problem of looking for a function ρ^* satisfying **(i)** and **(ii)** which minimizes the first eigenvalue $\lambda_1(\rho)$ of (20.3) is very similar to classical problems in optimization of eigenvalues, see e.g. [4] or [5]. In particular, it is easy to check that the solution is a *bang-bang* function: there exists $\xi_1 \in [0,\ell_1]$ such that

$$\rho^*(y) := \begin{cases} \rho_1 & \text{if } y \in [0,\xi_1[; \\ \rho_0 & \text{if } y \in]\xi_1, l_1]. \end{cases}$$

We deduce from the previous analysis that a^* should be the solution of the following ODE :

$$\begin{cases} a' = \varepsilon\dfrac{\sqrt{\rho_1^2 - a^6}}{a^3} & \text{if } x \in [0,\gamma_1[; \\ a' = \tilde{\varepsilon}\dfrac{\sqrt{\rho_0^2 - a^6}}{a^3} & \text{if } x \in]\gamma_1, l_1]. \end{cases}$$

with the conventions $\xi_1 = \displaystyle\int_0^{\gamma_1} \frac{dt}{a^2(t)}$ and $(\varepsilon,\tilde{\varepsilon}) \in \{-1,+1\}^2$.

We will conclude the talk with examples and a discussion to know whether the solution we got is a good one or not. More precisely: have we chosen a good criterion or not?

Bibliography

[1] W. Rall. *Theory of physiological properties of dendrites*, Ann, NY Acad Sciences **96** (1962) 1071.

[2] W. Rall, H. Agmon-Snir. *Cable theory for dendritic neurons*, C. Koch, I. Segev (Eds) Methods in Neuronal Modeling second edition, MIT, Cambridge, MA, 1998.

[3] S.J. Cox, J.H. Raol. *Recovering the passive properties of tapered dendrites from single and dual potential recordings*, Math. Biosci. **190** (2004), no. 1, 9–37.

[4] M.G. Krein. *On certain problems on the maximum and minimum of characteristic values and on the Lyapunov zones of stability*, Amer. Math. Soc. Transl. (2) 1 (1955), 163–187.

[5] A. Henrot. *Extremum problems for eigenvalues of elliptic operators*, Frontiers in Mathematics, Birkhäuser, Basel to appear.

Prediction and Errors for Geophysical Fluids

François-Xavier Le Dimet[1]

21.1 Introduction

Geophysical fluids (atmosphere, ocean, continental water) have some particularities, which are important to take into account when they are modelized in view of their prediction.

- Each situation is unique and therefore the model is not seeking for some asymptotic behavior, steady state or periodic solution.
- Geophysical fluids are non closed, they is always an interface with another fluid e.g. the fluxes of heat and humidity between the ocean and the atmosphere are fundamental to understand the evolution of climate. Therefore if the fluxes at the interfaces can't be explicitly set in the model they have to be parametrized.
- Geophysical fluids are non linear and consequently there are interaction between all the scales both in time and space. The discretization introduced in numerical model will be a truncature in the scales, nevertheless the subgrid fluxes of energy and matter must be taken into account by some empirical parametrization.

A consequence of these particularities is that the equation are not sufficient for predicting the evolution of the fluid the initial condition and some parameters must be taken into account and they will be obtained from direct or remote observations of the fluid.

Mixing models and data is a fundamental problem for environmental fluids. This problem with the associated algorithms is named : Data Assimilation.

21.2 Errors

In the process of forecasting the evolution of a fluid there are several kind of errors which are introduced:

- Errors in the model itself , some processes are modelized by empirical parametrization with errors. The boundary conditions have errors due to an approximate knowledge of the topography.
- Errors in the data due to physical measurements or sampling.

[1]Université Joseph Fourier (Grenoble, France) and INRIA Project MOISE

- Errors in the numerical methods issued from the discretization or by stopping criterion in the iterative methods that should be used with non linear models.

At first sight these errors sound independent but this is not the case: the same observation e.g. of the wind can be used in a very local model with a scale of some decimeters or in a synoptic model. The confidence in the observation will vary according to the context (i.e. the model) in which it is used.

21.3 Variational Data Assimilation

A way to link together data and model is to link them through a variational principle. The model is defined by :

$$\begin{cases} \dfrac{dX}{dt} = F(X) + B.V \\ X(0) = U \end{cases} \tag{21.1}$$

- X is the state variable and describes the evolution of the fluid.
- V is a control term, error and/or boundary condition.
- U is the initial condition, it's a control variable.

The discrepancy between the solution of the model associated to U and V and the observation X_{obs} is given by the cost-function

$$J(U,V) = \int_0^T \|CX - X_{\text{obs}}\|^2 dt + \|U - U_0\|^2 \tag{21.2}$$

U_0 is an a priori estimation of the initial condition. Therefore the problem is to determine (U^*, V^*) minimizing J.

The Euler-Lagrange equation, the optimality system (O.S) is deduced :

$$\begin{cases} \dfrac{dX}{dt} = F(X) + B.V \\ X(0) = U \\ \dfrac{dP}{dt} + \left[\dfrac{\partial F}{\partial X}\right]^t P = C^t(CX - X_{\text{obs}}) \\ P(T) = \\ \nabla_U J == P(0) + (U - U + 0) = 0 \\ \nabla_V J = -B^t.P = 0 \end{cases} \tag{21.3}$$

P is the adjoint variable, in the dual space of the state variable X Another source of information is provided by the statistics on the fields, it can be plugged in the analysis via the norms which are used in the space of observations and in the space of the initial condition taking into account the matrix of correlations of these fields. For sake of simplicity we won't use this information here. The optimal solution is obtained by carrying out a method of unconstrained optimization (BFGS, Quasi or Truncated Newton), the direction of descent, depending in the gradient of the cost function which is obtained by solving the adjoint model.

This method is presently used by the main meteorological services in the world.

It worth to point out that all the available information is contained in the optimality system. Thanks to the variational principle it has been possible to make a link between heterogeneous sources of information : mathematical information (the model), physical information (data) and statistical information.

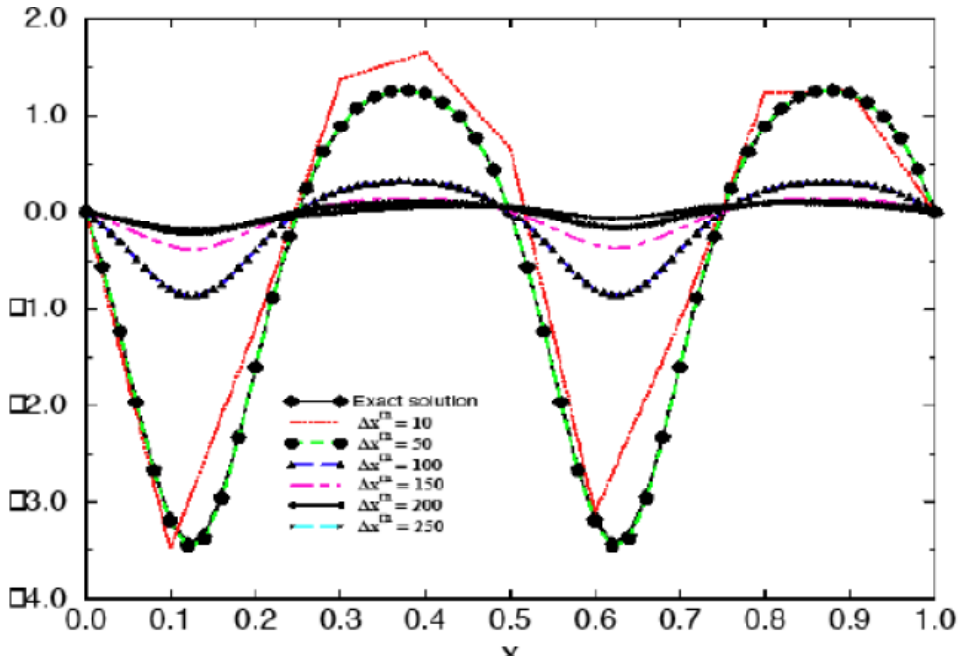

21.4 Errors and prediction

We would like to illustrate the propagation of errors on a simple one dimension model: the Burger's equation. The state variable is the velocity $w(x,t)$, the right hand side of the equation f is chosen such the exact of the continuous problem is known. The problem is discretized by a standard finite difference method. Therefore the only error introduced is the error of discretization. The observations are the values of the exact solution at fifty grid points.

$$\frac{\partial w}{\partial t} + w\frac{\partial w}{\partial x} - v\frac{\partial^2 w}{\partial x^2} = f \tag{21.4}$$

$$w(0,t) = w(1,t) = 0 \tag{21.5}$$

$$w(x,0) = u(x) \tag{21.6}$$

$$J(u) = \frac{1}{2}\int_0^1 \int_0^T (Cu - u_{\text{obs}})dtdx \tag{21.7}$$

In this case the only control is the initial condition. The assimilation has been done with several discretization ranging from $h = 1/10$ to $h = 1/250$ on the time interval between 0 and 1, therefore the initial condition was retrieved, then the prediction was carried out at tile $T = 2$

This simple example demonstrates that if the model is improver, in this case by decreasing the discretization error then the prediction can be downgraded, and therefore the important item to be studied is where all the available information is gathered: the optimality system.

21.5 Sensitivity and estimation of errors

Sensitivity is an important notion in modeling it permit to estimate the impact of perturbations. It can be stated as follow.

$$\Phi(\alpha, \beta) = 0$$

is the model with a unique solution $\alpha(\beta)$ for β given. α is the state variable, β a parameter, $\Psi(\alpha, \beta)$ is a scalar "response" function. How to estimate the sensitivity of Ψ with respect to β. Usually done by finite difference, small perturbations on β. If the dimension of β is large, it's impossible to explore the domain of β.

γ is the adjoint variable of α. If it is a solution of

$$\left[\frac{\partial \Phi}{\partial \alpha}\right]^t \gamma = \frac{\partial \Psi}{\partial \alpha}$$

the the sensitivity is given by

$$S = \left[\frac{\partial \Phi}{\partial \beta}\right]^t \gamma + \frac{\partial \Psi}{\partial \beta}$$

and therefore the sensitivity is obtained by just one run of the adjoint model.

In the situation of data assimilation, if we look for the impact of an error of observation, this sensitivity analysis must be carried out not on the model itself –it doesn't contain the observations– but on the optimality system. Therefore we need to take into account the second order properties. We will see how this procedure permits to estimate the covariance of the error on the initial condition from the covariance of the error on the observations or from some error on the model.

21.6 Conclusion

Most of the time the adjoint model is considered as a tool to compute a gradient in view of carrying out a algorithm of optimization. In fact the Optimality System must be considered as a generalized models and all the perturbations studies must be done on this Optimality System.

Bibliography

[1] F.-X. Le Dimet, I.M. Navon, D.N. Daescu. Second Order information in dataassimilation, Monthly Weather Review, vol.130, **3**:629-648, 1996.

[2] F.-X. Le Dimet, V. Shutyaev. On deteministic error analysis in variatonal data assimilation, Nonlinear Processes in Geophysics, vol 12, pp 481-490, 2005.

A Riemannian framework for the averaging, smoothing and interpolation of constrained data

Maher Moakher[1]

Abstract

The availability of new technologies in many fields of science has made it possible to acquire and store quite easily a huge amount of data. However, these data are generally corrupted with noise of different sources. It is therefore necessary to remove or reduce the noise before meaningful information could be extracted from them. In many situations, these data are subjected to nonlinear constraints. Symmetric positive-definite diffusion tensors from Diffusion Tensor Magnetic Resonance Imaging (DT-MRI) data, special Euclidean matrices from motion data, rotation matrices from orientation data, and unit vectors from directional data, are but few examples of constrained data. We use a Riemannian framework for the introduction of properly invariant means of element in some Riemannian symmetric spaces. We describe the use of these means for the smoothing of noisy data, and for the interpolation and averaging of discrete data on some smoothly constrained data. Some applications of these procedures for problems in engineering and biology are discussed.

22.1 Introduction

The availability of new technologies in many fields of science has made it possible to acquire and store quite easily a huge amount of data. These data are generally corrupted with noise whose origin can be related to the data acquisition devices, to the operator, to the environment, etc. It is therefore necessary to remove or reduce the noise before meaningful information could be extracted from them. As a consequence, there has been a growing demand for reliable, robust and efficient methods of data processing and analysis such as estimation, registration, averaging, smoothing, and interpolation. In many situations, these data are subject to nonlinear constraints. Symmetric positive-definite diffusion tensors from Diffusion Tensor Magnetic Resonance Imaging (DT-MRI) data [3, 19], special Euclidean matrices from motion data [1, 17], rotation matrices from orientation data [20], and unit vectors from directional data [7, 8, 11], are but few examples of constrained data.

Many of the data processing tasks mentioned above can be formulated as minimization problems of some cost functions over a smoothly constrained space. The classical approach to

[1] National Engineering School at Tunis, Tunis El-Manar University; ENIT-LAMSIN, B.P. 37, 1002 Tunis-Belvédère, Tunisia; maher.moakher@enit.rnu.tn

these problems is to use tools of optimization on Euclidean spaces together with a set of Lagrange multipliers that account for the constraints. However, if the cost function is directly related to the Riemannian structure of the constrained space, then it may be more appropriate to treat the minimization problem as an unconstrained one but on the constrained space. Over the past few years, there has been an increasing interest in the use of differential-geometric methods for the analysis and computation of optimization problems on manifolds. Some examples of such studies are quoted here. Edelman *et al.* [6] have used differential-geometric tools to intrinsically account for the constraints and to design efficient methods for minimization problems on the Stiefel manifold. Smith [21] analyzed optimization algorithms, like Newton's methods, on Riemannian manifolds. Mahony and Manton [9] studied the geometry of Newton's method on non-compact Lie groups. Marthinsen [12] presented a method of interpolation on Lie groups.

In the unconstrained case, the are basically two different classes to the smoothing and regularization of noisy data. The first one is based on the smoothing effects of diffusion. In this class we find PDE and variational methods that are based on isotropic linear diffusion, anisotropic linear diffusion, or nonlinear diffusion [2, 18, 23]. The second class consists of smoothing methods based on filtering techniques. For example, mean, median, Gaussian, Fourier and Kalman filters are used to smooth data.

The use of the first approach for the smoothing and regularization of constrained data are being pursued, see e.g., [5, 22]. In this work, we shall adapt the second approach to smooth and interpolate constrained data. A fundamental tool to this approach is the introduction of the notion of a *geometric mean* on constrained spaces. The use of this mean for the smoothing of noisy data and for the interpolation of discrete data on some Riemannian matrix spaces are discussed. Some applications of the means and interpolation procedures for some problems in imaging and biology are described.

22.2 Geometric mean of matrices

Geometric mean of symmetric positive-definite matrices

Recall that the set of all positive-definite matrices, denoted by $\mathcal{P}(n)$, is a Riemannian symmetric space of dimension $n(n+1)/2$. The Riemannian distance between two matrices $\mathbf{A}$ and $\mathbf{B}$ in $\mathcal{P}(n)$ is given by

$$d_{\mathcal{P}(n)}(\mathbf{P}_1, \mathbf{P}_2) = \| \operatorname{Log}(\mathbf{P}_1^{-1/2}\mathbf{P}_2\mathbf{P}_1^{-1/2})\|_F = \sqrt{\sum_{i=1}^{n} \ln^2 \lambda_i}, \tag{22.1}$$

where $\lambda_i,\ i = 1, \ldots, n$ are the (positive) eigenvalues of $\mathbf{P}_1^{-1}\mathbf{P}_2$ and $\|\cdot\|_F$ denotes the Frobenius norm.

The geometric mean of m given symmetric positive-definite matrices $\mathbf{P}_1, \ldots, \mathbf{P}_m$ is defined as [14]

$$\mathcal{G}(\mathbf{P}_1, \ldots, \mathbf{P}_m) := \operatorname*{arg\,min}_{\mathbf{P}\in\mathcal{P}(n)} \sum_{k=1}^{m} d^2_{\mathcal{P}(n)}(\mathbf{P}, \mathbf{P}_k). \tag{22.2}$$

Using differential-geometric tools, we show that the Riemannian mean of $\mathbf{P}_1, \ldots, \mathbf{P}_m$ is given by the unique solution to the nonlinear matrix equation [14]

$$\sum_{k=1}^{m} \operatorname{Log}(\mathbf{P}_k^{-1}\mathbf{P}) = \mathbf{0}. \tag{22.3}$$

Due to the non-commutative nature of matrix multiplication in $\mathcal{P}(n)$, equation (22.3) cannot be solved in closed form except for special cases. For instance, the Riemannian mean of two symmetric positive-definite matrices $\mathbf{P}_1$ and $\mathbf{P}_2$ is given explicitly by the equivalent expressions

$$\begin{aligned}\mathcal{G}(\mathbf{P}_1,\mathbf{P}_2) &= \mathbf{P}_1(\mathbf{P}_1^{-1}\mathbf{P}_2)^{1/2} = (\mathbf{P}_2\mathbf{P}_1^{-1})^{1/2}\mathbf{P}_1 \\ &= \mathbf{P}_1^{1/2}(\mathbf{P}_1^{-1/2}\mathbf{P}_2\mathbf{P}_1^{-1/2})^{1/2}\mathbf{P}_1^{1/2}.\end{aligned} \tag{22.4}$$

Despite their appearance, the first two expressions given in (22.4) are indeed symmetric positive-definite matrices. We note also that three other equivalent expressions are obtained by the exchange of $\mathbf{P}_1$ and $\mathbf{P}_2$ in (22.4).

For more than two matrices, in general, it is not possible to obtain an explicit solution for the geometric mean equation (22.3). It can be solved numerically using the fixed-point algorithm introduced in [16].

Geometric mean of special orthogonal matrices

Let $SO(n)$ denotes the Lie group of special orthogonal matrices. It is well known that $SO(n)$ is a Riemannian manifold of dimension $n(n-1)/2$. The Riemannian distance between two special orthogonal matrices is given by

$$d_{SO(n)}(\mathbf{R}_1,\mathbf{R}_2) = \frac{1}{\sqrt{2}}\|\operatorname{Log}(\mathbf{R}_1^T\mathbf{R}_2)\|_F. \tag{22.5}$$

The geometric mean rotation of m given rotation matrices $\mathbf{R}_1,\ldots,\mathbf{R}_m$ is defined as [13]

$$\mathfrak{G}(\mathbf{R}_1,\ldots,\mathbf{R}_m) := \underset{\mathbf{R}\in SO(n)}{\arg\min}\sum_{k=1}^{m} d^2_{SO(n)}(\mathbf{P},\mathbf{P}_k). \tag{22.6}$$

The minimum here is understood to be the global minimum. We remark that the objective function in (22.6) is not geodesically convex, and therefore the mean may not be unique.

Local minima of the objective function in (22.6) are characterized by [13]

$$\sum_{k=1}^{m}\operatorname{Log}(\mathbf{R}_k^T\mathbf{R}) = \mathbf{0}. \tag{22.7}$$

In general, closed-form solutions to (22.7) cannot be found. However, the geometric mean of two non-antipodal rotation matrices $\mathbf{R}_1$ and $\mathbf{R}_2$ is given explicitly by [13]

$$\begin{aligned}\mathfrak{G}(\mathbf{R}_1,\mathbf{R}_2) &= \mathbf{R}_1(\mathbf{R}_1^{-1}\mathbf{R}_2)^{1/2} = (\mathbf{R}_2\mathbf{R}_1^{-1})^{1/2}\mathbf{R}_1 \\ &= \mathbf{R}_1^{1/2}(\mathbf{R}_1^{-1/2}\mathbf{R}_2\mathbf{R}_1^{-1/2})^{1/2}\mathbf{R}_1^{1/2}.\end{aligned} \tag{22.8}$$

Three other equivalent expressions are obtained by the exchange of $\mathbf{R}_1$ and $\mathbf{R}_2$ in (22.8).

22.3 Applications to averaging, smoothing and interpolation

Applications to diffusion-tensor magnetic resonance imaging

Diffusion tensor magnetic resonance imaging (DT-MRI) is a new modality that provides a non-invasive probe into the microstructure of materials by measuring the probability density function, p, for the displacements of particles that undergo Brownian motion due to thermal fluctuations.

In the biomedical context, as water is a major constituent of biological tissues, the particles of interest are generally water molecules. Diffusion tensor magnetic resonance imaging of *in vivo* biological tissues produces a three-dimensional second-order tensor field, $\mathbf{D}$, based on the assumption that the probability density function, p, for the displacements of water molecules is a zero-mean trivariate Gaussian distribution

$$p(\mathbf{x}, \mathbf{x}_0; \tau) = \frac{1}{\sqrt{(4\pi\tau)^3 \det \mathbf{D}}} \exp\left(-\frac{(\mathbf{x}-\mathbf{x_0})^T \mathbf{D}^{-1}(\mathbf{x}-\mathbf{x}_0)}{4\tau}\right),$$

where τ is the diffusion time. The diffusion tensor $\mathbf{D}$ is evaluated by measuring the diffusion of water in many directions. From the theoretical point of view, six independent directions suffices to fully determine the diffusion tensor. In practice, however, due to noise more than six directions are usually needed.

Currently, brain imaging is the most common application of DT-MRI. The anatomical structure of the brain is composed of grey-matter regions connected by white-matter fibers. Grey matter is a dense tissue containing many barriers to water mobility such as cell walls and membranes. These barriers are randomly oriented and thus they hinder the displacement of water molecules equally in all directions. The white matter is composed of bundles of parallel fibers and the cell walls and membranes are aligned with the fibers. Therefore, the mobility of water molecules in the direction parallel to the fibers is greater than that in perpendicular directions.

The anisotropy of the diffusion tensor is evident in the MR measurements, which can be used noninvasively to explore the white matter structures *in vivo*. In the last decade, the quantitative description of this anisotropy with DT-MRI has become well established in research environments and its first applications in the clinic are now being reported. Several measures of anisotropy are used within the DT-MRI community and the most common one is the fractional anisotropy given by [3]

$$FA(\mathbf{D}) = \sqrt{\frac{3}{2}} \sqrt{\frac{(\lambda_1-\bar{\lambda})^2 + (\lambda_2-\bar{\lambda})^2 + (\lambda_3-\bar{\lambda})^2}{\lambda_1^2+\lambda_2^2+\lambda_3^2}},$$

where λ_1, λ_2 and λ_3 are the eigenvalues of $\mathbf{D}$, and $\bar{\lambda} = (\lambda_1+\lambda_2+\lambda_3)/3$. In the general context of symmetric positive-definite tensors in $\mathbb{R}^n$, the fractional anisotropy writes

$$FA(\mathbf{D}) = \sqrt{\frac{n}{n-1}} \frac{\|\mathbf{D} - \frac{1}{n}\operatorname{Tr}(\mathbf{D})\mathbf{I}\|_F}{\|\mathbf{D}\|_F}.$$

It turns out, as we showed in [15], that $\frac{1}{n}\operatorname{Tr}(\mathbf{D})\mathbf{I}$ is the closest (in the Frobenius distance) isotropic tensor to $\mathbf{D}$. Therefore, modulo a normalizing factor, the fractional anisotropy is a measure of the nearness of the tensor $\mathbf{D}$ to the axis of isotropic tensors. We used this characterization together with the Riemannian distance on $\mathcal{P}(n)$ to define another measure of anisotropy [15, 4]

$$GA(\mathbf{D}) = \|\operatorname{Log}\mathbf{D} - \tfrac{1}{n}\operatorname{Tr}(\operatorname{Log}\mathbf{D})\mathbf{I}\|_F,$$

which we called the geodesic anisotropy. The range of this anisotropy index over $\mathcal{P}(n)$ is $[0,\infty)$. Normalized forms, i.e., such as their range is $[0,1)$, can be obtained by any increasing map from $[0,\infty)$ to $[0,1)$. The main features of this anisotropy index is that it is defined on $\mathcal{P}(n)$, becomes infinite (or 1 in its normalized form) as $\mathbf{D}$ approaches the boundary of $\mathcal{P}(n)$, it is rotationally invariant, and is invariant under inversion.

Among the other DT-MRI data processing tasks are the regularization and smoothing of noisy diffusion tensor data, and the interpolating of diffusion tensor fields. The smoothing of

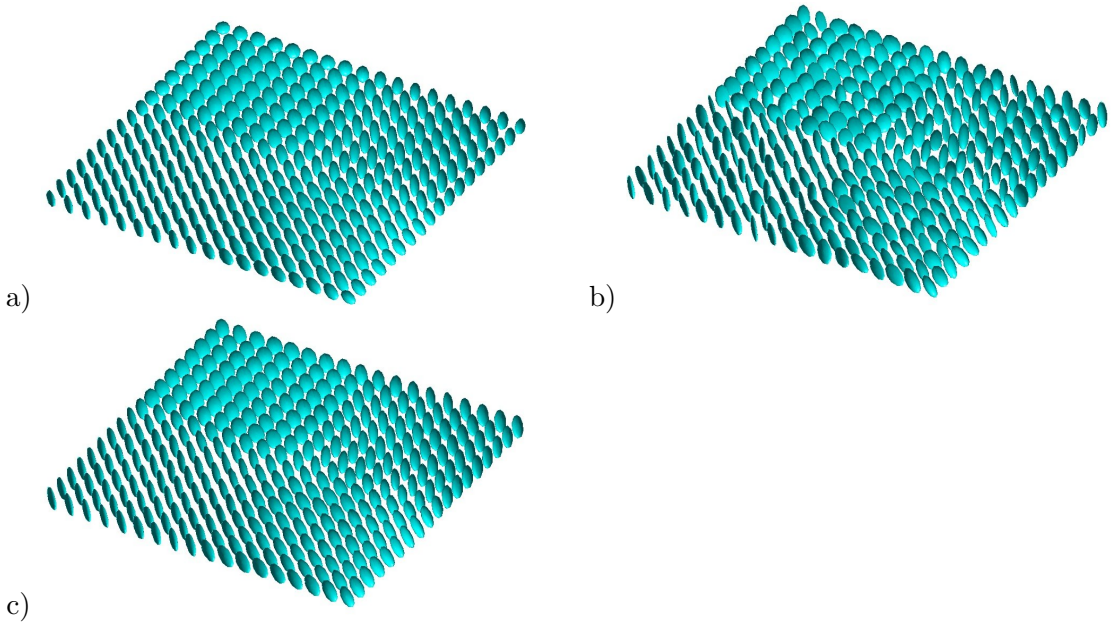

Figure 22.1: *Synthesized diffusion tensor image, a) original, b) perturbed, c) denoised.*

noisy diffusion tensor data can be performed by a smoothing filter that consists of a moving weighted average. This smoothing procedure can be seen to be similar to the commonly used PDE smoothing methods based on the heat equations, e.g. see [2, 23]. In fact, the spatial and temporal discretization of the heat equation by finite differences leads to a weighted average.

In Fig. 22.1a we show a synthesized diffusion tensor image comprised of four homogeneous regions. The diffusion tensors are represented by ellipsoids that have semi-axis equal to the diffusivities, i.e., the eigenvalues of the tensors, and orientations given by the corresponding eigenvectors. Then we show the perturbed image (with added noise) and the image regularized by a weighted geometric mean filter.

In [15] we introduced a new paradigm for the multivariate interpolation of diffusion tensor fields over simplical domains which is based on the geometric mean of symmetric positive-definite tensors. For example, if we know the values of the diffusion tensor $\mathbf{D}_1$, $\mathbf{D}_2$ and $\mathbf{D}_3$ at the three vertices of a non degenerate triangle, then the value of the tensor at any point inside this triangle with barycentric coordinates μ_1, μ_2 and μ_3 is given by the geometric mean of $\mathbf{D}_1$, $\mathbf{D}_2$ and $\mathbf{D}_3$ weighted by μ_1, μ_2 and μ_3. The latter is given by the unique solution of the nonlinear matrix equation

$$\mu_1 \operatorname{Log}(D^{-1}D_1) + \mu_2 \operatorname{Log}(D^{-1}D_2) + \mu_3 \operatorname{Log}(D^{-1}D_3) = \mathbf{0},$$

which can be efficiently solved by the fixed-point algorithm introduced in [16].

Applications to smoothing the DNA intrinsic shape

The continuum elastic theory of rods has been used with success to determine the equilibrium structures of supercoiled DNA. However, most of the published works assume uniform physical properties (bending and torsional stiffnesses) and intrinsic shape (minimum energy shape). Some numerical works did account for sequence dependent physical properties and intrinsic shape. However, the methods employed to construct continuum physical properties and intrinsic shape from the discrete experimental data (X-ray crystal structures) are ad-hoc. With the availability

of efficient computational tools for elastic rods the need for a rational method to construct continuum properties from the discrete base-pair structure is now increasing.

In the continuum approach, the DNA double helix is described by a centerline $\mathbf{r}(s)$ giving the location of the axis of the double helix at arclength s and a triad $(\mathbf{d}_1(s), \mathbf{d}_2(s), \mathbf{d}_3(s))$ that gives the orientation of the DNA axis at arclength s with respect to a fixed orthogonal coordinates system. At the discrete level, each base pair of the DNA double helix is described by the location $\mathbf{r}_i$ of its center and a triad $(\mathbf{d}_1^i(s), \mathbf{d}_2^i(s), \mathbf{d}_3^i(s))$ that gives the orientation of the base pair with respect to a fixed orthogonal coordinates system.

The sequence-dependent discrete stiffnesses and intrinsic shape are obtained from the experimental or computational data by the so-called wedge model which is a nearest neighbor model. The underlying assumptions of this model are that the origin of the triad $(\mathbf{d}_1^i(s), \mathbf{d}_2^i(s), \mathbf{d}_3^i(s))$ is at the center of the base-pair i, the $\mathbf{d}_3^i$ vector points to the next base-pair center, and the $\mathbf{d}_1^i$ axis tracks the rotation of the DNA sugar-phosphate double helix.

The transformation that gives the relation between the triads of two successive base pairs is obtained by the wedge angle set that gives the tilt, roll and twist for the 16 combinations of dimers (AA, AC, AG, AT, CA, CC, CG, CT, GA, GC, GG, GT, TA, TC, TG and TT). Several wedge angle sets have been proposed by researchers in the field of molecular biology.

The DNA intrinsic shape obtained from the wedge angle model contains a substantial amount of noise and thus is not suitable to be used in the sequence-dependent continuum modeling of DNA [10]. Therefore, smoothing the discrete intrinsic shape given by the wedge model is required to effectively eliminate or attenuate the noise.

We note that each base pair can be thought of as an element $\mathbf{T}^{[i]} = (\mathbf{R}^{[i]}, \mathbf{x}^{[i]})$ of the special Euclidean group $SE(3) \equiv SO(3) \ltimes \mathbb{R}^3$, the group of orientation-preserving isometries in $\mathbb{R}^3$, where $\mathbf{R}^{[i]}$ is in $SO(3)$ and $\mathbf{x}^{[i]}$ is in $\mathbb{R}^3$. Now, for two elements $\mathbf{T}_1 = (\mathbf{R}_1, \mathbf{u}_1)$ and $\mathbf{T}_2 = (\mathbf{R}_2, \mathbf{x}_2)$ in $SE(3)$ we can use the Euclidean distance given by $\mathrm{D}_E(\mathbf{T}_1, \mathbf{T}_2)^2 = d_E(\mathbf{R}_1, \mathbf{R}_2)^2 + \|\mathbf{u}_1 - \mathbf{u}_2\|^2$, or use the Riemannian distance given by $\mathrm{D}_R(\mathbf{T}_1, \mathbf{T}_2)^2 = d_R(\mathbf{R}_1, \mathbf{R}_2)^2 + \|\mathbf{u}_1 - \mathbf{u}_2\|^2$. We define the means of elements in $SE(3)$ associated with Euclidean and Riemannian distances in a similar fashion as we did for elements of $SO(3)$. It turns out that the minimizing problem in $SE(3)$ for the mean associated with either distance is equivalent two independent minimizing problems, one in $SO(3)$ and the other in $\mathbb{R}^3$. Therefore, the mean of $\mathbf{T}_n = (\mathbf{R}_n, \mathbf{u}_n),\ n = 1, \ldots, N$ associated with the Euclidean or the Riemannian distance, is given by $\mathbf{T} = (\mathbf{R}, \mathbf{u})$ where $\mathbf{R}$ is the corresponding mean in $SO(3)$ of $\mathbf{R}_n,\ n = 1, \ldots, N$ and $\mathbf{u}$ is the mean in $\mathbb{R}^3$ of $\mathbf{u}_n,\ n = 1, \ldots, N$.

The smoothing process is thus reduced to a smoothing process of the centerline, i.e., smoothing in $\mathbb{R}^3$, which is standard, and a smoothing process for the directors, i.e., smoothing in $SO(3)$. We use a running window filter of length $N = 2k+1$ in which the output of the filtering operation at base pair i is given by a weighted mean of $\mathbf{R}^{[i-k]}, \ldots, \mathbf{R}^{[i]}, \ldots, \mathbf{R}^{[i+k]}$.

Conclusions

In this work we presented a unified approach to several aspects of data processing, such as averaging, smoothing and interpolation, on some Riemannian symmetric spaces. The methods and ideas described are general enough to be applied to data processing on other manifolds. There are many things to be explored in both the theoretical and numerical aspects, and the applications. For instance, the numerical analysis of the algorithms of averaging and interpolation could be pursued. The Finsler geometry of divergences could be another direction to be studied further.

Bibliography

[1] C. Altafini. *Geometric motion control for a kinematically redundant robotic chain: application to a holonomic mobile manipulator*, Journal of Robotic Systems, **20**/5 (2003), pp. 211–227.

[2] G. Aubert and P. Kornprobst. Mathematical Problems in Image Processing: Partial Differential Equations and the Calculus of Variations, Springer-Verlag, New York, 2002.

[3] P. Basser and C. Pierpaoli. *Microstructural and physiological features of tissues elucidated by quantitative-diffusion-tensor MRI*, J. Magn. Reson. B, **111**/3 (1996), pp. 209–219.

[4] P. G. Batchelor, M. Moakher, D. Atkinson, F. Calamante, and A. Connelly. *A Rigorous Framework for Diffusion Tensor Calculus*, Magn. Reson. Med., **53**/1 (2005), pp. 221–225.

[5] C. Chefd'hotel, D. Tschumperlé, R. Deriche and O. D. Faugeras. *Constrained flows of matrix-valued functions: application to diffusion tensor regularization*, Proceedings of the 7th European Conference on Computer Vision, Part I, pp. 251–265, 2002.

[6] A. Edelman, T. A. Arias and S. T. Smith. *The Geometry of Algorithms with Orthogonality Constraints*, SIAM J. Matrix Anal. Appl., **20**/2, (1998), pp. 303–353.

[7] N. I. Fisher, T. Lewis, and B. J. J. Embleton. Statistical Analysis of Spherical Data, Cambridge University Press, Cambridge, 1987.

[8] P. E. Jupp and J. T. Kent. *Fitting smooth paths to spherical data*, Appl. Statist., **36** (1987), pp. 34–46.

[9] R. Mahony and J. Manton. *The geometry of the Newton method on non-compact Lie groups*, J. Global Optimization, **23** (2002), pp. 309–327.

[10] R. S. Manning, J. H. Maddocks and J. D. Kahn. *A continuum rod model of sequence-dependent DNA structure*, J. Chem. Phys., **105** (1996), pp. 5626–5646.

[11] K. V. Mardia. *Statistics of directional data*, Probability and Mathematical Statistics, No. 13, Academic Press, London-New York, 1972.

[12] A. Marthinsen. *Interpolation in Lie groups*, SIAM Numer. Anal., **37**/1 (1999), pp. 269–285.

[13] M. Moakher. *Means and Averaging in the Group of Rotations*, SIAM J. Matrix Anal. Appl., **24**/1 (2001), pp. 1–16.

[14] M. Moakher. *A Differential Geometric Approach to the Geometric Mean of Symmetric Positive Definite Matrices*, SIAM J. Matrix Anal. Appl., **26**/3 (2005), pp. 735–747.

[15] M. Moakher and P. G. Batchelor. *The Symmetric Space of Positive-Definite Tensors: From Geometry to Applications and Visualization*, in: Visualization and Processing of Tensor Fields, J. Weickert and H. Hagen, Eds., Springer, Berlin, 2005.

[16] M. Moakher. *On the Averaging of Symmetric Positive-Definite Tensors*, J. Elasticity, in Press.

[17] R. M. Murray, Z. Li and S. S. Sastry. A Mathematical Introduction to Robotic Manipulation, CRC Press, Florida, 1996.

[18] P. Perona and J. Malik. *Scale-space and edge detection using anisotropic diffusion*, Proceedings, IEEE Computer Society Workshop on Computer Vision, 1987, pp. 16–27.

[19] C. Pierpaoli, P. Jezzard, P. J. Basser, A. Barnett and G. Di Chiro. *Diffusion-tensor MR imaging of the human brain*, Radiology, **201**/3 (1996), pp. 637–648.

[20] M. J. Prentice. *Fitting smooth paths to rotation data*, Appl. Statist., **36** (1987), pp. 325–331.

[21] S. T. Smith, *Optimization techniques on Riemannian manifolds*, in: Hamiltonian and gradient flows, algorithms and control, A. Bloch, ed., Amer. Math. Soc., Providence, Rhode Island, 1994, pp. 113–136.

[22] D. Tschumperlé and R. Deriche, *Orthonormal vector sets regularization with PDE's and Applications*, International Journal of Computer Vision, **50**/3, (2002), pp. 237–252.

[23] J. Weickert, B. M. ter Haar Romeny and M. Viergever, *Efficient and reliable schemes for nonlinear diffusion filtering*, IEEE Transactions on Image Processing , **7** (1998), pp. 398–410.

The Control Variational Method

P. Neittaanmäki[1] *Dan Tiba*[2]

The variational method is a very powerful tool in the theory of partial differential equations. A thorough presentation of this approach may be found in the books of J.-L. Lions and E. Magenes [2] or R. Dautray and J.-L. Lions [1]. An essential feature of the classical approach is the coercivity of the differential operator and the application of the Lax-Milgram lemma.

The control variational method uses modern control theory instead of the classical calculus of variations and offers more flexibility in the analysis of boundary value problems associated to various differential operators. It has been introduced in a sequence of papers by D.Tiba and his coauthors and we quote the recent monograph by P. Neittaanmäki, J. Sprekels and D. Tiba [3] for a description of such ideas. The presentation will concentrate on applications to the linear elasticity system, the Kirchhoff plate and a generalized Nagdhi model for curved rods. We underline that this new approach does not replace, in general, the usual variational method, but offers more insight and new advantageous ways of treating well-known problems.

Bibliography

[1] R. Dautray and J.-L. Lions. *Mathematical analysis and numerical methods for science and technology, Vol. 2, Functional and variational methods*. Springer-Verlag, Berlin, 1988.

[2] J.-L. Lions and E. Magenes. *Problèmes aux limites non homogènes et applications*. Dunod, Paris, 1968.

[3] P. Neittaanmäki, J. Sprekels, D. Tiba. *Optimization of elliptic systems. Theory and applications*. Springer-Verlag, New York, 2005.

[1]University of Jyväskylä, Finland
[2]Institute of Mathematics, Bucharest, Romania

The method of constrained approximation applied to inverse problems for PDEs

Jonathan R. Partington[1]

Acknowledgements

This is an account of joint work with many people, in particular J. Leblond and others who are cited in the references.

24.1 Introduction

The technique of constrained approximation as method of recovering analytic functions in a domain $\Omega \subset \mathbb{C}$ from corrupted measurements on part of the boundary $\partial\Omega$ has been applied to control theory for over ten years (see, for example, the survey articles [10, 5]). A more recent idea, which can be traced back to [8], for example, is to perform a similar reconstruction for harmonic functions, by regarding them as the real parts of analytic functions.

Consider, for example, the following Cauchy-type problem for a domain $\Omega \subset \mathbb{R}^m$ (we shall later restrict ourselves to the cases $m = 2$ and 3) and a suitable subset S of the boundary $\partial\Omega$:

$$\begin{aligned} \Delta u &= 0 \quad \text{in} \quad \Omega, \\ u &= u_0 \quad \text{on} \quad S, \\ \partial_n u &= \phi \quad \text{on} \quad S, \end{aligned} \tag{24.1}$$

where u_0 and ϕ are prescribed functions on S and ∂_n denotes the normal derivative; in the simplest case $u_0 \in W^{1,2}(S)$ (the Sobolev space) and $\phi \in L^2(S)$, but smoother versions of the problem can also be considered. Typically, u_0 represents a measured temperature and ϕ a heat flux; alternatively, the same equations can arise through electrical measurements.

A further question that may be considered is the recovery of a Robin exchange coefficient, which has applications to corrosion detection. Assuming further that $\partial_n u + qu = 0$ on $\partial\Omega$, we may also wish to recover the unknown Robin coefficient q, at least assuming suitable smoothness and non-vanishing conditions on u. Some related problems have been considered in [1, 9, 15]

An important issue here is how to achieve stability (robustness) of the solution with respect to the data.

[1] j.r.partington@leeds.ac.uk

24.2 Constrained approximation

Suppose that u is harmonic in Ω, and that it can be written as the real part of an analytic function h (in the disc this is always the case, by solving the Cauchy–Riemann equations; with suitable modifications, this approach can also be made to work in the annulus or ball). The problem is now to identify the unknown analytic function h from partial and corrupted measurements on the boundary of its domain.

Let $H^2(\mathbb{D})$ denote the Hardy space of functions in the unit disc $\mathbb{D}$, of form

$$g(z) = \sum_{k=0}^{\infty} g_k z^k, \qquad \text{with} \quad \|g\|^2 = \sum_{k=0}^{\infty} |g_k|^2 < \infty.$$

Such functions have traces on $\mathbb{T}$, which are in $L^2(\mathbb{T})$. Also, let S be an appropriate subset of the boundary $\mathbb{T}$ (e.g. an arc). A much-studied problem is the following Bounded Extremal problem (BEP).

Problem 24.1 *Given $f_1 \in L^2(S)$, $f_2 \in L^2(\mathbb{T} \setminus S)$ and $M > 0$, let*

$$\mathcal{B} = \{h \in H^2(\mathbb{D}) : \|h_{|\mathbb{T}\setminus S} - f_2\|_{L^2(\mathbb{T}\setminus S)} \leq M\}.$$

Find $h \in \mathcal{B}$ to minimize $\|h_{|S} - f_1\|_{L^2(S)}$.

Typically, we think of f_1 as a corrupted measurement of h, and M and f_2 reference data, required to make the approximation problem well-posed. Often $f_2 = 0$. See [7] for more details.

In [12], a more general problem (GBEP) was considered (an L^p version for $1 < p < \infty$ was given in [13]).

Problem 24.2 *Let H, K_1, K_2 be Hilbert spaces, and let $A : H \to K_1$ and $B : H \to K_2$ be linear operators, satisfying the well-posedness condition that for some $\eta > 0$ one has $\|Ag\|^2 + \|Bg\|^2 \geq \eta\|g\|^2$ for each $g \in H$. Fix $f_1 \in K_1$, $f_2 \in K_2$ and $M > 0$. Let*

$$\mathcal{B} = \{h \in H : \|Bh - f_2\|_{K_2} \leq M\}.$$

Find $h \in \mathcal{B}$ to minimize $\|Ah - f_1\|_{K_1}$.

The case $H = H^2$, $K_1 = L^2(S)$ and $K_2 = L^2(\mathbb{T} \setminus S)$, with A and B restriction mappings, gives the problem (BEP). The extension to Hardy–Sobolev spaces is similar.

In general the solution is given by

$$(A^*A + \lambda B^*B)h = A^*f_1 + \lambda B^*f_2,$$

where $\lambda > 0$ is the unique parameter such that $\|Bh - f_2\| = M$. Here * denotes the adjoint of an operator. When we are working with analytic functions as in (BEP), the solution involves Toeplitz operators.

The following crucial stability result was proved in [17]: *for each fixed $f_2 \in K_2$, the solution to (GBEP) (and hence to (BEP)) depends continuously in norm on f_1 and M.* However, there is a trade-off here, in that a small value of $\|Ah - f_1\|$ can be obtained only at the expense of a large error $M = \|Bh - f_2\|$. In the (BEP) version this means that, when the data is perturbed, we can approximate well on S but only at the expense of a large error on $\mathbb{T} \setminus S$.

24.3 Three applications of the method

24.3.1 The disc

By means of conformal mapping, the problem for a sufficiently regular simply-connected plane domain can be reduced to the case of the disc. The procedure in Section 24.2 has been considered in [6, 9, 17], for example. In [17] the constrained approximation approach was used to study inverse diffusion problems: for instance, to find a crack $\sigma \subset \mathbb{D}$ given by a simple curve, such that one has

$$\begin{aligned} \Delta u &= 0 \quad \text{in} \quad \mathbb{D} \setminus \sigma, \\ \partial_n u &= \phi \quad \text{on} \quad \mathbb{T}, \\ \partial_n u &= 0 \quad \text{on} \quad \sigma, \\ u &= u_0 \quad \text{on} \quad S. \end{aligned}$$

Similar approximation problems have been used in the detection of point sources.

24.3.2 The annulus

For a fixed s with $0 < s < 1$, let $\mathbb{A}$ denote the annulus $\{z \in \mathbb{C} : s < |z| < 1\}$. The Hardy space $H^2(\mathbb{A})$ consists of all analytic functions with L^2 boundary values, that is, Laurent series of the form

$$g(z) = \sum_{k=-\infty}^{\infty} g_k z^k, \qquad \text{with} \quad \|g\|^2 = \sum_{k=-\infty}^{\infty} (1 + s^{2k})|g_k|^2 < \infty.$$

Constrained approximation problems in these spaces have been considered in [11, 18]. A typical issue here is the recovery of a function in $H^2(\mathbb{A})$ given values on $L^2(S)$, where S is a subset of $\partial\mathbb{A}$, for example the exterior circle. Applications of this to inverse problems for Robin coefficients have been given in [16, 14]. Note that there is an additional subtlety here, in that $\mathbb{A}$ is not simply connected, and so a harmonic function on $\mathbb{A}$ cannot be written directly as the real part of an analytic function (a term of the form $c \log |z|$ has to be allowed for).

24.3.3 The sphere

Let $\mathbb{B}$ denote the open unit ball in $\mathbb{R}^3$ and $\mathbb{S}$ its boundary, the unit sphere. In the Stein theory of harmonic analysis in 3 dimensions, a function $h : \mathbb{B} \to \mathbb{R}^3$ is said to be analytic if $h = \nabla U$ for some harmonic function U on $\mathbb{B}$ [4, 19]. The Hardy space $H^2(\mathbb{B})$ consists of all such $h = (h_1, h_2, h_3)$ such that the $L^2(\rho\mathbb{S})$ norms of the components h_j, restricted to $\rho\mathbb{S}$, are uniformly bounded over $0 < \rho < 1$.

For a subset $S \subset \mathbb{S}$ (typically, a hemisphere), we also require the space

$$L^2_\nabla(S) \subset L^2(S, \mathbb{R}^3),$$

of functions of the form $f_1\mathbf{n} + \nabla_{\mathbb{S}} f_2$ for $f_1 \in L^2(S)$ and $f_2 \in W^{1,2}(S)$, the Sobolev space. Here $\mathbf{n}$ is a unit vector normal to the sphere, and $\nabla_{\mathbb{S}} f_2$ is the tangential component of ∇f_2. The spaces $L^2_\nabla(S)$ and $L^2_\nabla(\mathbb{S} \setminus S)$ now play roles equivalent to those of $L^2(S)$ and $L^2(\mathbb{T} \setminus S)$ in the standard (BEP).

In this situation there are applications to inverse EEG problems, as well as the possibility of working with a domain consisting of the area between two concentric spheres (which models the skull) [3, 2].

Bibliography

[1] G. Alessandrini. Examples of instability in inverse boundary-value problems. *Inverse Problems*, 13(4):887–897, 1997.

[2] B. Atfeh, L. Baratchart, M. Clerc, J. Leblond, J.-P. Marmorat, T. Papadopoulo, and J. R. Partington. The Cauchy problem applied to cortical imaging: comparison of a boundary element and a bounded extremal problem. In preparation. Poster presented at ISBET 2005, Berne.

[3] B. Atfeh, L. Baratchart, J. Leblond, and J. R. Partington. Bounded extremal problems and Cauchy–Laplace problems on 3D spherical domains. In preparation.

[4] S. Axler, P. Bourdon, and W. Ramey. *Harmonic function theory*, volume 137 of *Graduate Texts in Mathematics*. Springer-Verlag, New York, second edition, 2001.

[5] L. Baratchart. Identification and function theory. In J.-D. Fournier, J. Grimm, J. Leblond, and J. R. Partington, editors, *Harmonic analysis and rational approximation: their roles in signals, control and dynamical systems theory*, volume 327 of *Lecture Notes in Control and Information Sciences*, pages 211–230. Springer-Verlag, Berlin, 2006.

[6] L. Baratchart, A. Ben Abda, F. Ben Hassen, and J. Leblond. Recovery of pointwise sources or small inclusions in 2D domains and rational approximation. *Inverse Problems*, 21(1):51–74, 2005.

[7] L. Baratchart and J. Leblond. Hardy approximation to L^p functions on subsets of the circle with $1 \leq p < \infty$. *Constr. Approx.*, 14(1):41–56, 1998.

[8] L. Baratchart, J. Leblond, F. Mandréa, and E. B. Saff. How can the meromorphic approximation help to solve some 2D inverse problems for the Laplacian? *Inverse Problems*, 15(1):79–90, 1999.

[9] S. Chaabane, M. Jaoua, and J. Leblond. Parameter identification for Laplace equation and approximation in Hardy classes. *J. Inverse Ill-Posed Probl.*, 11(1):33–57, 2003.

[10] I. Chalendar, J. Leblond, and J. R. Partington. Approximation problems in some holomorphic spaces, with applications. In *Systems, approximation, singular integral operators, and related topics (Bordeaux, 2000)*, volume 129 of *Oper. Theory Adv. Appl.*, pages 143–168. Birkhäuser, Basel, 2001.

[11] I. Chalendar and J. R. Partington. Approximation problems and representations of Hardy spaces in circular domains. *Studia Math.*, 136(3):255–269, 1999.

[12] I. Chalendar and J. R. Partington. Constrained approximation and invariant subspaces. *J. Math. Anal. Appl.*, 280(1):176–187, 2003.

[13] I. Chalendar, J. R. Partington, and M. Smith. Approximation in reflexive Banach spaces and applications to the invariant subspace problem. *Proc. Amer. Math. Soc.*, 132(4):1133–1142, 2004.

[14] M. Jaoua, J. Leblond, M. Mahjoub, and J. R. Partington. Analytic extensions and Cauchy-type inverse problems on annular domains: numerical results. In preparation.

[15] V. A. Kozlov, V. G. Maz'ya, and A. V. Fomin. An iterative method for solving the Cauchy problem for elliptic equations. *U.S.S.R. Comput. Math. and Math. Phys.*, 31(1):45–52, 1992.

[16] J. Leblond, M. Mahjoub, and J. R. Partington. Analytic extensions and Cauchy-type inverse problems on annular domains: stability results. *J. Inverse Ill-posed Problems*, to appear, 2006.

[17] J. Leblond, J.-P. Marmorat, and J. R. Partington. Analytic approximation under real constraints, with applications to inverse diffusion problems. Submitted, 2005.

[18] M. Smith. The spectral theory of Toeplitz operators applied to approximation problems in Hilbert spaces. *Constr. Approx.*, 22(1):47–65, 2005.

[19] E. M. Stein. *Singular integrals and differentiability properties of functions.* Princeton Mathematical Series, No. 30. Princeton University Press, Princeton, N.J., 1970.

About Regularity of Optimal shapes

Michel Pierre [1]

Introduction

The goal of this talk is to describe some ideas and techniques, and some recent results as well, concerning the study of *the regularity of optimal shapes*.

For most of the shape functionals we are considering, existence of optimal shapes is derived via the use of topological and functional analytic tools which generally provide optimal shapes with very poor regularity: they may be only open sets, sometimes even only measurable sets, while we expect them to be regular or even very regular like having an analytic boundary.

There are quite a lot of analysis tools to prove that optimal shapes are regular once they are known to have a little bit of regularity. For instance, if one knows that the boundary may locally be represented as the graph of some function, then it has become classical in many situations to prove that this function is actually regular: this is often done by using —deep, but now classical— results of the regularity theory for partial differential equations.

We will mainly be interested in the very first step consisting in starting from "scratch" and reaching *some* information on the regularity of the optimal shape: for instance, a given optimal shape is obtained as a measurable set and we want to prove that it is at least an open set and, next, that its boundary is at least Lipschitz or C^1.

The shape functionals

We may consider optimal shape functionals of the form

$$\Omega \subset D \to E(\Omega) = \tau P(\Omega) + J(\Omega),$$

where D is a *given* open subset of $\mathbb{R}^d$, $\tau \in [0, +\infty[$ is *given*, the Ω's are variable measurable subsets of D and
– $P(\Omega)$ denotes the perimeter of Ω,
– $J(\Omega) = \inf\{\int_\Omega \frac{1}{2}|\nabla v|^2 - f\, v;\ v \in H^1_0(\Omega)\}$ is the Dirichlet energy of Ω for a *given* $f \in L^2(D)$.

Given $m \in (0, |D|)$ (where we denote by $|\cdot|$ the Lebesgue measure), we are interested in the regularity of the optimal shapes $\hat{\Omega}$ of

$$\hat{\Omega} \subset D, |\hat{\Omega}| = m,\ E(\hat{\Omega}) = \min\{\ E(\Omega);\ \Omega \subset D \text{ measurable}, |\Omega| = m\ \}. \tag{25.1}$$

Let us recall what happens in the two limit cases "$\tau = +\infty$" and $\tau = 0$.

[1] michel.pierre@bretagne.ens-cachan.fr, Ecole Normale Supérieure de Cachan, Antenne de Bretagne & Institut de Recherche Mathématique de Rennes, France

The case $\tau = +\infty$

This is the classical isoperimetric problem:

$$\hat{\Omega} \subset D,\ |\hat{\Omega}| = m,\ P(\hat{\Omega}) = \min\{\ P(\Omega);\ \Omega \subset D \text{ measurable},\ |\Omega| = m\ \}. \tag{25.2}$$

It is classical that, if $D = \mathbb{R}^d$, or if D is large enough to contain a ball of measure m, then the solution of (25.2) is precisely this ball. This is a consequence of the classical isoperimetric inequality which states that

$$\forall\, \Omega \subset \mathbb{R}^d \text{ measurable},\ P(\Omega) \geq c_d |\Omega|^{(d-1)/d},\ \text{where } c_d = d\,|B(0,1)|^{1/d}, \tag{25.3}$$

and *the equality holds if and only if* Ω *is a ball* (see a.e. [20],[32] for proofs and references). If D does not contain a ball of measure m but is bounded, it is easy to prove the existence of a *measurable* optimal shape $\hat{\Omega}$ (see e.g. [28]).

With respect to the regularity of this optimal set $\hat{\Omega}$, the following holds:

Theorem 25.1 *Let* $\hat{\Omega}$ *be a solution of* (25.2)*. Then,*
– if $d \leq 7$*,* $\partial\hat{\Omega} \cap D$ *is an analytic hypersurface,*
– if $d \geq 8$*, then there exists a "small" set* $\Sigma \subset \partial\hat{\Omega}$*, which is of* $s-$*Hausdorff measure zero for all* $s > d-8$*, and such that* $\partial\hat{\Omega} \setminus \Sigma$ *is an analytic hypersurface.*

We find the above result in [23] or also in [22], [33]. It follows and uses a series of previous results by E. De Giorgi [15], M. Miranda [31], H. Federer [19], E. Bombieri, E. De Giorgi & E. Giusti [5] (see also more references in these articles).

The case $\tau = 0$

Here, the question is the regularity of the optimal set $\hat{\Omega}$ of

$$\hat{\Omega} \subset D,\ |\hat{\Omega}| = m,\ J(\hat{\Omega}) = \min\{\ J(\Omega);\ \Omega \subset D,\ |\Omega| = m\}. \tag{25.4}$$

Note that for each Ω, $J(\Omega) = \int_\Omega \frac{1}{2}|\nabla u_\Omega|^2 - f u_\Omega$ where u_Ω is the solution to the Dirichlet problem

$$u_\Omega \in H_0^1(\Omega),\ \forall\, v \in H_0^1(\Omega),\ \int_D \nabla u_\Omega \nabla v = \int_D f\, v. \tag{25.5}$$

This problem appears in many applications (see for instance [27], the books [16], [28] and the references in them). It is not hard to show that the problem (25.4) has a solution (see e.g. [13], or [25], or [9]). However, the general existence theory does not provide an open set, but only *a quasi-open* set. Thus, it is already a regularity result to prove that we may obtain an open set as an optimal set (this is not true if for instance f is only in H^{-1}). Actually, a first result is the following, assuming $f \in L^\infty(D)$.

Theorem 25.2 *Let* $\hat{\Omega}$ *be a solution of (25.4). Then,* $u_{\hat{\Omega}}$ *is Lipschitz continuous on* $D_\delta = \{\xi \in D; d(\xi, \partial D) \geq \delta\}$ *for all* $\delta > 0$*.*

This is the first step in studying the regularity of $\hat{\Omega}$ itself. The case where $f \geq 0$ (or more generally when $u_{\hat{\Omega}} \geq 0$) is a little easier. It may be found in [25] and [6], or in [24] for a penalized version, and the proof relies on tools from [2]. See also [1] for a similar problem. The case where u changes sign is more involved (see [7]) and requires the monotonicity lemma of [3] in its nonhomogeneous form given in [10].

Now, we come to the regularity of $\partial\hat{\Omega}$ itself. We cannot expect full regularity in all cases: for instance, it is easy to prove that, if the solution $u_{\hat{\Omega}}$ changes sign near the boundary of $\hat{\Omega}$, then necessarily *the boundary has a singularity (like a cusp), this even in dimension 2.* On the other hand, we do expect regularity in the positive case. One can indeed prove the following:

Theorem 25.3 *Let $\hat{\Omega}$ be a solution of (25.4) and assume $f \geq 0, f \in L^\infty(D)$. Then, there exists a set $\Sigma \subset \partial\hat{\Omega}$ such that*
– the $(d-1)-$Hausdorff measure of Σ is zero,
– $\partial\hat{\Omega} \setminus \Sigma$ is regular.
If moreover $d = 2$, then the full boundary $\partial\hat{\Omega}$ is regular.

Here, by regular, we mean that the boundary is at least $C^{1,\alpha}$. If f is more regular, like $\mathcal{C}^\infty$, then so is the boundary.

We refer to [6] for a proof (based on tools from [2]) and for more general assumptions. See also [24], [1], [34] for results of this kind and to [11], [17] indicating for similar problems that the situation may change whether $d \leq 6$ or $d > 6$ (however, our problem is different since singularities occur even for $d = 2$ when positivity does not hold).

The full problem (25.1)

The state function u_Ω is shown to be 1/2-Hölder continuous in all cases and regularity is obtained when $f \geq 0$ (see N. Landais [30]).

More examples

We may also consider the regularity question of the optimal shapes for the eigenvalues of the Laplacian operator with Dirichlet boundary conditions, for instance

$$\hat{\Omega} \subset D,\ |\hat{\Omega}| = m,\ \lambda_1(\hat{\Omega}) = \min\{\lambda_1(\Omega);\ \Omega \subset D,\ |\Omega| = m\},$$

where $\lambda_1(\Omega)$ is the first eigenvalue defined by

$$\lambda_1(\Omega) = \inf\{\int_\Omega |\nabla v|^2;\ v \in H_0^1(\Omega), \int_\Omega v^2 = 1\}.$$

Here again, if D contains a ball of measure m, then the ball is the minimum (see [18, 29]). If not, there exists at least a quasi-open minimal set (see [9]). Next, regularity results similar to Theorems 25.2 and Theorem 25.3 may be proved (see [26], [8]).

Let us mention that regularity questions turn out to be an important issue in many mathematical models. We may refer to [4] for a design problem, to [12] for a compliance problem and to the book [14] for the famous conjecture on the Mumford-Shah problem.

Bibliography

[1] N. Aguilera, H.W. Alt and L.A. Caffarelli. *An optimization problem with volume constraint*, SIAM J. Control Optimization, 24 (1986), 191-198.

[2] H.W. Alt and L.A. Caffarelli. *Existence and regularity for a minimum problem with free boundary*, J. reine angew. Math. 325 (1981), 105-144.

[3] H.W. Alt, L.A. Caffarelli and A. Friedman. *Variational Problems with Two Phases and Their Free Boundaries*, Trans. AMS Vol. 282, Nr2 (1984), 431-461.

[4] L. Ambrosio and G. Buttazzo. *An optimal design problem with perimeter penalization*, Calc. Var. **1** n^{o}1 (1993), 55–69.

[5] E. Bombieri, E. De Giorgi and E. Giusti. *Minimal cones and the Bernstein problem*, Invent. Math. 7 (1969), 243-268.

[6] T. Briançon. *Regularity of optimal shapes for the Dirichlet's energy with volume constraint*, ESAIM: COCV, Vol. 10 (2004), 99-122.

[7] T. Briançon, M. Hayouni and M. Pierre. *Lipschitz continuity of state functions in some optimal shaping*, Calc. Var. PDE 18 (2005), 13-32.

[8] T. Briançon. *Regularity of the optimal shape for the first eigenvalue of the Laplacian with volume and inclusion constraints*, to appear

[9] G. Buttazzo and G. Dal Maso. *An Existence Result for a Class of Shape Optimization Problems*. Arch. Ration. Mech. Anal. 122 (1993), 183-195.

[10] L.A. Caffarelli, D. Jerison and C.E. Kenig. *Some New Monotonicity Theorems with Applications to Free Boundary Problems*, Annals of Math., 155 (2002), 369-404.

[11] L.A. Caffarelli, D. Jerison and C.E. Kenig. *Global energy minimizers for free boundary problems and full regularity in three dimensions*, Contemp. Math., 350 (2004).

[12] A. Chambolle and Ch. J. Larsen. *$\mathcal{C}^\infty$ regularity of the free boundary for a two-dimensional optimal compliance problem*, Calc. Var. PDE, 18 Nr 1 (2003), 77-94.

[13] M. Crouzeix. *Variational approach of a magnetic shaping problem*, Eur. J. Mech. B Fluids 10 (1991), 527-536.

[14] G. David. *Singular Sets of Minimizers for the Mumford-Shah Functional*, book, Progress in Mathematics, Birkhäuser.

[15] E. De Giorgi. *Frontiere orientate di misura minima*, Sem. Mat. Sc. Norm. Sup. Pisa, 1960-1961

[16] M. Delfour, J.P. Zolésio. *Shapes and geometries. Analysis, differential calculus and optimization*, Advances in Design and Control SIAM, Philadelphia, PA, 2001.

[17] De Silva and D. Jerison. to appear.

[18] G. Faber. *Beweis, dass unter allen homogenen Membranen von gleicher Fläche und gleicher Spannung die kreisförmige den tiefsten Grundton gibt*, Sitz. Ber. Bayer. Akad. Wiss. (1923), 169-172.

[19] H. Federer. *The singular set of area minimizing rectifiable currents with codimension one and of area minimizing flat chains modulo two arbitrary codimension*, Bull. Amer. Math. Soc. 76 (1970), 767-771.

[20] H. Federer. *Geometric Measure Theory*, Springer-Verlag, N.-Y., 1969.

[21] E. Giusti. *Minimal surfaces and functions of bounded variation*. Monographs in Mathematics, 80. Birkhauser Verlag, Basel-Boston, Mass., 1984.

[22] E. Giusti. *The equilibrium configuration of liquid drops*, J. reine angew. Math., 321 (1981), 53-63.

[23] E. Gonzalez, U. Massari and I. Tamanini. *On the Regularity of Boundaries of Sets Minimizing Perimeter with a Volume Constraint*, Indiana U. Math. J., Vol. 32, No1 (1983) 25-37.

[24] B. Gustafsson and H. Shahgholian. *Existence and geometric properties of solutions of a free boundary problem in potential theory*, J. reine angew. Math. 473 (1996), 137-179.

[25] M. Hayouni. *Lipschitz Continuity of the State Function in a Shape Optimization Problem,* J. Conv. Anal., Vol. 6 (1999), No 1, 71-90.

[26] M. Hayouni. *Sur la minimisation de la première valeur propre du laplacien*, CRAS 330 (2000), No 7, 551-556.

[27] A. Henrot and M. Pierre. *Un problème inverse en formage de métaux liquides*, RAIRO Modél. Math. Anal. Num. 23 (1989), 155-177.

[28] A. Henrot and M. Pierre. *Variation et optimisation de formes: une analyse géométrique*, July 2005, Springer

[29] E. Krahn. *Über eine von Rayleigh formulierte Minimaleigenschaft des Kreises*, Math. Ann., **94** (1924), 97-100.

[30] N. Landais. *A regularity result in a shape optimization problem with perimeter*, to appear

[31] M. Miranda. *Sul minimo dell-integrale del gradiente di una funzione*, Ann. Scuola Norm. Sup. Pisa (3) 18 (1964), 27-56.

[32] F. Morgan. *Geometric Measure Theory: A Beginner's Guide*, Academic Press, 1995.

[33] I. Tamanini. *Variational Problems of Least Area Type with Constraints*, Ann. Univ. Ferrara-Sez. VII -Sc. Mat., Vol. XXXIV, (1988) 183-217.

[34] G.S. Weiss. *Partial regularity for weak solutions of an elliptic free boundary problem*, J. Geom. Anal. 9 (1999), No2, 317-326.

Unique continuation from Cauchy data for harmonic functions in a domain with unknown and nonsmooth parts of the boundary

Luca Rondi[1]

An electrically conducting body occupies a region Ω, which we assume to be a bounded domain in $\mathbb{R}^N$, $N \geq 2$, with a reasonably smooth boundary. We suppose that the conductor is homogeneous and isotropic. Let us assume that such a conductor presents some perfectly insulating defects, such as cracks (either interior or surface breaking), cavities or material losses at the boundary, which might be caused by different phenomena, like for instance fractures or corrosion. The boundaries of these defects are collected into a closed set which we call K. If we prescribe a current density $f \in L^2(\partial\Omega)$, with $\int_{\partial\Omega} f = 0$ and such that its support is contained in $\tilde{\gamma}$, a part of the boundary of Ω which is accessible, known and disjoint from K, then the electrostatic potential $u = u(f, K)$ inside the conductor solves the following Neumann type boundary value problem

$$\begin{cases} \Delta u = 0 & \text{in } \Omega \backslash K, \\ \dfrac{\partial u}{\partial \nu} = f & \text{on } \tilde{\gamma}, \\ \dfrac{\partial u}{\partial \nu} = 0 & \text{on } \partial(\Omega \backslash K) \backslash \tilde{\gamma}. \end{cases} \tag{26.1}$$

Let us consider the following kind of inverse problem. Assuming that the defect K is unknown, we might wish to determine it by performing boundary measurements of voltage and current type. That is, we prescribe one or more currents f and we measure on γ, an accessible and known part of $\partial\Omega$, the value of the corresponding potentials u. Through these measurements we obtain additional information with which we would like to recover the unknown defect K. For what concerns the determination of cracks we refer to the recent review paper [3], where uniqueness, stability and reconstruction procedures, in two and three dimensions, are discussed. For the determination of other defects, such as cavities or material losses at the boundary, we refer to the following papers and to the references therein. The uniqueness and stability issues are treated in [7], for the two dimensional case, and in [1], for the higher dimensional case.

A two step procedure is usually employed to deal with these kinds of inverse problems. In the first step, the potential is recovered from the boundary measurements of voltage and current type. Subsequently, in the second step, features of the potential such as singularities, level sets or critical points are used to determine the unknown defect K. For instance, in our case, that

[1]Università degli Studi di Trieste, Italy. E-mail: rondi@dmi.units.it

is when the defects are perfectly insulating, the jump set of u, $S(u)$, is contained in K. Thus $S(u)$ would identify at least a part of our defect. Repeating the procedure for different and suitable choices of f, the union of the jump sets of the corresponding potentials would cover the whole K. The uniqueness results which are available in the literature give us information on how many and which kind of measurements we need to take in order to identify uniquely, at least in a suitable class of admissible defects, the unknown K. Here we limit ourselves to notice that in many interesting cases a finite number (usually one or two) of suitably chosen measurements is enough. However, in dimension higher than 2, for what concerns insulating cracks, still a general uniqueness result with a finite number of measurements is missing, the only available result, [2], deals with planar cracks only.

We investigate the first step of the previous scheme. Let us suppose that K is the unknown defect. Fixed a current density f, we measure $g = u(f, K)|_\gamma$, where $u(f, K)$ solves (26.1). Given f and g, we ask whether the potential inside the conductor is uniquely identified by the Cauchy data (g, f). In other words, we ask when the following result holds: whenever another defect K_1 gives rise to the same boundary measurement g, that is we have $u(f, K)|_\gamma = u(f, K_1)|_\gamma$, then $u(f, K) = u(f, K_1)$ in Ω. Such a unique continuation result is relatively easy to prove if we assume K and K_1 smooth. However, when the unknown defect K is very irregular, various technical difficulties arise. We show that uniqueness holds for a very large class of admissible defects.

The main result is the following. When K is formed, up to a set of zero capacity, by Lipschitz hypersurfaces and K_1 has finite $(N-1)$-dimensional Hausdorff measure, then $u(f, K)|_\gamma = u(f, K_1)|_\gamma$ implies $u(f, K) = u(f, K_1)$ in Ω. The proof is strongly based on harmonic analysis techniques on Lipschitz domains, in particular for what concerns the Neumann problem. In fact, see [5], a Lipschitz condition on the boundary allows us to pass from a weak formulation of the Neumann datum to a pointwise formulation, through the nontangential maximal function and the nontangential limit. This procedure allows us to deal with the weak smoothness of K. In order to deal with the roughness of K_1, we use another key ingredient, namely the Gauss-Green formula for sets of finite perimeter. Furthermore, in two dimensions, we may take advantage of the duality provided by the use of harmonic conjugates, thus other kinds of unique continuation results may be proved.

As a first application of our unique continuation results to inverse problems, we deduce uniqueness with a single measurement for the inverse problem of determining cavities or material losses at the boundary. On the other hand it is well known that a single measurement is not enough, in general, to determine cracks.

In order to implement the reconstruction procedure of (a part of) K from the Cauchy data (g, f), through the determination of the potential $u = u(f, K)$ and of its jump set $S(u)$, we might set the problem into the following least square formulation. We look for

$$\min_{\tilde{K}} \|u(f, \tilde{K})|_\gamma - g\|_{L^2(\gamma)}, \tag{26.2}$$

where $\tilde{K}$ varies in a suitable class of admissible defects. The minimum is zero and is obviously reached for $\tilde{K} = K$. Although other $\tilde{K}$ may be minimizers, the previous uniqueness results imply that for any minimizer $\tilde{K}$ we have $u(f, \tilde{K}) = u(f, K)$. However, one usually has to deal with noisy measurements, that is f, the prescribed current density, and in particular g, the measured potential at the boundary, are known up to some noise which is due to the errors the measurements are subject to. Hence, we need to investigate the stability of the unique continuation results described before. We require at least a qualitative type of stability, that is convergence in a suitable sense to the looked for potential when the noise goes to zero. We

prove two kinds of, strictly related, stability results, under minimal assumptions of regularity on the admissible defects, whose main features are that we treat the three dimensional case and that the admissible defects may include cracks.

First, we show stability of the direct problem (26.1) under the variation of K, with respect to the Hausdorff distance, which corresponds to the stability of Neumann problem under domain variations. We refer to [4] and its references for a detailed account on this problem. Up to our knowledge, in dimension higher than two, previously known results require quite strong assumptions on K, which usually do not include cracks, for instance. On the other hand, in dimension 2, again by making use of duality arguments, stronger results have been proved even for nonlinear problems, see again [4] and its references.

Then, we prove stability of the unique continuation in Ω of u from the Cauchy data. As an application to inverse problems of these two stability results, we show that, in the class of admissible defects for which stability holds, the least square problem (26.2) is stable with respect to noise on the Cauchy data.

We observe that the difficulty of proving such stability results is due to the ill-posedness of these unique continuations from the Cauchy data. We remark that the ill-posedness of the inverse boundary value problems we are considering is strictly linked to the one of the unique continuation problem. We recall that, however, under stronger assumptions on the admissible defects, quantitative stability results for the inverse problems have been obtained, see for instance [7] and, for what concerns cracks, [8] for the two dimensional case, and [1] for cavities and material losses in higher dimensions. Although such quantitative estimates of stability are very weak, indeed of logarithmic type, they are essentially optimal, since these kinds of inverse problems are severely ill-posed.

An interesting prosecution of this work would be to develop a numerical procedure for the determination of the potential, and in particular of its jump set, from the Cauchy data, by variational methods, for instance in $SBV(\Omega)$, the space of special functions of bounded variation to which the potential u belongs. Such a numerical method should take into account the noise of the data, the conditions under which stability occurs and the fact that the jump sets of SBV functions are quite difficult to handle from a numerical point of view. For example, a quite natural attempt would be to use a modification of the so-called Mumford-Shah functional which has been introduced in [6] as an image segmentation method. However such an issue requires further investigation and it will be the subject of future research.

Bibliography

[1] G. Alessandrini, E. Beretta, E. Rosset and S. Vessella. *Optimal stability for inverse elliptic boundary value problems with unknown boundaries*, Ann. Scuola Norm. Sup. Pisa Cl. Sci. **29** (2000), pp. 755–806.

[2] G. Alessandrini and E. Di Benedetto. *Determining 2-dimensional cracks in 3-dimensional bodies: uniqueness and stability*, Indiana Univ. Math. J. **46** (1997), pp. 1–82.

[3] K. Bryan and M. S. Vogelius. *A review of selected works on crack identification*, in C. B. Croke, I. Lasiecka, G. Uhlmann and M. S. Vogelius eds., *Geometric Methods in Inverse Problems and PDE Control*, Springer-Verlag, New York, 2004, pp. 25–46.

[4] G. Dal Maso, F. Ebobisse and M. Ponsiglione. *A stability result for nonlinear Neumann problems under boundary variations*, J. Math. Pures Appl. **82** (2003), pp. 503–532.

[5] D. S. Jerison and C. E. Kenig. *The Neumann problem on Lipschitz domains*, Bull. Amer. Math. Soc. (N.S.) **4** (1981), pp. 203–207.

[6] D. Mumford and J. Shah. *Optimal approximations by piecewise smooth functions and associated variational problems*, Comm. Pure Appl. Math. **42** (1989), pp. 577–685.

[7] L. Rondi. *Uniqueness and Optimal Stability for the Determination of Multiple Defects by Electrostatic Measurements*, Ph.D. thesis, S.I.S.S.A.-I.S.A.S., Trieste, 1999 (downloadable from `http://www.sissa.it/library/`).

[8] L. Rondi. *Optimal stability of reconstruction of plane Lipschitz cracks*, SIAM J. Math. Anal. **36** (2005), pp. 1282–1292.

Experimental inversion algorithms for quantum control

Gabriel Turinici[1]

Abstract

The purpose of this paper is to introduce the framework of quantum experimental inversion. We first set the stage with the presentation of quantum control and then describe some recent works that pertain to the potential and / or dipole inversion. Both theoretical and experimental aspects will be considered.

27.1 Introduction

The prospect of influencing the outcome of chemical reactions, or on a more general level the outcome of quantum phenomena, through tailored laser pulses has been investigated ever since the introduction of the laser technology half of century ago. However, the successful implementation of experimental protocols [1, 13, 21, 3, 2, 8, 11] only came after the problem was reformulated as a control situation and proper engineering control theory tools were applied, among which the optimal control.

In such a context the time scales range from femtosecond (10^{-15}) to the picosecond (10^{-12}) and the space scales range from several atoms to large polyatomic or metallic structures. Historically, first applications involved isotopic separation and chemical reactions, but now the field extended to encompass High Harmonic Generation (generation of output laser pulses having larger frequency than the input pulse), manipulation of atoms and molecules toward constructing logical gates for quantum computers [4, 17], study of excited states of proteins [9], etc.

This control situation requires a modelisation; we will explore here a formulation where the system can be characterized by its wave-function evolving from an initial state $\Psi(x, t = 0) = \Psi_0(x)$. Here x denote the relevant spacial variables. In absence of any external interaction, the evolution of the (nuclear) wave-function is given by the Time Dependent Schrödinger Equation which involves an internal Hamiltonian H. $H = H_0 + V$ is made up of two terms :

- a kinetic energy part H_0 which can be the Laplacian operator $-\frac{1}{2m}\sum_i \frac{\partial^2}{\partial x_i^2}$ in the x coordinates

- and a potential $V(x)$ part which characterizes the electronic interactions. This potential can be given through a previous "ab initio" computation or has to be find through inversion (we

[1]CEREMADE, Université Paris Dauphine
Place Du Maréchal de Lattre de Tassigny, 75775 Paris Cedex 16
The author acknowledge financial support from INRIA Rocquencourt and from a PICS CNRS-NSF collaboration between the Department of Chemistry, Princeton University, and the Laboratoire J.L.Lions, Université Paris 6.

will come to this latter).

By hypothesis this Hamiltonian does not produces the desired target state or the desired inversion quality so an external interaction is introduced to control the system; here the control is a dipole modeled by a self-adjoint operator $C(x,t) = -\mu(x)\epsilon(t)$ where $\mu(x)$ is the coupling term and $\epsilon(t)$ is the intensity of the electric field (other higher order models can also be considered, see for instance [5]). The evolution equation can be written as (we used atomic units i.e., $\hbar = 1$):

$$\begin{cases} i\frac{\partial}{\partial t}\Psi(x,t) = (H_0 + V - \epsilon(t)\mu)\Psi(x,t) \\ \Psi(x,t=0) = \Psi_0(x). \end{cases} \tag{27.1}$$

The dipole operator $\mu(x)$ may be or may not be known in practice. The control is realized through the selection of the intensity $\epsilon(t)$ which is at our disposal.

The target to be reached can either be given in a strong form as a target wave-function Ψ_T or in a weak form through the introduction of an self-adjoint observable operator O with the requirement that $\langle \Psi, O\Psi \rangle$ be maximized. In the latter case the optimal control theory is invoked and a cost functional is constructed $J(\epsilon)$, e.g. $J(\epsilon) = \alpha \int_0^T \epsilon^2(t)dt - \langle \Psi, O\Psi \rangle$ that is minimized ($\alpha > 0$ is a penalization factor).

A large body of literature concerns the control aspect of these equations. We refer the interested reader to [10, 16, 14, 22]. Suffices to say here that algorithms to find the controls are available in theoretical framework, but more importantly, very specific procedures also exist that apply in practice. In fact, the experimental realization of quantum control is based on the so called "closed loop" [10] methodology which exploits the crucial observation that many experiments can be performed in very short time (repetition rate of a quantum control experiment is as high as 10^5 a second!). The "closed loop" operates by combining a zero-order search algorithm (i.e., no gradient required) (see [18] for recent works on these algorithms) to the experimental machinery: the search algorithm explores the cost functional surface $J(\epsilon)$ and each time it requires the evaluation of $J(\epsilon_k)$ for a solution candidate ϵ_k an experiment is performed to measure $J(\epsilon_k)$.

27.2 Theoretical studies

Although the control of quantum phenomena is a goal in itself, sometimes further interest arises in connection with these experimental capabilities. More precisely, it turns out that is some situations the potential $V(x)$ and / or the dipole $\mu(x)$ are not known with a high precision. Moreover, since we are in a quantum framework the state itself $\Psi(t)$ may be unknown at some time instants (e.g. initial time); furthermore, according to quantum theory principles, any measurement on the state Ψ will necessarily disturb it and as such obtaining the full information on the state Ψ may not be an option. However, some observables $\langle O_k \rangle = \langle \Psi, O_k\Psi \rangle$ may still be available: in this case the system is measured and then is discarded (replaced with a new one).

Thus we can consider the question of inverting the Schrödinger equation (27.1) to find the potential $V(x)$ and or the dipole $\mu(x)$. One of the earliest studies that treated the inversion of the potential [23] considered the situation where is no control

$$\begin{cases} i\frac{\partial}{\partial t}\Psi(x,t) = \left(-\frac{1}{2m}\frac{\partial^2}{\partial x^2} + V(x)\right)\Psi(x,t) \\ \Psi(x,t=0) = \Psi_0(x). \end{cases} \tag{27.2}$$

If $\rho(x,t) = |\Psi(x,t)|^2$ can be measured at all times t and spatial locations x one can use the identity:

$$\int_{-\infty}^{\infty} \rho(x,t)\frac{\partial V(x)}{\partial x}dx = -m\frac{d^2}{dt^2}\int_{-\infty}^{\infty} x\rho(x,t)dx. \tag{27.3}$$

to recover V. An interesting conceptual application is observed when we can suppose that, e.g., by initially controlling the system, one can bring it to a state which ensure $\rho_j(x, t = \tau_k) = \delta(x - x_j)$ which tells that

$$\left.\frac{\partial V(x)}{\partial x}\right|_{x=x_j} = -m\frac{d^2}{dt^2}\left.\int_{-\infty}^{\infty} x\rho_j(x,t)dx\right|_{t=t_j}. \tag{27.4}$$

In general however, no such simple expression exist and inversion must resort on one hand to more demanding numerical algorithms and on the other hand ensure that recovery of V and / or μ is possible from the given partial measurements.

A situation that was recently treated [12] concerns a finite-dimensional discretization of (27.1): now H_0, V and μ are all $N \times N$ complex self-adjoint matrices. We denote by $\{\phi_i\}_{i=1}^N$ the eigenvectors of $H_0 + V$ and $\{\lambda_i\}_{i=1}^N$ the associated eigenvalues. The measured quantities are for all instants $t \geq 0$ the *populations* of the eigenstates ϕ_i, i.e. $p_i(t) = |\langle\phi_i, \Psi(t)\rangle|^2, i = 1, 2, ...$, or their analogues $|\langle\Psi, e_i\rangle|^2$ with respect to elements e_i of a basis of $\mathbb{C}^N$. Any control intensity $\epsilon(t)$ can be considered. Both V and the dipole moment μ are to be identified; we will suppose that H_0 is known (by spectroscopy or otherwise). The following result can be obtained:

Theorem 27.1 *Suppose that there exist two Hamiltonians H_1 and H_2 and two dipole moments μ_1 and μ_2, giving rise to two evolving states Ψ_1 and Ψ_2 respectively solving*

$$i\dot{\Psi}_1 = (H_1 + \epsilon(t)\ \mu_1)\ \Psi_1, \tag{27.5}$$

$$i\dot{\Psi}_2 = (H_2 + \epsilon(t)\ \mu_2)\ \Psi_2, \tag{27.6}$$

that produce identical observations for all times $t \in [0, \infty)$ and all fields $\epsilon(t)$

$$|\langle\Psi_1(t)\ |\ e_i\rangle|^2 = |\langle\Psi_2(t)\ |\ e_i\rangle|^2 \qquad i = 1, .., N, \tag{27.7}$$

where $\{e_i\}_{i=1}^N$ is the canonical basis of the state space $\mathbb{C}^N$. Assume for both Hamiltonians

1. *Equation* (27.1) *is wavefunction controllable [15].*
2. *The transitions of the Hamiltonian H are non-degenerate: $\lambda_{i_1} - \lambda_{j_1} \neq \lambda_{i_2} - \lambda_{j_2}$ for $(i_1, j_1) \neq (i_2, j_2)$ [19, 20].*
3. *The diagonal part of the dipole moment μ, when written in the eigenbasis of the Hamiltonian H, is zero: $\langle\phi_i\ |\ \mu\ |\ \phi_i\rangle = 0, \quad i = 1, .., N$.*
4. *the Hamiltonians H_1 and H_2 have the same eigenvalues.*
5. *there does not exist a subspace of dimension one or two spanned by the vectors $\{e_i\}$, which remains invariant during the free evolution ($\epsilon \equiv 0$) of the first system (H_1 and μ_1).*

Then, there exists a set of phases $\{\alpha_i\}_{i=1}^N$ such that, for all $1 \leq i, j \leq N$,

$$(\mu_1)_{ij} = e^{i(\alpha_i - \alpha_j)}(\mu_2)_{ij}, \tag{27.8}$$

$$(H_1)_{ij} = e^{i(\alpha_i - \alpha_j)}(H_2)_{ij}. \tag{27.9}$$

Such a result instructs us that the information contained in the $|\langle\Psi|e_i\rangle|^2$ is sufficient to recoved the potential V, the dipole μ and implicitelly some information on the initial state ϕ_0. Further results can also be obtained in terms of the populations p_i, see [12].

27.3 Practical implementations

The Theorem above links essentially the controllability of the nonlinear system (27.1) to the possibility of identifying the potential and the dipole moment through quantum control experiments. However, it does not provide an analytical formula to evaluate these quantities. Experimental protocols are thus required to realize the inversion. We will present briefly below one such protocol [7, 6, 12]: the *optimal identification* which is a mixed laboratory-computer simulation procedure that aims to recovered the information on the system Hamiltonian from experimental data. The optimal identification combines optimal control with inversion techniques exploiting once again the capability of performing a large number of control experiments. The algorithm employed is the following :

1/ for any laser field $\epsilon(t)$ and any proposal for the dipole moment /potential μ, V we define a cost functional $J(\epsilon, \mu, V)$ as the distance between

– the experimental measure of a given observable obtained with the field $\epsilon(t)$ on the real quantum system and

– the measure obtained from a numerical simulation with the Hamiltonian H_0 (known) the potential V, dipole μ and field ϵ.

2/ Let τ be a given tolerance; for any ϵ one can define the set $S(\epsilon) = \{\mu, V; J(\epsilon, \mu, V) \leq \tau\}$. Let $m(\epsilon)$ be its measure (precise definitions may vary, see the references above). Then an optimization algorithm is considered to minimize $m(\epsilon)$. The solution to this procedure $\bar{\epsilon}$ will be called *discriminating field*; any element of $S(\bar{\epsilon})$ will then be a possible solution of the initial inversion (identification) problem.

In practice there is still much to be done to find satisfactory procedures that combine robustness with algorithmic efficacity. Note that the above formulation solves for each ϵ an inverse problem, which is a very demanding task not only due to the nonlinearity but also to the demanding computational ressources required to numerically solve (27.1). Procedures are needed that make optimal use of resolutions of the Time Dependent Schrödinger Equations.

Bibliography

[1] A. Assion, T. Baumert, M. Bergt, T. Brixner, B. Kiefer, V. Seyfried, M. Strehle, and G. Gerber. Control of chemical reactions by feedback-optimized phase-shaped femtosecond laser pulses. *Science*, 282:919–922, 1998.

[2] C. J. Bardeen, V. V. Yakovlev, J. A. Squier, and K. R. Wilson. Quantum control of population transfer in green fluorescent protein by using chirped femtosecond pulses. *J. Am. Chem. Soc.*, 120:13023–13027, 1998.

[3] C.J. Bardeen, V. V. Yakovlev, K. R. Wilson, S. D. Carpenter, P. M. Weber, and W. S. Warren. Feedback quantum control of molecular electronic population transfer. *Chem. Phys. Lett.*, 280:151–158, 1997.

[4] D. Deutsch. Quantum theory, the Church-Turing principle and the universal quantum computer. *Proc. R. Soc. Lond. A*, 400:97–117, 1985.

[5] C.M. Dion, A. Keller, O. Atabek, and A.D. Bandrauk. Laser-induced alignment dynamics of HCN: Roles of the permanent dipole moment and the polarizability. *Phys. Rev. A*, 59(2):1382, 1999.

[6] H. Geremia, and .JM. Rabitz. Optimal identification of hamiltonian information by closed-loop laser control of quantum systems. *Phys. Rev. Lett.*, 89(26):263902, 2002.

[7] J. M. Geremia and H. Rabitz. Optimal hamiltonian identification: The synthesis of quantum optimal control and quantum inversion. *J. Chem. Phys*, 118(12):5369–5382, 2003.

[8] T. Hornung, R. Meier, and M. Motzkus. Optimal control of molecular states in a learning loop with a parameterization in frequency and time domain. *Chem. Phys. Lett.*, 326:445–453, 2000.

[9] Daniel G. Jay. Selective Destruction of Protein Function by Chromophore-Assisted Laser Inactivation. *PNAS*, 85(15):5454–5458, 1988.

[10] R.S. Judson and H. Rabitz. Teaching lasers to control molecules. *Phys. Rev. Lett*, 68:1500, 1992.

[11] J. Kunde, B. Baumann, S. Arlt, F. Morier-Genoud, U. Siegner, and U. Keller. Adaptive feedback control of ultrafast semiconductor nonlinearities. *Appl. Phys. Lett.*, 77:924, 2000.

[12] C. Le Bris, M. Mirrahimi, H. Rabitz, and G. Turinici. Hamiltonian identification for quantum systems : well posedness and numerical appraoches. *ESAIM: COCV, accepted*, 2006.

[13] R. J. Levis, G.M. Menkir, and H. Rabitz. Selective bond dissociation and rearrangement with optimally tailored, strong-field laser pulses. *Science*, 292:709–713, 2001.

[14] Herschel Rabitz, Gabriel Turinici, and Eric Brown. Control of quantum dynamics: Concepts, procedures and future prospects. In Ph. G. Ciarlet, editor, *Computational Chemistry, Special Volume (C. Le Bris Editor) of Handbook of Numerical Analysis, vol X*, pages 833–887. Elsevier Science B.V., 2003.

[15] V. Ramakrishna, M. Salapaka, M. Dahleh, and H. Rabitz. Controllability of molecular systems. *Phys. Rev. A*, 51(2):960–966, 1995.

[16] S. Rice and M. Zhao. *Optical Control of Quantum Dynamics*. Wiley, 2000. Many additional references to the subjects of this paper may also be found here.

[17] P. W. Shor. Algorithms for quantum computation: Discrete logarithms and factoring. In S. Goldwasser, editor, *Proceedings of the 35th Annual Symposium on the Foundations of Computer Science*, pages 124–134, Los Alamitos, CA, 1994. IEEE Computer Society.

[18] G. Turinici, C. Le Bris, and H. Rabitz. Efficient algorithms for the laboratory discovery of optimal quantum controls. *Phys. Rev. E*, 70:016704, 2004. Virtual Journal of Ultrafast Science, issue of August 2004.

[19] Gabriel Turinici and Herschel Rabitz. Quantum wave function controllability. *Chem. Phys.*, 267:1–9, 2001.

[20] Gabriel Turinici and Herschel Rabitz. Wavefunction controllability in quantum systems. *J. Phys.A.*, 36:2565–2576, 2003.

[21] T.C. Weinacht, J. Ahn, and P.H. Bucksbaum. Controlling the shape of a quantum wavefunction. *Nature*, 397:233–235, 1999.

[22] M. Zhao and S. Rice. Optimal control of product selectivity in reactions of polyatomic molecules: a reduced-space analysis. In J. Hepburn, editor, *Laser techniques for State-selected and State-to-Chemistry II, ed.*, volume SPIE 2124, pages 246–257, 1994.

[23] W. Zhu and H. Rabitz. Potential surfaces from the inversion of time dependent probability density data. *J. Chem. Phys.*, 111:472–480, 1999.

PICOF'06

Avec le soutien de :

AUF

CIMPA

CONSEIL GENERAL
DES ALPES-MARITIMES

Région
Provence-Alpes-Côte d'Azur

Liberté • Égalité • Fraternité
RÉPUBLIQUE FRANÇAISE
MINISTÈRE
DES AFFAIRES
ÉTRANGÈRES